



Vitória Gonçalves dos Santos Souza Pina

**Synthesis and photophysical properties evaluation of
purely organic dyes with potential application in
optoelectronic devices**

Dissertação de Mestrado

Dissertation presented to the *Programa de Pós-Graduação em Química* of PUC-Rio in partial fulfilment of the requirements for the degree of *Mestre em Química*.

Advisor: Prof. Dr. Jones Limberger

Co-advisor: Dr. Rodrigo da Costa Duarte

Rio de Janeiro
August 2024



Vitória Gonçalves dos Santos Souza Pina

**Synthesis and photophysical properties evaluation of
purely organic dyes with potential application in
optoelectronic devices**

Dissertation presented to the *Programa de Pós-Graduação em Química* of PUC-Rio in partial fulfilment of the requirements for the degree of *Mestre em Química*. Approved by the Examination Committee:

Prof. Dr. Jones Limberger

Advisor

Departamento de Química – PUC-Rio

Dr. Rodrigo da Costa Duarte

Co-advisor

UNESC

Profa. Dra. Camilla Djenne Buarque Muller

Departamento de Química – PUC-Rio

Profa. Dra. Aurora Pérez Gramatges

Departamento de Química – PUC-Rio

Profa. Dra. Nanci Câmara de Lucas Garden

Instituto de Química - UFRJ

Rio de Janeiro

August 2024

All rights reserved. Reproduction of all or part of this work is prohibited without the permission of the university, the author, and the advisor.

**Vitória Gonçalves dos
Santos Souza Pina**

Graduated in Chemistry from *Universidade Federal Fluminense*, 2022, with experience in electrochemistry and corrosion inhibition.

Bibliographic data

Pina, Vitória Gonçalves dos Santos Souza

Synthesis and photophysical properties evaluation of purely organic dyes with potential application in optoelectronic devices / Vitória Gonçalves dos Santos Souza Pina ; advisor: Jones Limberger ; co-advisor: Rodrigo da Costa Duarte. – 2024.

114 f. : il. color. ; 30 cm

Dissertação (mestrado)–Pontifícia Universidade Católica do Rio de Janeiro, Departamento de Química, 2024.

Inclui bibliografia

1. Química – Teses. 2. Chalconas. 3. DSSCs. 4. Camada emissiva. 5. OLEDs. I. Limberger, Jones. II. Duarte, Rodrigo da Costa. III. Pontifícia Universidade Católica do Rio de Janeiro. Departamento de Química. IV. Título.

CDD: 540

Acknowledgements

I would like to start thanking my family for all the support, love and understanding they provided for me throughout this master's journey and my life. To my grandmother Lola, my mother and father, thank you for everything and I love you more than words could ever express.

To my professor Dr. Jones Limberger for his guidance, patience, understanding, partnership and generosity. The academic life is tough by itself, and I feel very lucky to have been tutored by a professor and researcher as excellent as you. Your professionalism is cherished and admired by me.

To my co-tutor Dr. Rodrigo Duarte, for guiding my first steps at the lab, for the availability even from far away and for the friendship. *Saúde!*

To the LaSOQF group of students, for all the help provided and the laughter we had at the lab. Thanks to Daniella Grego for helping and teaching me at the first moments. A very special thanks to Carolina Vesga-Hernández for all the support, all the good moments and all the *arepas* and friendship.

To the LOEM group, led by professor Dr. Marco Cremona, for the photovoltaic experiments. Special thanks to Dr. Aline Magalhães for the partnership. To LEEA, led by professor Dr. Ricardo Aucélio. Special thanks to Dr. Marlin Peñafiel for the electrochemical measurements. To Dr. Andrea Barbieri, from *Istituto per la Sintesi Organica e la Fotoreattività*, for the solid-state measurements.

To Matheus Menezes and Henrique Hollauer. I am grateful for all the support and good moments we shared.

And finally, for the strength I had at moments when I thought I would not handle it and the happiness I experienced at moments when I thought it was not possible, I would like to thank my spiritual guides.

This study was financed in part by the *Coordenação de Aperfeiçoamento de Pessoal de Nível Superior* – Brasil (CAPES) – Finance code 001.

Abstract

Pina, Vitória Gonçalves dos Santos Souza; Limberger, Jones; Duarte, Rodrigo da Costa. **Synthesis and photophysical properties evaluation of purely organic dyes with potential application in optoelectronic devices.** Rio de Janeiro, 2024. 114p. Dissertação de Mestrado – Departamento de Química, Pontifícia Universidade Católica do Rio de Janeiro.

Traditional energy sources significantly contribute to environmental degradation and climate change, underscoring the need for innovative, energy-efficient solutions. This dissertation explores advancements in optoelectronic technologies as promising alternatives. The study is divided into two main applications: dye-sensitized solar cells (DSSCs) and organic light-emitting diodes (OLEDs). In the DSSC project, D- π -A chalcone-cored molecules with cyano-carboxylate and carboxylate as acceptor groups were synthesized, utilizing electron-rich aldehydes as donor precursors. These compounds exhibited intense, narrow absorption bands (322 to 429 nm) and blue to yellow emissions (431 to 579 nm) with moderate to large Stokes shifts. Solid-state testing showed broad UV to NIR absorption, excellent blue wavelength absorption, and effective anchoring onto TiO₂. Photovoltaic evaluation revealed short-circuit currents between 0.18 and 0.36 mA cm⁻², open-circuit voltages from 0.52 to 0.56 V, and a maximum power conversion efficiency of 0.13% for the molecule with a diphenylamino donor group and cyano-carboxylate acceptor. In the OLED project, four novel aryloxy-benzothiadiazole and 2,6-diphenyl-dicyanopyridine derivatives were synthesized, featuring carbazole and triphenylamino donor units, aiming for potential emissive layers in OLEDs. These compounds demonstrated absorption bands in the visible region (around 346 and 438 nm), with dicyanopyridine derivatives showing positive solvatochromic shifts. Fluorescence spectroscopy indicated emission maxima from 461 to 697 nm and moderate to large Stokes shifts. Aggregation-induced emission studies revealed enhanced emission in the aggregated state. Cyclic voltammetry showed energy gaps from 2.09 to 2.43 eV, with the smallest energy gap observed in the triphenylamino-substituted aryloxy-BTD molecule. In the future, the most promising molecules will be applied in OLEDs.

Keywords

Chalcones; DSSCs; Emissive layer; OLEDs.

Resumo

Pina, Vitória Gonçalves dos Santos Souza; Limberger, Jones; Duarte, Rodrigo da Costa. **Síntese e avaliação de propriedades fotofísicas de corantes puramente orgânicos com potencial aplicação em dispositivos optoeletrônicos.** Rio de Janeiro, 2024. 114p. Dissertação de Mestrado – Departamento de Química, Pontifícia Universidade Católica do Rio de Janeiro.

Fontes energéticas tradicionais contribuem significativamente para a degradação ambiental e mudanças climáticas, ressaltando a necessidade de soluções inovadoras e eficientes em termos de energia. Esta dissertação explora os avanços nas tecnologias optoeletrônicas como alternativas promissoras. O estudo é dividido em duas principais aplicações: células solares sensibilizadas por corante (DSSCs) e diodos emissores de luz orgânicos (OLEDs). Para o projeto de DSSC, moléculas D- π -A baseadas em núcleo de chalcona, contendo grupos aceptores de ciano-carboxilato e carboxilato, foram sintetizadas, utilizando aldeídos ricos em elétrons como precursores da unidade doadora. Esses compostos exibiram bandas de absorção intensas (322 a 429 nm) e emissões de azul a amarelo (431 a 579 nm) com deslocamentos de Stokes moderados a grandes. Os testes no estado sólido mostraram absorção ampla na região UV a NIR, boa absorção em comprimento de onda azul e ancoragem eficaz no TiO_2 . A avaliação fotovoltaica revelou correntes de curto-circuito entre 0,18 e 0,36 mA cm^{-2} , tensões de circuito aberto de 0,52 a 0,56 V e uma eficiência de conversão máxima de 0,13% para o composto com grupo doador difenilamino e aceitador de ciano-carboxilato. Para o projeto de OLED, quatro novos derivados de ariloxi-benzotiadiazola e 2,6-difenil-dicianopiridina foram sintetizados, apresentando unidades doadoras de carbazol e trifenilamino, com potencial aplicação em camadas emissivas para OLEDs. Os compostos demonstraram bandas de absorção na região visível (346 e 438 nm), com os derivados de dicianopiridina mostrando deslocamentos solvatocrômicos positivos. A espectroscopia de fluorescência indicou máximos de emissão variando de 461 a 697 nm e deslocamentos de Stokes moderados a grandes. Estudos de emissão induzida por agregação revelaram emissão ou emissão aumentada no estado agregado em todos os casos. A voltametria cíclica mostrou diferenças de energia variando de 2,09 a 2,43 eV, com a menor sendo observada no composto ariloxi-BTD substituído por trifenilamino. Futuramente, as moléculas mais promissoras serão aplicadas em OLEDs para teste.

Palavras-chave

Chalconas; DSSCs; Camada emissiva; OLEDs.

Table of Contents

List of Acronyms and Abbreviations	12
1. General Introduction	13
2. Dye sensitized solar cells	15
2.1. DSSC evaluation	18
2.2. the dye sensitizer's structure	20
2.3. Chalcones	23
3. Objectives	27
4. Methodology	27
4.1. Materials and Methods	27
4.2. Synthesis	29
4.2.1. Cyanoacrylic boronic acid (compound 2)	29
4.2.2. Butoxy-methoxy-benzaldehyde (compound 4a)	30
4.2.3. Brominated chalcones (compounds 5a-c)	30
4.2.4. Photosensitizers (compounds 6a-c and 7b)	31
4.3. DSSC studies	33
5. Results and Discussion	34
5.1. Design and synthesis	34
5.2. Photophysical properties	37
5.3. Electrochemical evaluation	40
5.4. Evaluation of the dyes as photosensitizers for DSSCs	41
6. Conclusions	44

7. Organic light emitting diodes	45
7.1. OLEDs operation	46
7.2. Time resolved fluorescence studies.....	49
7.3. Operation parameters of OLEDs.	50
7.4. Emitting layer.....	51
7.5. Benzothiadiazole	53
7.6. Cyanopyridine	56
7.7. Carbazole and triphenylamino groups	59
8. Objectives	63
9. Methodology	63
9.1. Synthesis of the intermediates	65
9.1.1. Aryloxy-BTD	65
9.1.2. Pyridine-3,5-carbonitrile derivative (DCP)	65
9.2. Synthesis of the luminophores	66
9.2.1. Carbazole-benzothiadiazole (CB-BTD)	66
9.2.2. Triphenylamine-benzothiadiazole (TF-BTD).....	67
9.2.3. Carbazole-dicyanopyridine (CB-DCP)	67
9.2.4. Triphenylamine-dicyanopyridine (TF-DCP)	68
10. Results and Discussion.	68
10.1. Design and synthesis.	68
10.2. Photophysical properties	73
10.3. Aggregation induced emission experiments	77
10.4. Electrochemical evaluation.....	82

11. Conclusions.....	83
Bibliography	85
Appendix	93

List of Acronyms and Abbreviations

ΔE_{ST}	Energy gap between S_1 and T_1
ϕ_f	Fluorescence quantum yield
f_w	Water fraction
A	Acceptor
AIE	Aggregation-induced Emission
AIEE	Aggregation-induced Enhanced Emission
BTD	Benzothiadiazole
CB	Carbazole
D	Donor
DCP	Dicyanopyridine derivatives
DSSC	Dye sensitized solar cell
EQE	External quantum efficiency
IQE	Internal quantum efficiency
ISC	Intersystem crossing
OLED	Organic light-emitting diode
RISC	Reverse intersystem crossing
S_0	Singlet ground state
S_1	Singlet
TF	Triphenylamino
TADF	Thermally activated delayed fluorescence
THF	Tetrahydrofuran
T_1	Triplet

1. General Introduction

One of the main concerns faced by humankind of the 21st century, as a result of unstoppable nature resources exploitation, is the energy crisis and a possible future energy collapse especially due to the depletion of fossil fuels. This scenario pushes authorities towards finding alternatives to mitigate the environmental impact caused by oil and gas, as well as covering the energy demands imposed by modern society life.^{1,2}

With an important role in this issue, the scientific community, alongside with the governments, has been working to understand, predict and create alternatives to overcome the problems caused by the overconsumption of non-renewable energy sources. Figure 1 depicts the world's energy consumption, highlighting our deep dependence of these non- renewable sources throughout the years.³

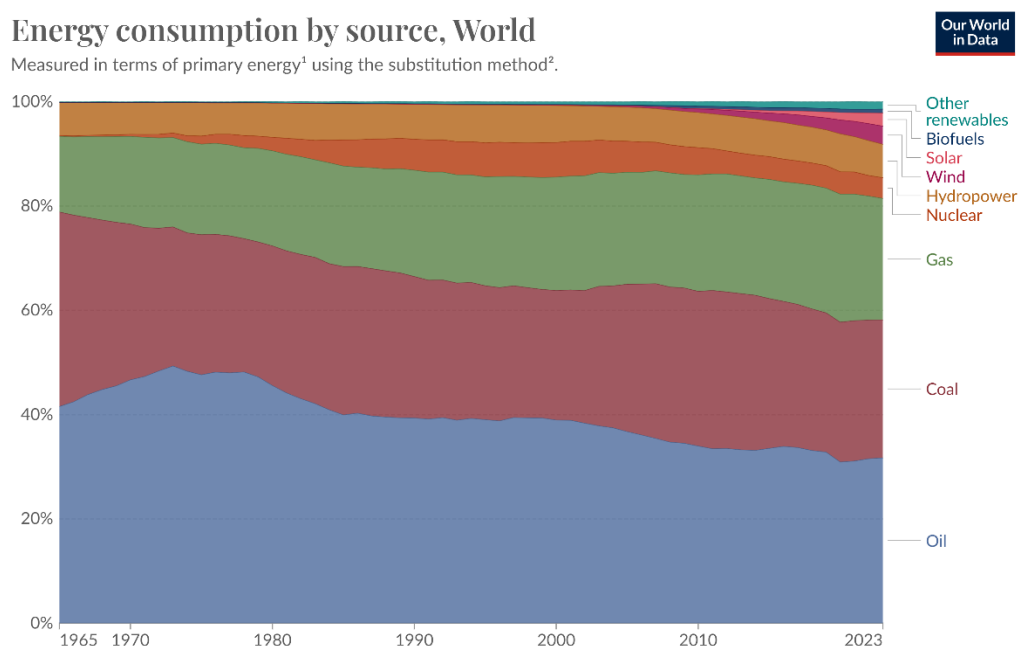


Figure 1: Energy consumption over the years by energy source.³

As can be seen, more than 80% of all the energy use is originated from oil, coal and gas, although from the 1980s onwards, the use of nuclear and hydroelectric energy began to appear in a somewhat more significant manner. Even though it is in a slow rate, other types of energy approaches are gaining importance and having its gradual implementation in society and domestic use.

This event is due to scientific advancements that enable these technologies to work efficiently and at good cost, popularizing their use by making them more accessible and affordable.

In this view, one of the technologies that can be mentioned when talking about saving energy alternatives is the optoelectronics. These types of devices are electric apparatus that can interact with light in different ways, capturing it and transforming it into an electric sign, or receiving an electric stimulus and producing light. Being employed as light-emitting devices, photodetectors, lasers and optical sensors (Figure 2), optoelectronics are able to harness light and be more effective in energy use and generation.^{4,5}



Figure 2: Optoelectronic devices examples, such as solar cells, LEDs and OLEDs and blue laser.

The present dissertation is divided into two topics related to organic compounds in optoelectronics applications: dye sensitized solar cells (DSSCs) and organic light-emitting diodes (OLEDs). For the DSSCs, sunlight interacts with the device and produce electric current, while OLEDs, in turn, receive the electric stimulus and produce visible light. Throughout this work, the synthesis, characterization and photophysical properties of different organic materials with potential applications in devices will be described.

In chapters 2 to 6, new chalcone-cored molecules featuring different donating substituents were studied in the context of their application in DSSCs. Regarding OLEDs, the development of benzothiadiazole and dicyanopyridine derivatives with carbazole and triphenylamino groups were presented in the chapters 7 to 11.

2. Dye sensitized solar cells

The solar cells history started in the XIX century, at the end of the 1830 decade, with the conceptualization of the photovoltaic (PV) effect, by the French scientist Edmond Becquerel.⁶ The effect can be explained as a generation of tension on a semiconductor material when exposed to a determined radiant light frequency. When the light frequency is absorbed, the electrons migrate to an excited state of energy and freely flow on the material's conduction band.^{7,8} This discovery is considered the prelude of solar power energy, because it made possible a series of developments, such as the first PV cell in 1883, by the north-american inventor Charles Fritts, using selenium and gold as raw materials.⁹ Throughout time, the explanation of other physical-chemical phenomena enabled, for example, the use of silicon crystals for new solar panels. In fact, many consider the silicon cell, developed in the 1950 decade as the true first PV cell, due to its capacity to generate enough current to power an electric device.^{10,11}

Until the current days, without disregarding its technological advancement, silicon-based cells are the most conventional solar panels used, representing more than 90% of the panels worldwide market, with photovoltaic solar power representing, in 2023, 5.5% of the electric power matrix on Earth.^{12,13} The importance of this market and the scientific progress behind it is due to the necessity for new alternative energy generation, especially environmentally friendly ones, as an attempt to decrease the deep dependence of fossil fuels. The development of these alternatives comes along with the need of optimization and technological evolution, which encourages the use of other types of resources and contribute to decelerate the high oil and gas consumption. Thus, not only the silicon cells were intensely studied throughout the years, but also other solar panels were developed with new materials.

Highlighting organic materials, an interesting and emerging class of solar power system are the dye-sensitized solar cells (DSSCs), devices that offer low cost, flexibility, and good indoor efficiency. Developed by Michael Grätzel in 1991, DSSCs work based on a redox process of an organic dye (sensitizer) to generate electric current. These types of cells explore a photoelectrochemical process, based on promoting the sensitizer's electron to an excited state of energy by absorbing sunlight photons. These excited electrons are injected into a semiconductor layer, promoting the oxidation of the dye sensitizer. The electron

then flows through a conductive electrode to the external circuit, reaching the counter-electrode and reducing a redox mediator, which, in turn, reduces back the oxidized dye, completing the redox circuit, as shown in figure 3.¹⁴⁻¹⁶

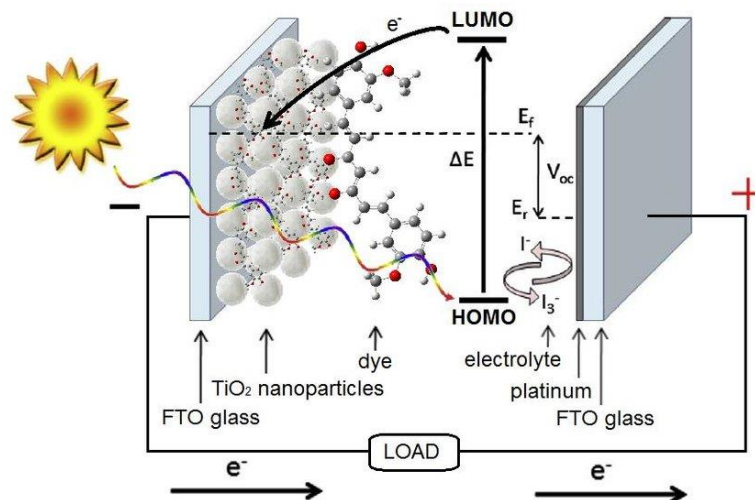


Figure 3: Operating mechanism of a dye sensitized solar cell.¹⁷

As can be seen, each part of the system is responsible for a step on the electron circuit. The DSSCs is composed by the following parts:¹⁸

Dye sensitizer: Organic compound (or coordinating compound) that absorbs the sunlight's photons, promoting electrons from HOMO to LUMO energy level.

Semiconductor (usually TiO₂ nanoparticles): Layer where the dye is anchored onto and acts as a semiconductor, enabling the electrons flow towards the photocathode.

FTO glass: Fluorine doped tin oxide transparent glass that acts as the photoanode (with a deposition of TiO₂ nanoparticles on its surface) or photocathode (with a deposition of a thin layer of platinum on its surface).

Counter-electrode (usually Platinum): Counter-electrode that receives the electron, reducing the mediator redox pair.

Electrolyte (usually ionic liquids or ammonium salts): Liquid containing the redox pair (usually I⁻/I₃⁻) that regenerates the dye.

When studying and designing DSSCs, an important characteristic to be considered is the energy level difference of the components involved (Figure 4).

The diagram shows that, to make the electron flow possible according to the correct direction, it is necessary to respect the potential gaps that allow the electron transfer and the circuit completion. The negative charge will be transferred to a lower state of energy in the 2, 3 and 4 processes, as they refer to oxidation-reduction steps. In 1 to 2, instead of redox, the sensitizer reaches a higher state of energy due to sunlight absorption. At this step, the molecule becomes excited, enabling the electron to be injected into the TiO₂ film.¹⁹

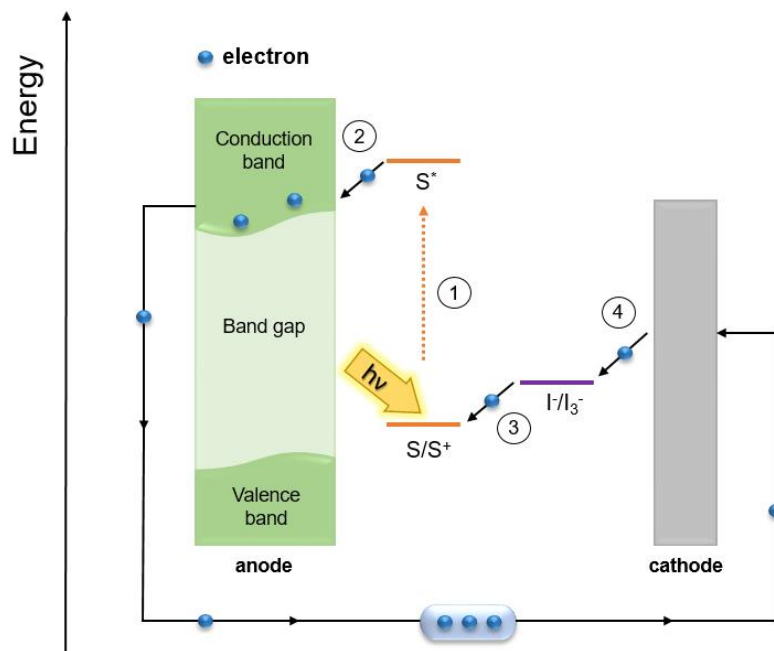


Figure 4: Generic energy diagram for DSSCs.

To elucidate the electron flow, it is possible to represent the 4 main processes as:^{20,21}

- 1) Dye excitation by sunlight: $S/S^+ \rightarrow S^*$
- 2) Electron injection: $S^* \rightarrow S^+ + e^-$ (on TiO₂ conduction band)
- 3) Dye regeneration: $S^+ + 3I^- \rightarrow S + I_3^-$
- 4) Redox pair regeneration: $I_3^- + e^- (\text{Pt}) \rightarrow 3I^-$

In addition to the aforementioned, other undesired processes must be contemplated when studying solar cells operation. The recombination processes can be related to the sensitizer and the I⁻/I₃⁻ pair. One of the possibilities is the return of the electron on the TiO₂ conduction band to the oxidized sensitizer, instead of generating work by flowing towards the photocathode. The mentioned event will happen if the recombination is faster than the electron injection velocity

on the semiconductor. It is also important that the velocity of this injection is greater than the velocity of the sensitizer decay to its fundamental energy level, in order to promote a considerable charge separation time on the system. The reduction of the sensitizer by the redox pair must also be fast, avoiding its regeneration by the semiconductor electron. Other recombination possible is the redox pair reacting with the TiO₂ electron, since this reaction happens faster than the sensitizer decay and the dye being on the adequate energy level to be regenerated. All of the mentioned processes will directly interfere with the cell's efficiency since the electrons are being deviated from the current generation. It is essential, thus, to respect the energy gaps of the TiO₂, dye and redox pair, as shown in figures 3 and 4, with the dye's LUMO being more energetic than the semiconductor's conduction band and the HOMO less energetic than the redox potential of the I^{+/I₃⁻}.^{20,22}

2.1. DSSCs evaluation

To evaluate a PV solar cell, the most important element to be determined is the current generation from light absorption. With a current vs potential (I vs V) graph, it is possible to find the essential parameters to understand the operation of the cell, as described below and shown in figure 5:²³

Open circuit potential (V_{oc}): Measured potential when current is null.

Short circuit current (I_{sc}): Measured current when the potential is null.

Fill factor (FF): A parameter that varies from 0 to 1 and describes how close to the ideal I vs V curve is from the real graph, represented by the darker blue square. Its value is determined by the equation (1):

$$FF = \frac{I_m \cdot V_m}{I_{sc} \cdot V_{oc}} \quad (1)$$

Where I_m and V_m are the maximum values found for current and potential.

Photoconversion efficiency (η): The ratio value between the maximum power (P_m) and incident light density (ρ_{in}), described by the equations (2) and (3) are:

$$P_m = I_m \cdot V_m \quad (2)$$

$$\eta = \frac{P_m}{\rho_{in}} = \frac{I_{sc} \cdot V_{oc} \cdot FF}{\rho_{in}} \quad (3)$$

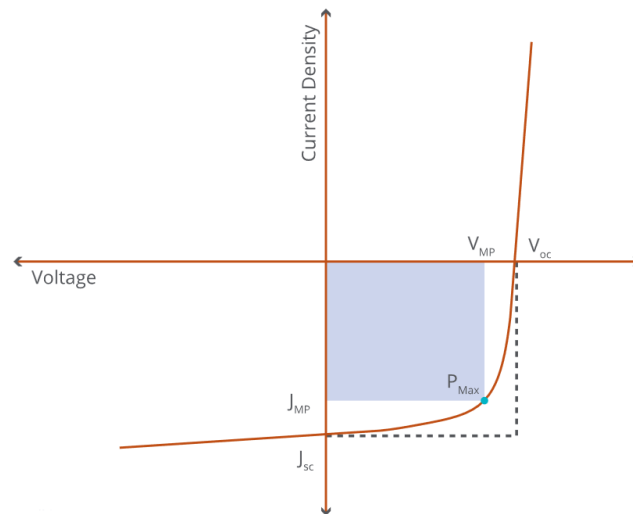


Figure 5: Current vs potential graph of a generic cell (Adapted from OSSILA).²⁴

Another relevant element that is analyzed is the incident photon-to-current efficiency (IPCE). This parameter correlates the generated photocurrent with the incident photons rate, at a specific wavelength. It is measured by shining monochromatic light onto the solar cell to obtain the resulting current. This test must follow the AM 1.5G standard measurement, which refers to a specific condition of realistic global solar simulation, allowing a consistent evaluation of the cell's performance. Figure 6 shows an example of an IPCE graph.^{25,26}

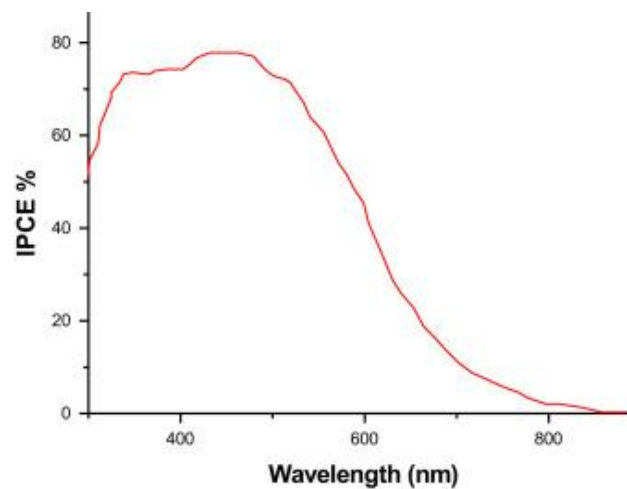


Figure 6: IPCE vs wavelength graph as an example for the percentage of current generation with determined wavelengths.

2.2. The dye sensitizers' structure

When it comes to the dyes used in DSSCs, some characteristics are required for a compound to be employed as a sensitizer, such as good photophysical properties. Amongst the already reported structures, ruthenium complexes stand out for their excellent stability and capacity to lead to DSSCs with the highest efficiencies described to date, as example the commercial N719 dye (**I**), reaching 12.3% of photoconversion efficiency (figure 7).^{27,28} However, as an important disadvantage, the synthesis of metal complexes can be highly expensive and difficult to achieve when compared to metal-free molecules.²⁹ For these reasons, several purely organic sensitizers have been produced and evaluated in DSSCs.

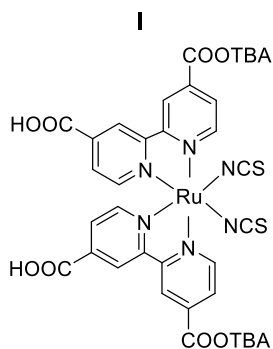


Figure 7: The structure of N719 dye (**I**), where TBA⁺ is the tetrabutylammonium cation.

Drawing inspiration from the operational mechanism of these cells, the aim in designing organic photosensitizers is to engineer molecules with a robust capacity for photon absorption spanning a broad range of wavelengths, coupled with efficient electron injection into the semiconductor's conduction layer. To accomplish this, the photosensitizer's architecture must revolve around molecular configurations conducive to streamlined electron transport and injection. This design incorporates a donor group tethered to a π -conjugated bridge, conjugately linked to an electron acceptor unit. Furthermore, nestled within the electron acceptor unit lies a pivotal moiety tasked with anchoring and facilitating electron injection into the semiconductor (figure 8).^{30,31}

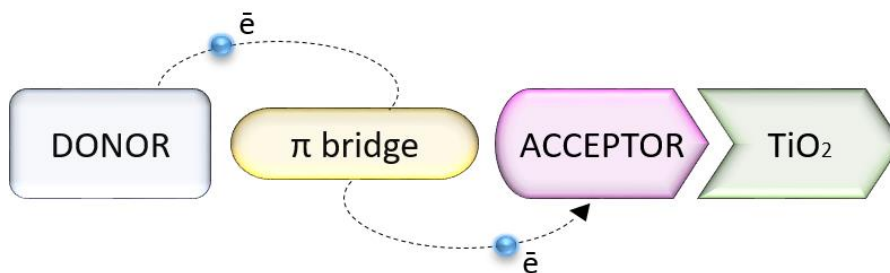


Figure 8: Sensitizer's desired structure.

In literature, it is possible to find a variety of D- π -A organic structures with potential to work as sensitizer. Siddiqui *et al.* synthesized a dithiophene cored molecule with triphenylamine as the donor moiety (**II**), reaching 23.01 mA cm⁻¹ of photocurrent density due to triphenylamine good electrical properties.³²

Cyanoacrylic-based organic dyes with different π -bridge groups, such as benzothiadiazole (**III**), thiophene (**IV**) and imidazopyridine (**V**), were synthesized by Ren and coworkers. The molecules showed absorption maxima wavelength around 500 and 600 nm. Molecule IV presents the narrowest energy gap with best charge separation ability. In turn, molecule III showed good electron-accepting abilities and electron transfer promotion. It was observed that the introduction of the imidazopyridine portion increased the steric hindrance, exhibiting good distortion.³³

Cai *et al.* developed new fused azacycle donor with D-A- π -A structure. Varying the number of members in the cycles, it was reached 6.22% of photoconversion efficiency, fill factor of 0.69 and 63% of maximum IPCE value for the seven membered ring, the most promising molecule synthesized (**VI**).³⁴

Yang *et al.* proposed phenothiazine dyes with different carbon chains length as potential sensitizers. The compound containing the octyloxyphenyl donor group showed high molar extinction coefficient, as well as higher absorption intensity, 6.66% of power conversion and 0.77 of fill factor (**VII**).³⁵

The molecules aforementioned are depicted in Figure 9 with a blue unit representing the donors and a red unit representing the acceptor/anchoring.

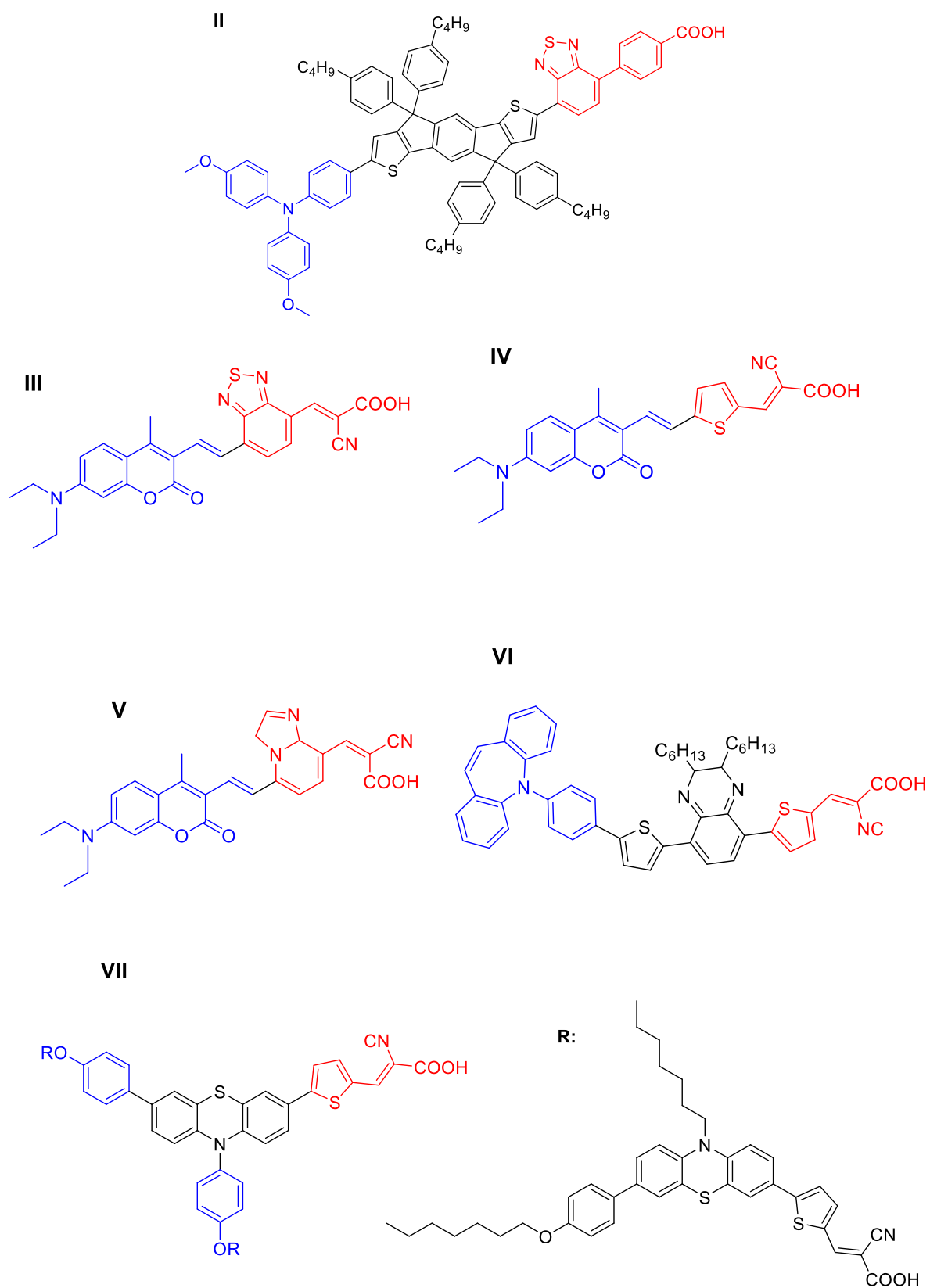


Figure 9: BTB derivatives as sensitizers for DSSC application.

2.3. Chalcones

Chalcones (**VIII**) represent α,β -unsaturated ketones bearing aryl/heteroaryl groups at both the carbonyl and β -carbon positions (figure 10). Numerous chalcones occur naturally, serving as pivotal intermediates in flavonoid biosynthesis.^{36,37} Moreover, these compounds can be readily synthesized via aldol condensation, involving the combination of substituted aryl aldehydes and acetophenones. Given the cost-effectiveness and accessibility of these starting materials, adjusting substituents and diversifying chalcone chemistry is a straightforward endeavor. Consequently, chalcones featuring varied substitution patterns find utility in (i) medicinal chemistry, displaying activities such as anti-inflammatory, antimicrobial, and antitumor effects; (ii) materials chemistry, where they serve as mechanochromic or luminescent materials; and (iii) analytical chemistry, employed as probes or biosensors.³⁸⁻⁴⁴

VIII

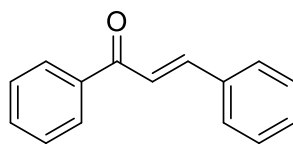


Figure 10: Chalcone structure.

In terms of optical applications, the fully conjugated structure of chalcones and the easiness of manipulating the aryl groups enable the creation of compounds capable of intensely absorbing radiation in a wide range of wavelengths, which can be valuable in the development of photosensitizers for dye-sensitized solar cells.^{45,46} In this context, selected chalcones have been tested as photosensitizers for DSSCs. Some examples reported in literature are described below with their respective molecular structures shown in Figures 11 and 12.

Teo *et al.* synthesized six new bischalcone compounds absorbing in the range of 268-421 nm. The highest conversion efficiency (0.054%) was obtained with a hydroxy-substituted bis-chalcone (**IX**). The better performance of this compound compared to other chalcones from same work was attributed to an improved electron injection to the TiO_2 layer, compared to non-hydroxylated analogs.⁴⁷

Anizaim and coworkers synthesized two ferrocenyl chalcones by Claisen-Schmidt condensation. In their study, the enone moiety presented in the

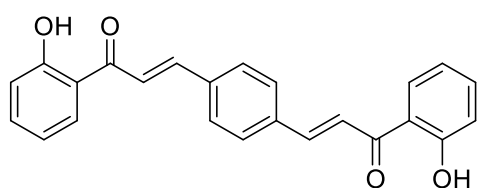
derivatives enabled a good linker between the ferrocene and the substituents bithiophene (**X**) and ethylfuran (**XI**). When these dyes were applied in DSSCs, power conversion efficiencies of 0.0034 and 0.041% were obtained, respectively.⁴⁸

Nizar *et al.* synthesized fluorinated (**XII**) and chlorinated (**XIII**) chalcones with A- π -A architecture. The fluoro-substituted chalcone showed enhanced charge transfer compared to the chloro-substituted analog, reaching up to 0.036% power conversion. This result was attributed to a better electron injection due to the electronegativity of the fluorine atom, which increased the dye regeneration in the circuit.⁴⁹

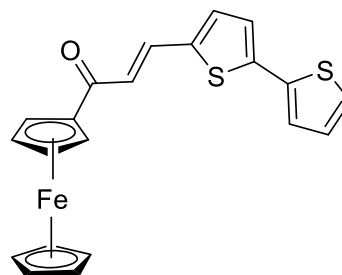
Karaca *et al.* worked with new tetra-substituted metallophthalocyanines-chalcones (of Zn, Cu and Ni), which showed suitable HOMO and LUMO energy for DSSCs application (**XIV**). The efficiencies obtained were 1.27, 0.51 and 1.11%, respectively, with the Zn substituted chalcone showing the highest power conversion due to its higher molar absorptivity coefficient and narrower absorption band.⁵⁰

For the same purpose, Rajakumar and coworkers synthesized hole-transporting and charge-separable dendrimers with chalcones at the periphery (**XV** and **XVI**), showing great light absorption. The DSSCs fabricated with these materials reached 7.1% conversion efficiency. According to the authors, such a good performance was due to the large number of donating atoms at the structure and the formation of a complex with the I₂ redox couple.⁵¹

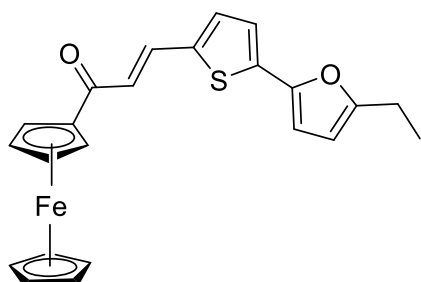
IX



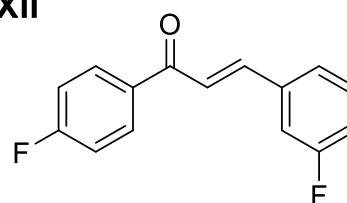
X



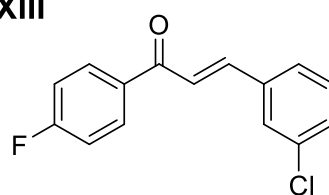
XI



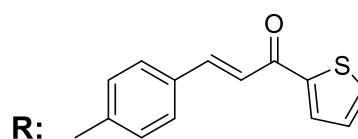
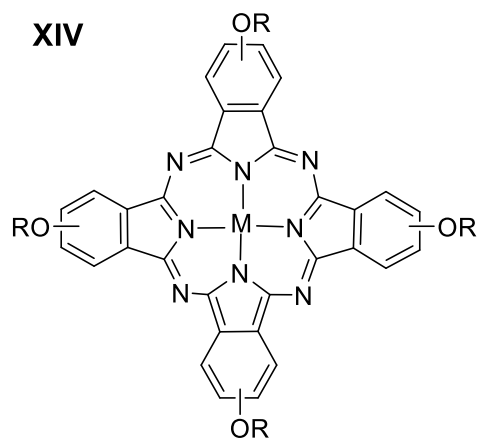
XII



XIII



XIV



M: Zn, Cu, Ni

Figure 11: Chalcone-cored structures evaluated as potential sensitizers.

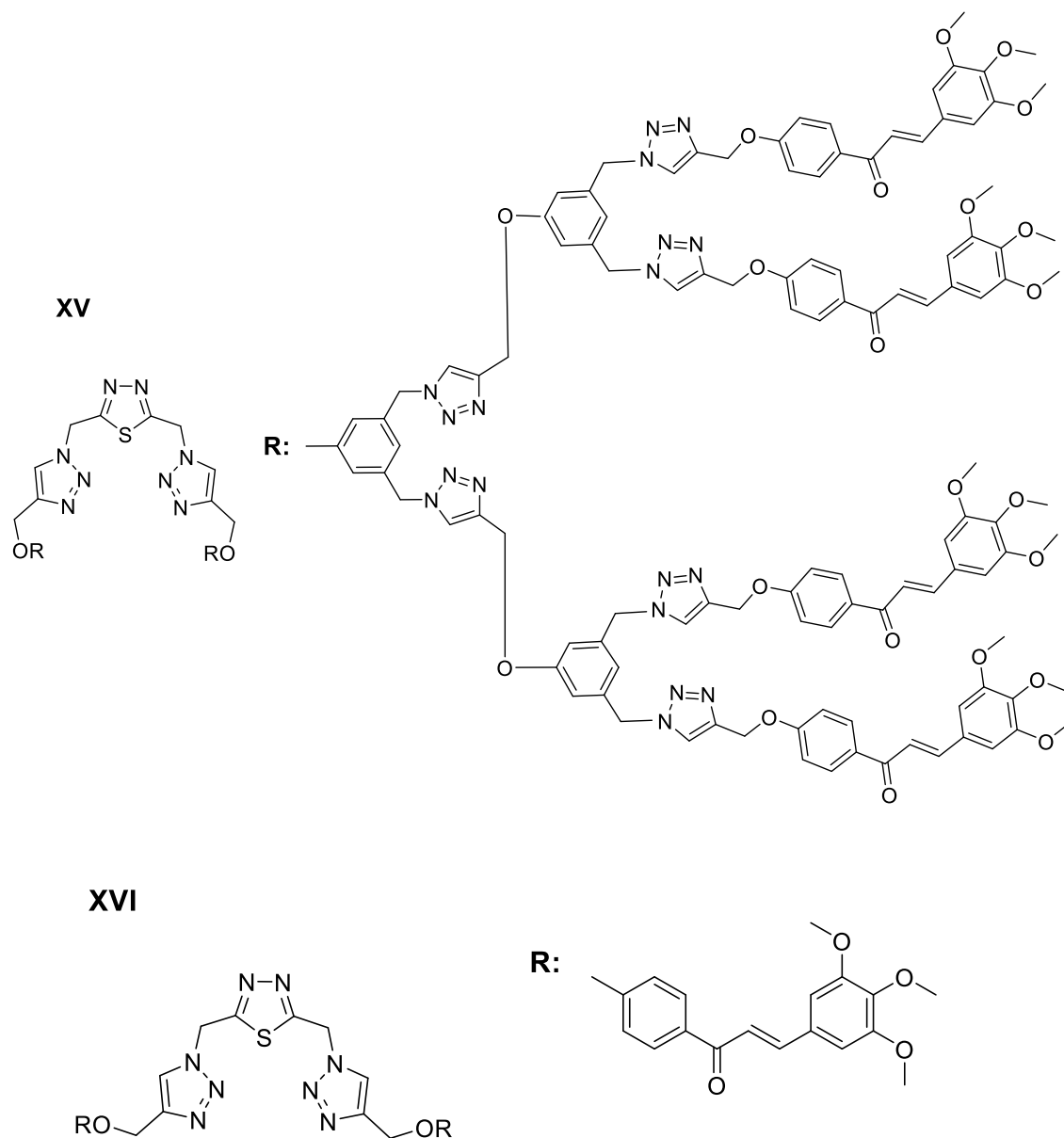


Figure 12: Chalcone-cored structures evaluated as potential sensitizers.

Considering all the topics discussed throughout this section and the literature consulted during the elaboration of this project, the combination of different donor groups with carboxylate and cyano-carboxylate acceptors has not been explored for chalcones. In this study, the synthesis of four highly conjugated chalcones with a D- π -A architecture, using electron-rich aldehydes as precursors of the donor units and carboxylate and cyanoacrylate acceptors attached to an acetophenone substrate was design and planned. This dissertation aimed to evaluate these molecules and their properties, comparing the performances as photosensitizers.

3. Objectives

The main objective of this work is the design, synthesis and evaluation of the photophysics properties of novel chalcones possessing different D and A groups, as well as the assessment of these compounds as photosensitizers for dye sensitized solar cells.

The specific objectives of the work are described below:

- To synthesize new chalcone-cored molecules via Suzuki cross-coupling reaction, with different electron donor (dimethylaminophenyl, butoxymethoxyphenyl and aryl groups) and electron acceptor/anchoring units (benzoate and cyanoacrylate groups), synthesizing also the intermediates materials when necessary.
- To perform photophysical and electrochemical characterization of the new compounds to determine absorption and emission maxima, fluorescence quantum yields in solution and solid state, as well as cyclic voltammetry to determine HOMO and LUMO energy levels.
- To fabricate and test the DSSC unit using the chalcone derivatives and determine their photoconversion efficiencies.

4. Methodology

4.1. Materials and methods

All chemicals and solvents utilized in this study were purchased from commercial suppliers and utilized without further purification unless specified otherwise. Solvents employed in cross-coupling reactions were previously degassed using a stream of nitrogen.

All the new molecules synthesized for this project were characterized via ^1H and ^{13}C NMR spectroscopy using a Bruker Advance III HD 400 MHz spectrometer. NMR analyses were carried out at the Analytical Facilities "Pe. Leopoldo Hainberger" of the Chemistry Department at PUC-Rio (CAPLH PUC-Rio).

The final products were characterized via the described technics:

High-resolution mass spectroscopy (HRMS), using a MICROTOF mass spectrometer (Bruker Daltonics) via direct infusion of the sample dissolved in acetonitrile solution and scanning range between 50 and 1200 m/z. The analysis was conducted in positive mode utilizing electrospray ionization at the Mass Spectrometry Laboratory within the Analytical Facilities of the Chemistry Institute at USP.

UV-Vis absorption spectra were performed on a Shimadzu UV-1900i spectrophotometer, with a 1 cm optical path quartz cuvette. Photoluminescence measurements were performed on a Shimadzu RF-6000 spectrofluorometer, using four clear faced 1 cm quartz cuvette, 6000 nm min⁻¹ scanning rate and 5.0 nm of spectral bandpass. Absorption and emission measurements were carried out using solutions with concentrations around 10⁻⁵ and 10⁻⁶ mol L⁻¹, respectively.

Relative fluorescence quantum yields of the four compounds synthesized were obtained by comparison with quinine solutions as standard. The photosensitizers' solutions were prepared at concentrations between 10⁻⁶ and 10⁻⁵ mol L⁻¹, using dichloromethane; quinine sulphate solutions were prepared at concentrations around 2.5 × 10⁻⁷ and 10⁻⁶ mol L⁻¹, using sulfuric acid 0.5 mol L⁻¹. It was used the equation (4) and considered 0.546 for the quinine's fluorescence quantum efficiency (ϕ_{st}).⁵²

$$\phi_{ch} = \phi_{st} \cdot \frac{A_{st}(\lambda_{ex})}{A_{ch}(\lambda_{ex})} \cdot \frac{\int_{\lambda_{em}(initial)}^{\lambda_{em}(final)} F_{ch}(\lambda_{em})}{\int_{\lambda_{em}(initial)}^{\lambda_{em}(final)} F_{st}(\lambda_{em})} \cdot \frac{n_{ch}^2}{n_{st}^2} \quad (4)$$

In equation (4), the $\int_{\lambda_{em}(initial)}^{\lambda_{em}(final)} F_{ch}(\lambda_{em})$ portion refers to the integrated area of the fluorescence emission band, with (st) representing the standard and (ch) the chalcones **6a-c** and **7b**; the n incognita refers to the refractive index of the chalcone solutions, which was considered the solvent refractive index, dichloromethane, with a $n = 1.4228$.⁵³

Electrochemical analyses were conducted employing a potentiostat/galvanostat (μ -AUTOLAB Type III, Metrohm) connected to a computer, operating in cyclic voltammetric analysis mode. The working electrode comprised glassy carbon, while the Ag|AgCl (KCl_(sat)) electrode served as the reference, and a platinum wire functioned as counter-electrode.

The electrochemical cell, with a volume of 15 mL, was constructed from Pyrex glass and equipped with a Teflon cap featuring openings for electrode adaptation. Cyclic voltammetric experiments were executed at a scanning rate of 50 mV s⁻¹ at room temperature, under N₂ purging. The electrolyte solution consisted of a 0.04 mol L⁻¹ solution of tetrabutylammonium phosphorus hexafluoride (TBAPF₆) in a blend of DMSO and acetonitrile (85/15% v/v). Ferrocene was employed to generate a reference voltammogram, with ΔV_{ref} of 0.1 eV. The determination of HOMO and LUMO energy levels from onset redox potentials were made by the equations (5) and (6).^{54,55}

$$E_{HOMO} = e^{(E_{ox}^{onset} + 4.4 - \Delta V_{ref})} \quad (5)$$

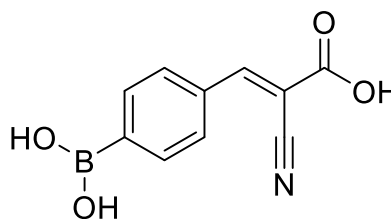
$$E_{LUMO} = e^{(E_{red}^{onset} + 4.4 - \Delta V_{ref})} \quad (6)$$

4.2. Synthesis of intermediates and photosensitizers

4.2.1. Cyanoacrylic-boronic acid (compound 2)

A blend containing 200 mg (1.34 mmol) of 4-formylphenylboronic acid, 131 mg (1.54 mmol) of 2-cyanoacetic acid, 578 mg (7.5 mmol) of ammonium acetate, and 6 mL of toluene was introduced into a Schlenk flask and stirred for 3 hours at 110°C. Subsequently, the reaction mixture was allowed to cool to room temperature, resulting in the formation of a solid corresponding to the crude product. The solid was then isolated by filtration and subjected to purification through recrystallization in a mixture of H₂O and acetonitrile (1:1).

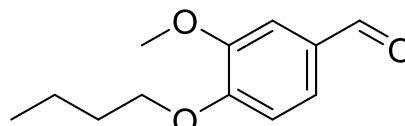
(E)-3-(4-boronophenyl)-2-cyanoacrylic acid (**2**): White solid; Yield: 77%; mp: 255-260 °C; FTIR-ATR (cm⁻¹): 3305, 2794, 2362, 2231, 1706, 1601, 1550, 1357, 1276, 1188, 1034, 825, 626. ¹H NMR (400 MHz, DMSO-d₆) δ ppm 8.03 (s, 1H); 7.89 – 7.84 (m, 4H). ¹³C NMR (100 MHz, DMSO-d₆) δ ppm 163.6; 151.6; 138.9; 135.0; 134.0; 129.3; 118.0; 109.0. HRMS (ESI) calculated for C₁₀H₇BNO₄ (M-H)⁻ = 216.0468; found: 216.0472.



4.2.2. Butoxy-methoxy-benzaldehyde (compound 4a)

In a Schlenk flask, 1.2 g (8.0 mmol) of 4-hydroxy-3-methoxybenzaldehyde (vanillin), 5.4 g (40 mmol) of 1-bromobutane, 0.05 g (3.6 mmol) of K_2CO_3 , and 10 mL of acetonitrile were combined and stirred at 80°C for 48 hours. Subsequently, the crude product was concentrated, dissolved in 50 mL of ethyl acetate, and subjected to washing with 2 mol L⁻¹ sodium hydroxide and brine. The organic layer was then dried over sodium sulfate, filtered, and the solvent was removed using a rotary evaporator. Purification of the product was achieved through silica plug chromatography using a hexane/ethyl acetate (7:3) eluent system.

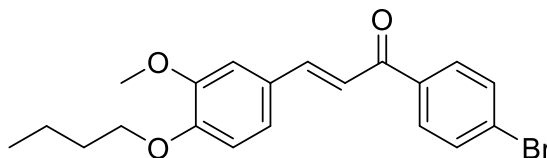
4-butoxy-3-methoxybenzaldehyde (**4a**): Colorless oil. Yield: 62%. ¹H NMR (400 MHz, CDCl₃) δ ppm 9.87 (s, 1H); 7.47 – 7.43 (m, 2H); 6.99 (d, J = 8.5 Hz, 1H); 4.13 (t, J = 6.4 Hz, 2H); 3.95 (s, 3H); 1.89 (m, 2H); 1.54 (m, 2H); 1.02 (t, J = 7.4 Hz, 3H). ¹³C NMR (100 MHz, CDCl₃) δ ppm 191.0; 154.2; 149.9; 130.0; 126.8; 111.4; 109.4; 68.7; 55.9; 30.9; 19.3; 13.9. Characterization data in accordance with literature.



4.2.3. Brominated chalcones (compounds 5a-c)

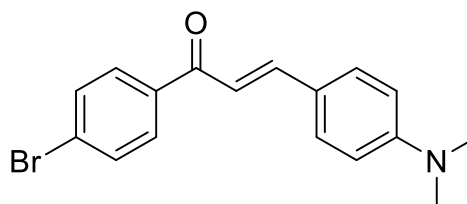
A round bottom flask was charged with the arylaldehyde (4-butoxy-3-methoxybenzaldehyde, 4-dimethylaminobenzaldehyde, or benzaldehyde) (2.0 mmol), 4-bromoacetophenone (2.0 mmol, 398 mg), and sodium hydroxide (2 mmol), along with 4 mL of ethanol. The mixture was stirred for 18 hours at room temperature. Subsequently, 1 mL of water was added, and the reaction flask was cooled to 0°C. The resulting solid was filtered and vacuum dried to yield compounds **5a-c**.

(E)-1-(4-bromophenyl)-3-(4-butoxy-3-methoxyphenyl)prop-2-en-1-one (**5a**): Yellow solid; Yield: 44%; mp: 76-78 °C; FTIR-ATR (cm⁻¹): 2960, 2937, 2874, 2163, 2052, 1650, 1580, 1508, 1340, 1240, 1137, 1026, 802, 527. ¹H NMR (400 MHz, CDCl₃) δ 7.88 (d, J = 8.6 Hz, 2H), 7.76 (d, J = 15.6 Hz, 1H), 7.64 (d, J = 8.6 Hz, 2H), 7.32 (d, J = 15.6 Hz, 1H), 7.21 (dd, J = 8.3, 2.0 Hz, 1H), 7.15 (d, J = 2.0 Hz, 1H), 6.90 (d, J = 8.3 Hz, 1H), 4.08 (t, J = 6.8 Hz, 2H), 3.93 (s, 3H), 1.90 – 1.80 (m, 2H), 1.57-1.45 (m, 2H), 0.99 (t, J = 7.4 Hz, 3H). ¹³C NMR (100 MHz, CDCl₃) δ ppm 189.4; 151.3;



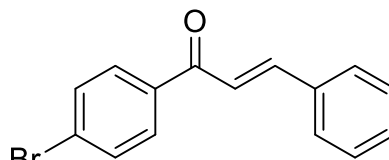
149.5; 145.6; 137.3; 131.9; 129.8; 127.6; 127.4; 123.3; 119.4; 112.3; 110.5; 68.7; 56.0; 30.9; 19.3; 13.6. HRMS (ESI) calculated for $C_{20}H_{22}BrO_3$ ($M+H$)⁺ = 389.0752; found: 389.0774.

(E)-1-(4-bromophenyl)-3-(4-(dimethylamino)phenyl)prop-2-en-1-one (**5b**): Yellow solid; Yield: 77%; mp: 146-148 °C; FTIR-ATR (cm^{-1}): 2888, 2802, 2165, 1898, 1646, 1580, 1527, 1334, 1188, 1065, 1005, 981, 808, 571. ¹H NMR (400 MHz, $CDCl_3$) δ ppm 7.89 (d, J = 8.4 Hz, 2H); 7.83 (d, J = 15.6 Hz, 1H); 7.64 (d, J = 8.4 Hz, 2H); 7.57 (d, J = 8.5 Hz, 2H); 7.33 – 7.27 (m, 3H); 6.72 (d, J = 8.4 Hz, 2H); 3.07 (s, 3H). ¹³C NMR (101 MHz; $CDCl_3$) δ 189.4; 152.2; 146.4; 137.8; 131.7; 130.5; 129.9; 127.0; 122.4; 116.2; 111.8; 40.1. HRMS (ESI in positive mode) calculated for $C_{17}H_{17}BrNO$ ($M+H$)⁺ = 330.0494; found: 330.0501.



Characterization data in accordance with the literature.

(E)-1-(4-bromophenyl)-3-phenylprop-2-en-1-one (**5c**): pale yellow solid; Yield: 73%; mp: 94-96 °C; FTIR-ATR (cm^{-1}): 2358, 1919, 1784, 1654, 1605, 1578, 1482, 1396, 1291, 1215, 1017, 979, 819, 685, 490. ¹H NMR (400 MHz, $CDCl_3$) δ ppm 8.02 (d, J = 8.5 Hz, 2H); 7.77 (d, J = 15.7 Hz, 1H); 7.62 – 7.52 (m, 8H). ¹³C NMR (100 MHz, $CDCl_3$) δ ppm 190.2; 143.4; 138.0; 133.8; 132.8; 132.3; 129.9; 128.6; 124.7; 122.4.



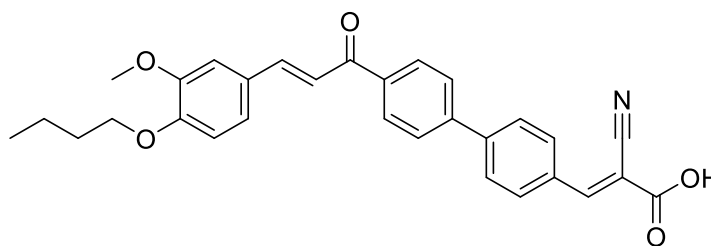
Characterization data in accordance with the literature.

4.2.4. Photosensitizers (compounds **6a-c** and **7b**)

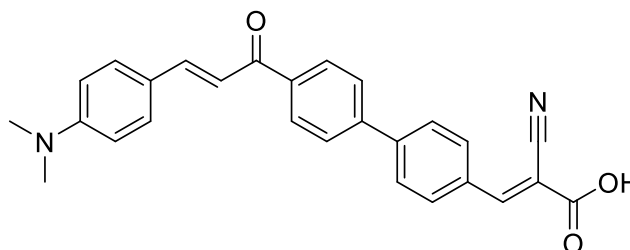
To synthesize the photosensitizers, 0.30 mmol of the monobrominated intermediates (**5a-c**) and 0.33 mmol of arylboronic acid (either compound 2 or 4-carboxyphenylboronic acid) were combined in a Schlenk flask previously evacuated and back-filled with nitrogen. Subsequently, 6.0 mg (0.027 mmol) of palladium acetate, 10.3 mg (0.042 mmol) of PPh_3 , 24 mg (0.6 mmol) of sodium hydroxide, and 6 mL of a 1:1 toluene/ethanol mixture were added. The flask was then sealed, and the reaction was carried out under constant stirring at 80°C for 18 hours. After cooling to room temperature, the crude reaction mixture was diluted with dichloromethane, filtered, and concentrated under vacuum. The resulting solid

product was purified via column chromatography using SiO₂ and a mixture of dichloromethane and methanol (95:5). The raw materials **5a**, **5b** and **5c**, in a combination with compound 2, originated the photosensitizers 6a, 6b and 6c, respectively; the raw material **5b**, in a combination with carboxyphenylboronic acid, originated the compound **7b**.

(E)-3-(4'-((E)-3-(4-butoxy-3-methoxyphenyl)acryloyl)-[1,1'-biphenyl]-4-yl)-2-cyanoacrylic acid (**6a**): Yellow solid; Yield: 39%; mp: 221-225 °C; FTIR-ATR (cm⁻¹): 3498, 2960, 2874, 2566, 2369, 1675, 1588, 1510, 1420, 1258, 1137, 969, 776. ¹H NMR (400 MHz, DMSO) δ 8.27 (d, J = 8.5 Hz, 2H), 8.14 – 8.02 (m, 3H), 7.99 – 7.85 (m, 5H), 7.73 (d, J = 15.4 Hz, 1H), 7.57 (d, J = 1.8 Hz, 1H), 7.39 (dd, J = 8.4, 1.8 Hz, 1H), 7.03 (d, J = 8.4 Hz, 1H), 4.03 (t, J = 6.5 Hz, 2H), 3.87 (s, 3H), 1.77 – 1.68 (m, 2H), 1.50 – 1.38 (m, 2H), 0.94 (t, J = 7.4 Hz, 3H). ¹³C NMR (101 MHz, DMSO) δ 188.46; 163.15; 150.85; 149.20; 148.38; 144.70; 142.98; 141.41; 137.28; 132.74; 130.40; 129.27; 127.55; 127.41; 127.11; 124.09; 119.53; 118.43; 112.53; 111.12; 67.92; 55.84; 30.71; 18.74; 13.69. HRMS (ESI) calculated for C₃₀H₂₆NO₅ (M-H)⁻ = 480.1811; found: 480.1822.

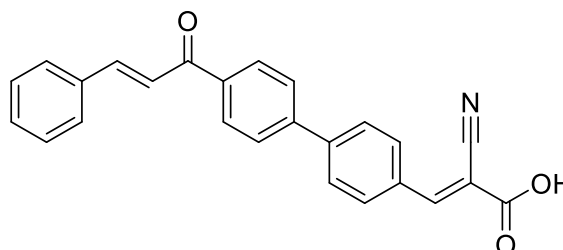


(E)-2-cyano-3-(4'-((E)-3-(4-(dimethylamino)phenyl)acryloyl)-[1,1'-biphenyl]-4-yl)acrylic acid (**6b**): Yellow solid; Yield: 50%; mp: 276-279 °C; FTIR-ATR (cm⁻¹): 3393, 2929, 2367, 2223, 1580, 1523, 1365, 1336, 1217, 1118, 1038, 810 ¹H NMR (400 MHz, DMSO) δ 8.22 (d, J = 8.5 Hz, 2H), 8.06 – 8.01 (m, 3H), 7.96 – 7.90 (m, 4H), 7.76 – 7.70 (m, 4H), 6.76 (d, J = 9.0 Hz, 2H), 3.02 (s, 3H). ¹³C NMR (100 MHz, DMSO-d₆) δ ppm 188.6; 158.3; 152.5; 148.3; 145.9; 143.0; 141.6; 138.1; 133.3; 131.2; 130.6; 129.4; 127.7; 127.5; 122.4; 119.0; 116.3; 112.2; 40.2. HRMS (ESI) calculated for C₂₇H₂₃N₂O₃ (M+H)⁺ = 423.1709; found: 423.1724.



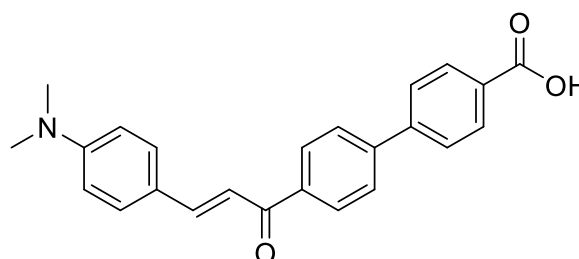
(E)-3-(4'-cinnamoyl-[1,1'-biphenyl]-4-yl)-2-cyanoacrylic acid (**6c**): Yellow solid; Yield: 36%; mp: 250-254 °C; FTIR-ATR (cm^{-1}): 3434, 2796, 2529, 2223, 1921, 1695, 1654, 1580, 1424, 1238, 1209, 979, 778; ^1H NMR (400 MHz, DMSO- d_6) δ ppm 8.41 (s, 1H); 8.19 (t, $J = 7.4$ Hz, 4H); 8.11 – 8.00 (m, 5H); 7.93 (d, $J = 8.4$ Hz, 2H); 7.82 (d, $J = 15.6$ Hz, 1H); 7.70 (t, $J = 7.3$ Hz, 1H); 7.60 (t, $J = 7.6$ Hz, 2H). ^{13}C NMR (100 MHz, DMSO- d_6) δ ppm 189.5; 163.8; 154.0; 143.7; 140.7; 137.9; 135.3; 133.7; 132.1; 131.5; 130.2; 129.3;

129.0; 127.9; 122.9; 116.7; 104.2.
HRMS (ESI) calculated for $\text{C}_{25}\text{H}_{17}\text{NO}_3$ (M-H) $^-$ = 378.1130; found: 378.1130.



(E)-4'-(3-(4-(dimethylamino)phenyl)acryloyl)-[1,1'-biphenyl]-4-carboxylic acid (**7b**): Yellow solid; Yield: 55%; mp: 275-278 °C; FTIR-ATR (cm^{-1}): 3077, 2800, 2557, 1677, 1572, 1519, 1424, 1338, 1297, 1180, 985, 810; ^1H NMR (400 MHz, DMSO- d_6) δ ppm 8.24 (d, $J = 8.5$ Hz, 2H); 8.07 (d, $J = 8.6$ Hz, 2H); 8.11 – 8.00 (m, 4H); 7.76 – 7.72 (m, 4H); 6.76 (d, $J = 8.5$ Hz, 2H); 3.03 (s, 6H). ^{13}C NMR (100 MHz, DMSO- d_6) δ ppm 188.5; 167.8;

152.5; 145.9; 143.5; 143.1; 138.2; 131.3; 130.4; 129.4; 127.6; 127.6(2); 122.4; 116.4; 112.2; 42.3. HRMS (ESI) calculated for $\text{C}_{24}\text{H}_{22}\text{NO}_3$ (M+H) $^+$ = 372.1600; found: 372.1617.



4.3. DSSCs studies

Solutions of chalcones **6a-c** and **7b**, as well as the ruthenium standard dye N719 (cis-diisothiocyanato-bis(2,2'-bipyridyl-4,4'-dicarboxylato) ruthenium(II) bis(tetrabutylammonium)), were prepared at a concentration of 5×10^{-4} mol L^{-1} using a mixture of methanol and dichloromethane in a 1:1 (v/v) ratio as the solvent. Chenodeoxycholic acid was added to the solutions at a 10:1 ratio to enhance the adsorption of the dyes onto the titania substrate. The solutions were prepared in volumetric flasks and covered with aluminum foil to prevent exposure to light.

The fabrication of the DSSCs utilized Solaronix® solar cell test kits. The photoanodes (titania electrodes) were submerged in solutions containing the dyes N719, **6a-c**, and **7b** for one day at room temperature. Subsequently, the electrodes were rinsed with a mixture of methanol and dichloromethane in a 1:1 (v/v) ratio to remove excess dye. The drop-casting method was then employed to apply the remaining dye solution onto the titania surface area. Following this, the electrodes were dried using airflow.

To assemble the DSSCs, platinum and titania electrodes were joined together using a 25 μm sealing polymeric film (Meltonix), creating a sandwich-type system. This sealing process was conducted on a hot plate at 100°C with gradual pressure application until the film completely melted. Following the sealing, 30 μL of the iodolyte AN-50 electrolyte (containing the iodide/triiodide couple) was added through the hole in the platinum electrode. Finally, the hole was sealed to prevent electrolyte leakage or drying.

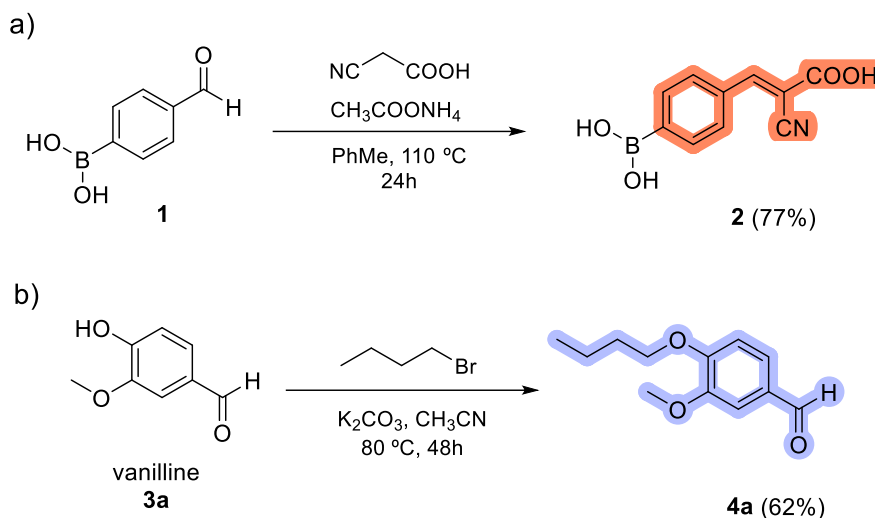
The tests aimed to assess the photovoltaic characteristics of the compounds under examination were conducted utilizing the Oriel 68805 universal power supply and Oriel lamp housing 66000, powered by a 300W Xenon lamp. Consistency was maintained throughout the measurements, employing a power density of 100 mW cm^{-2} from an Oriel xenon lamp irradiation system, in order to emulate sunlight.

5. Results and Discussion

5.1. Design and synthesis

Before synthesizing the π -extended chalcones, two crucial synthetic intermediates were produced to enable the synthetic route proposed. Given the widespread application of the cyanoacrylic acid unit as an acceptor/anchoring group in organic photosensitizers, notably present in dyes associated with excellent DSSC performance,^{56,57} the crucial component **2** was initially synthesized. This component facilitates the integration of the cyanoacrylic acid group and enhances the conjugation pathway of the chalcones. To achieve this, 4-formylphenylboronic acid (**1**) underwent a Knoevenagel condensation with cyanoacetic acid in the presence of ammonium acetate, yielding (**2**) at a 77% rate (Scheme 1a). Additionally, alkyl chains have been incorporated into dye structures for DSSCs. The objective behind this inclusion is to mitigate aggregate formation,

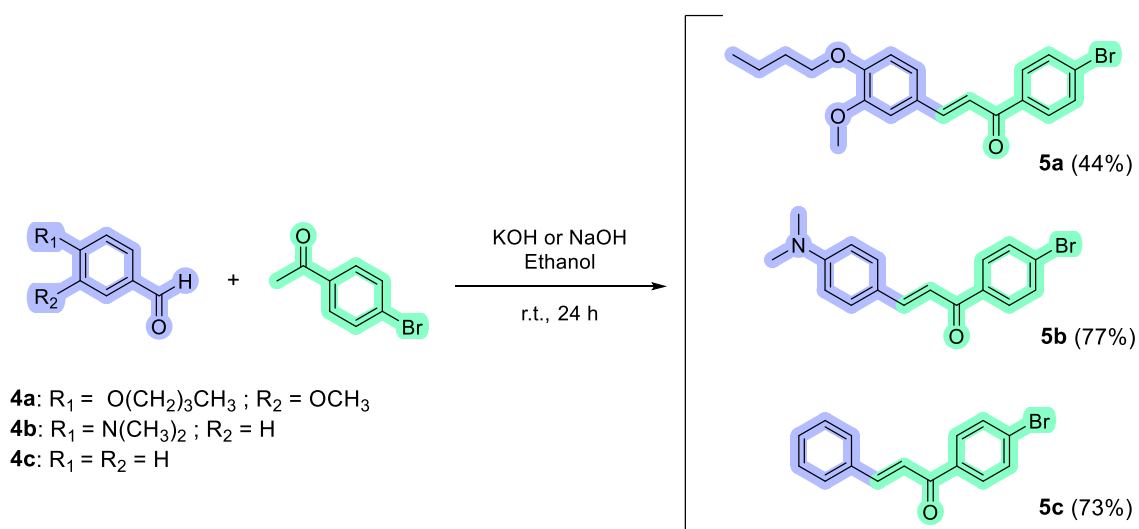
which impedes interaction between the photosensitizers and the semiconductor. Consequently, the alkylation of vanilline (**3a**) was conducted with butyl bromide, resulting in the aldehyde **4a**, a building unit possessing donor capacity, with a yield of 62% (Scheme 1b).



Scheme 1: a) Synthesis of the cyanoacrylic-boronic acid intermediate (**2**), via Knoevenagel reaction.

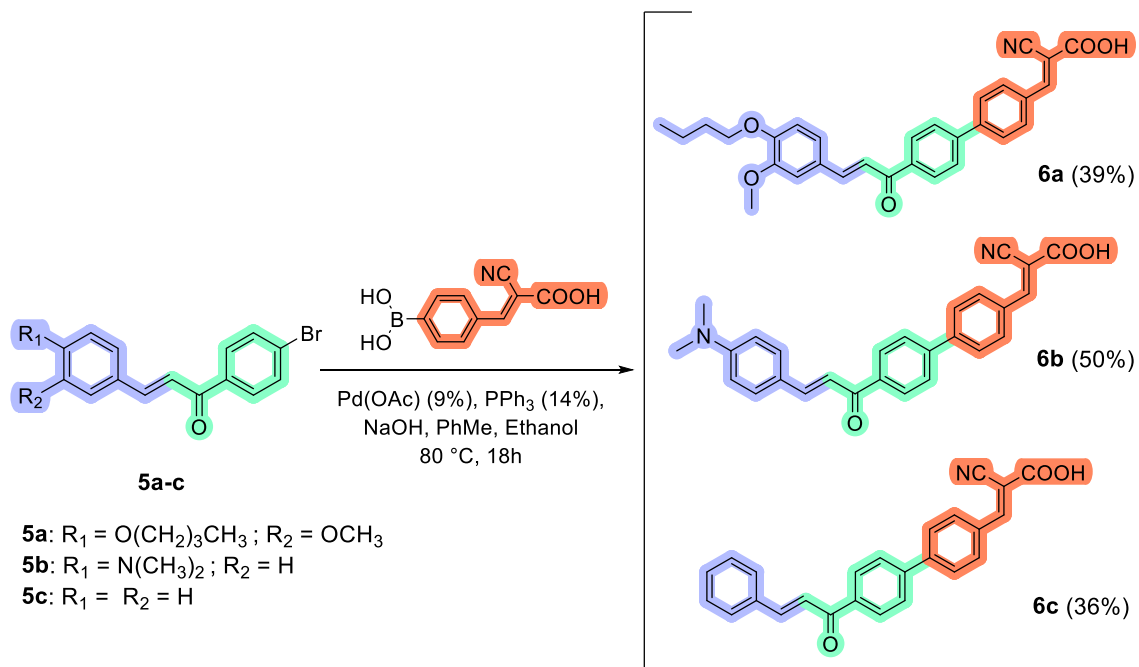
b) Alkylation of vanilline, producing the butoxy-methoxy-benzaldehyde (**4a**).

The synthesis of the chalcone's structures involved subjecting the vanillin-derived aldehyde (**4a**), 4-dimethylaminobenzaldehyde (**4b**), and benzaldehyde (**4c**) to aldol condensation conditions (using KOH or NaOH, ethanol, at room temperature) with 4-bromoacetophenone. This process yielded the chalcones **5a**, **5b**, and **5c** in yields of 44%, 77%, and 73%, respectively, as shown in Scheme 2.



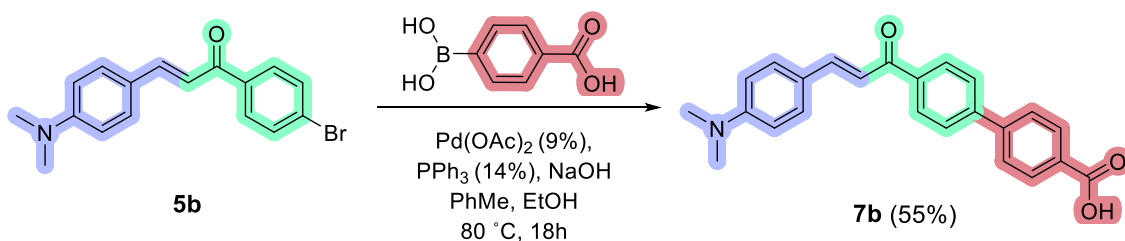
Scheme 2: Synthesis of the intermediate chalcones **5a-c**.

To synthesize the final products, the chalcones **5a-c**, together with the compound **2**, underwent a Suzuki cross-coupling reaction, in a system containing Pd(OAc)₂, PPh₃, and NaOH. After 18h, the chalcones **6a**, **6b** and **6c** were obtained with 39, 50 and 36% of yields, respectively (scheme 3).



Scheme 3: Synthesis of the final products 6a-c via Suzuki cross-coupling.

Likewise the process described above, aiming to produce a compound with a different anchoring group, the molecule **5b** was submitted to cross-coupling with 4-boronobenzoic acid, in the same reaction environment, originating the fourth compound with a carboxylic unit, yielding 55% of **7b**. The choice of the carboxylic group as an alternative regarding the anchoring unit comes, like the cyanoacrylic group, from its extensive application in dye synthesis for DSSCs. The reaction is elucidated in scheme 4.



Scheme 4: Synthesis of the final product 7b via Suzuki cross-coupling.

5.2. Photophysical properties

The photophysical characteristics of the π -extended chalcone dyes **6a-c** and **7b** were examined in various organic solvents with different dielectric constants (toluene, ethyl acetate, dichloromethane, and acetonitrile). Figures 13 and 14 illustrate the absorption and fluorescence emission profiles. Absorption peaks ranging from 322 to 429 nm, covering the ultraviolet to violet regions, with molar absorption coefficients around $10^4 \text{ mol L}^{-1} \text{ cm}^{-1}$, indicative of π - π^* transitions, were observed. These results denote a notable capacity for photon absorption, which can suggest promising prospects for solar radiation utilization in DSSCs when employing the compounds studied. Concerning structure-property relations, the $\text{N}(\text{CH}_3)_2$ -substituted chalcones **6b** and **7b** exhibited redshifted absorption compared to **6a** and **6c**, absorbing in less energetic wavelengths. Additionally, the benzoic acid chalcone derivative **7b** displayed the highest light absorption capacity.

Regarding fluorescence emission, the solutions were excited at the respective absorption maxima wavelength (λ_{abs}) of each solvent. The chalcones displayed emissions from blue to yellow, with peaks ranging from 431 to 579 nm, accompanied by Stokes shifts (72 to 192 nm), which can be considered moderate to large shifts. Compounds **6a-c** demonstrated very low fluorescence quantum yields (ϕ_{FL}), less than 0.01. In contrast, compound **7b** exhibited a more expressive value of ϕ_{FL} , 0.35. Comparing it to the other compounds, especially with the **6b** structure, which has the same dimethylamino donor group, it can suggest that substituting the cyanoacrylic unit with a benzoic acid acceptor unit enhances radiant decay processes through photon emission.

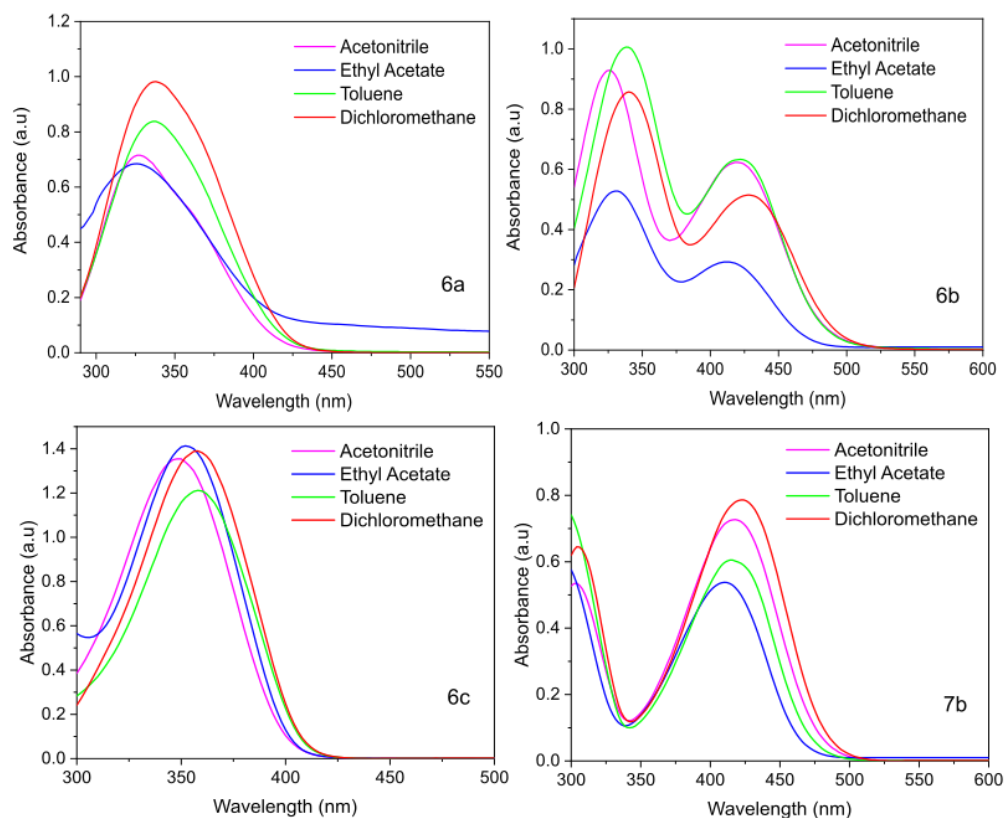


Figure 13: UV-Vis absorption spectra of the chalcones 6a-c and 7b.

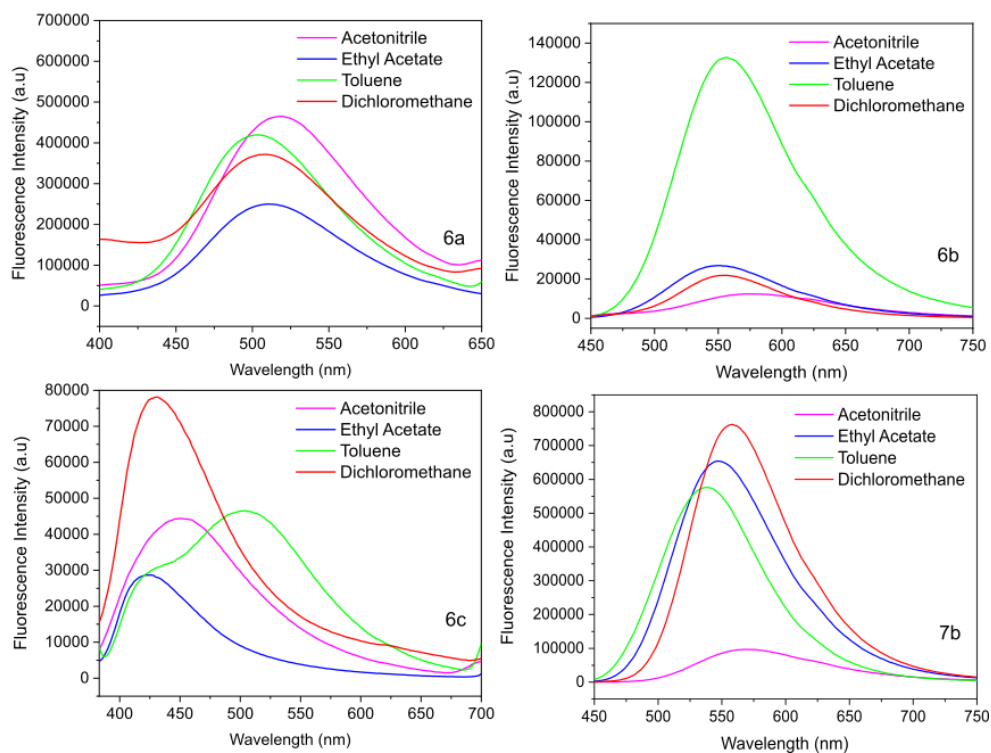


Figure 14: Fluorescence intensity emission spectra of the chalcones 6a-c and 7b.

In the following, table 1 summarizes the values found for the essays performed, where ε ($10^4 \text{ mol L}^{-1}\text{cm}^{-1}$) is the molar absorptivity coefficient, λ_{abs} and λ_{em} (nm) are the absorption and emission maxima, respectively, E_g (eV) is the optical bandgap energy, $\Delta\lambda_{\text{ST}}$ is the Stokes shift (nm) and ϕ_{FL} is the fluorescence quantum yield.

Table 1: Photophysical data of the chalcone dyes.

Dye	Solvent	λ_{abs}	ε	E_g	λ_{em}	$\Delta\lambda_{\text{ST}}$	ϕ_{FL}
6a	Acetonitrile	326	2.00	3.6	518	192	<0.01
	Ethyl Acetate	322	1.95	3.8	508	186	
	Toluene	338	2.36	3.8	502	164	
	Dichloromethane	338	2.76	3.6	508	170	
6b	Acetonitrile	420	1.84	2.9	578	158	<0.01
	Ethyl Acetate	412	0.88	3.0	550	138	
	Toluene	420	1.84	2.9	556	136	
	Dichloromethane	429	1.48	2.8	556	127	
6c	Acetonitrile	350	3.85	3.5	450	100	<0.01
	Ethyl Acetate	350	4.00	3.5	422	72	
	Toluene	358	3.42	3.4	503	145	
	Dichloromethane	358	3.71	3.4	431	73	
7b	Acetonitrile	414	2.30	3.0	569	155	0.35
	Ethyl Acetate	409	1.73	3.0	547	138	
	Toluene	414	1.91	3.0	537	123	
	Dichloromethane	424	2.50	2.9	558	134	

The absorption characteristics of the chalcones were also assessed in the solid state using diffuse reflectance UV-Vis measurements (DRUV/vis), shown in Figure 15. The compounds were examined either in powdered form (Figure 15a) or adsorbed onto TiO_2 films (Figure 15b). In the absence of TiO_2 , all compounds exhibited broad bands spanning from UV to NIR, with heightened absorption in the blue region. Chalcones **6a**, **6c**, and **7b** demonstrated similar absorption profiles, with a notable decline in absorption beyond 480 nm. Conversely, chalcone **6b** exhibited elevated absorptions in the green to red regions (500 to 650 nm), suggesting enhanced solar radiation capture potential.

The absorption profiles of all chalcones were influenced by the presence of TiO_2 , indicating their potential coordination with the semiconductor, a crucial property for their role as photosensitizers in DSSCs. When associated with TiO_2 , chalcones **6a** and **6c** displayed absorption primarily in the UV and blue regions, indicating limited solar radiation absorption. In contrast, compounds **6b** and **7b** showcased broader absorption bands extending into the green and orange regions, respectively. Given that these two compounds feature the dimethylamino donor group, it can be inferred that this group positively impacts by providing broader absorption bands.

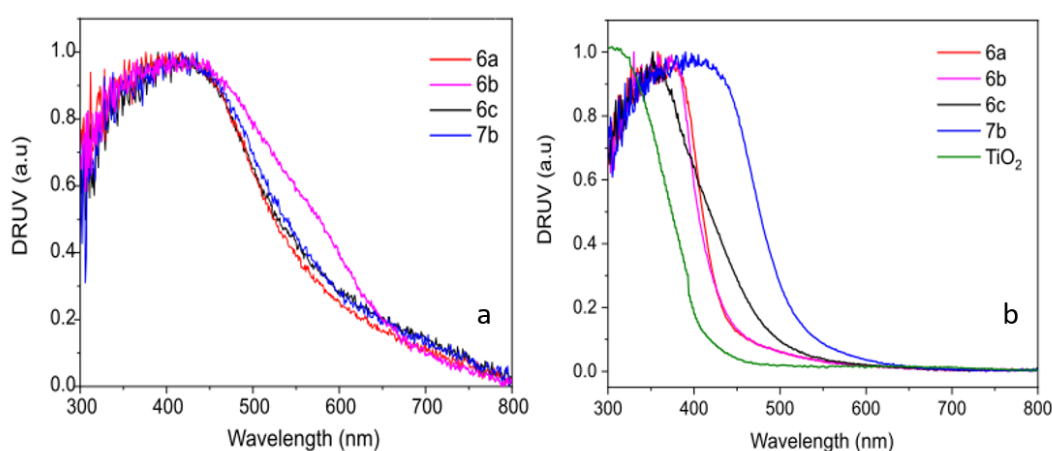


Figure 15: (a) UV-Vis-NIR spectra of compounds 6a-c and 7b in the solid-state. (b) UV-Vis-NIR spectra of compounds 6a-c and 7b adsorbed on TiO_2 film and TiO_2 pure.

5.3. Electrochemical evaluation

The electrochemical characteristics of photosensitizers **6a-c** and **7b** were evaluated through cyclic voltammetry measurements (Table 2) in dichloromethane, using tetrabutylammonium hexafluorophosphate as the supporting electrolyte. The resulting voltammograms are depicted in Figures A30-34 in the Appendix section. For this experiment, a glassy carbon electrode served as the working electrode (with Ag/AgCl (KCl_{sat}) reference). Oxidation peaks were observed within the range of 1.18 to 1.21 V, while reduction peaks ranged from -1.11 to -1.23 V. Subsequently, the HOMO and LUMO energy levels were estimated from these values using equations (2) and (3), previously described in experimental section. HOMO energy levels ranged from -5.48 eV to -5.51 eV, whereas LUMO levels varied between -3.07 and -3.19 eV. A distinct correlation between the donor or

acceptor group's nature and HOMO/LUMO energy levels was not observed. It is worth noting that the LUMO of all photosensitizers exceeded the conduction band edge of TiO₂, a prerequisite for efficient electron injection in DSSCs. Furthermore, the HOMO values were below the iodine/triiodine redox couple, facilitating dye regeneration by the electrolyte (Figure 16).

Table 2: Redox potential, HOMO and LUMO and energy band gap estimated via cyclic voltammetry for each dye.

Dye	E ^{ox} (V)	E ^{red} (V)	HOMO (eV)	LUMO (eV)	E _{gap} (eV)
6a	1.20	-1.23	-5.50	-3.07	2.43
6b	1.18	-1.11	-5.48	-3.19	2.29
6c	1.20	-1.14	-5.50	-3.16	2.34
7b	1.21	-1.21	-5.51	-3.09	2.42

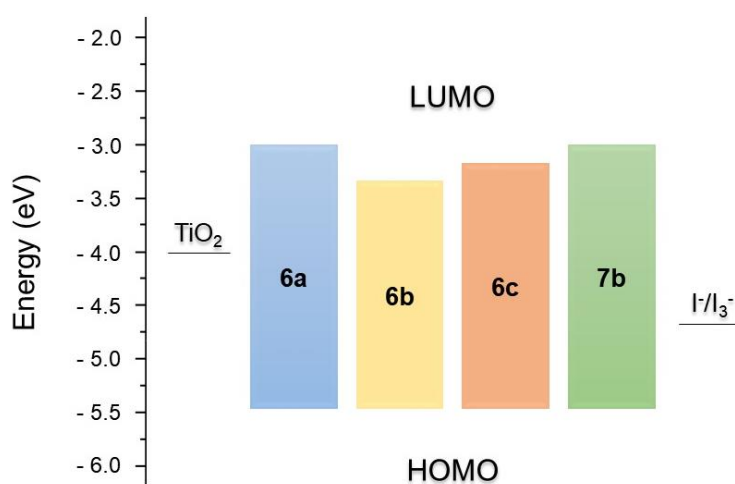


Figure 16: Energy diagram of chalcones 6a-c and 7b in comparison to TiO₂ valence band and I⁻/I₃⁻ redox couple energy.

5.4. Evaluation of the dyes as photosensitizers for DSSCs

Chalcones **6a-c** and **7b** were subsequently tested as photosensitizers for DSSCs. The solar cells were assembled using Solaronix® kits, featuring titania electrode (TiO₂ photoanode), platinum electrode (cathode), and the electrolyte (I⁻/I₃⁻ redox pair), shown in Figure 17. To sensitize the titania, the photoanode was immersed for 24 h in solutions containing chenodeoxycholic acid and the chalcones **6a-c** and **7b** (at 5 × 10⁻⁴ mol L⁻¹). After drying, sealing, and addition of

the electrolyte solution, current-voltage curves were obtained under irradiation from a Xe lamp, with an irradiance of 100 mW cm^{-2} . The results are illustrated in Figure 18 and summarized in Table 3.

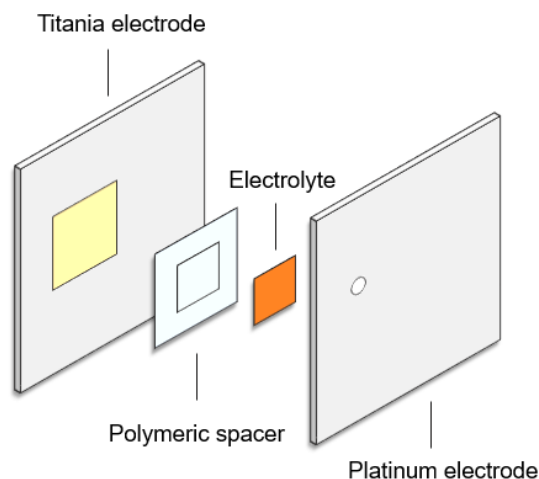


Figure 17: Schematic representation on a single DSSC unit.

The DSSCs exhibited a range of performance metrics: short-circuit current density (I_{sc}) varied from 0.18 to 0.36 mA cm^{-2} , open circuit voltage (V_{oc}) from 0.52 to 0.56 V, fill factor (FF) between 54% and 67%, and power conversion efficiency (η) from 0.05% to 0.13%. The lowest efficiency was observed with photosensitizer **6c**, characterized by a phenyl ring as the sole donating moiety. This result was already expected due to the lower donating capacity of the D portion of the molecule. In contrast, compound **7b** demonstrated the highest efficiency, combining both the stronger donating group (NMe_2) and an effective carboxylate anchoring group. This photosensitizer also exhibited higher molar absorptivity, and a broader absorption band compared to **6a-c**, contributing to its superior performance. The chalcone **6a** also exhibited an interesting conversion efficiency, similar to **7b**. This can be explained by the presence of the butoxy group, that enables the good anchoring of the cyanoacrilic group onto the titania by preventing the accumulation of the molecule on the semiconductor's surface, thus promoting a more efficient electron injection.

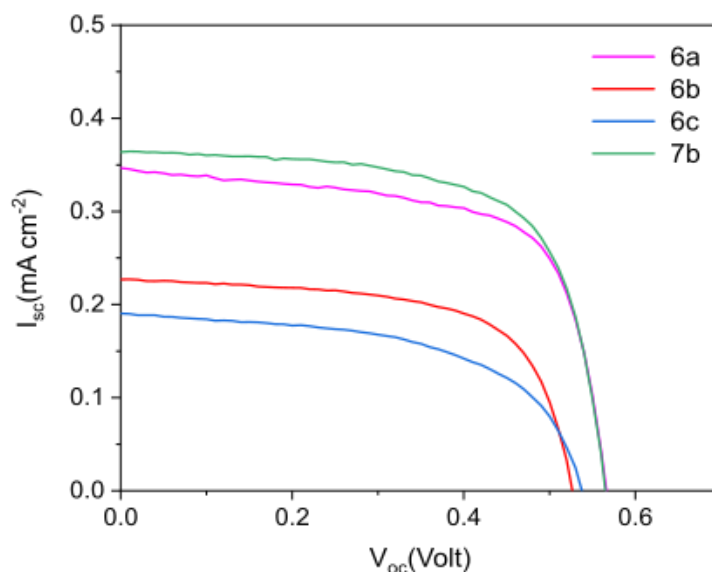


Figure 18: Open circuit voltage vs short-circuit current density graph for the four photosensitizers evaluated.

Table 3: Photovoltaic properties of DSSCs fabricated using chalcones **6a-c** and **7b** as photosensitizers.

Dye	I_{sc} (mA cm^{-2})	V_{oc} (V)	FF (%)	η (%)
6a	0.34	0.56	65	0.12
6b	0.23	0.52	63	0.07
6c	0.18	0.53	54	0.05
7b	0.36	0.56	67	0.13

While efficiencies of 0.12 and 0.13% might appear modest compared to dendrimer-based chalcones and polymer-linked benzimidazole-indole chalcones, the compounds **6a** and **7b** significantly outperformed various chalcone derivatives previously reported in the literature, including ferrocenyl-chalcones, bischalcones, and halogenated chalcones.

6. Conclusions

It was synthesized four novel π -extended chalcones designed with a D- π -A architecture, aiming to advance the development of chalcone-based photosensitizers specifically designed for DSSCs. These compounds were strategically synthesized by incorporating dimethylaminophenyl and alkylated vaniline derivatives as electron-donating units, complemented by benzoic acid and cyanoacrylic acid groups serving as acceptor and anchoring groups, respectively.

A key focus of this investigation was the photophysical characterization of these chalcones. It was observed that each compound exhibited distinct absorption bands characterized by their intensity and wavelength range. Despite their absorption being limited to narrower wavelength ranges, these bands were notably intense, which is crucial for efficient light absorption in solar energy applications.

Furthermore, the experimental results demonstrated that all synthesized chalcones effectively coordinated with TiO₂ semiconductor. This coordination highlighted the ability of these dyes to facilitate electron transfer from the photoexcited dye molecules to the titania surface, a pivotal step in the conversion of light energy to electrical current in solar cells. The evaluation of the HOMO and LUMO energy levels of these chalcones revealed promising properties for their application in DSSCs. The appropriate alignment of HOMO and LUMO energy levels ensures efficient charge separation and transport within the solar cell device, contributing to enhanced overall performance.

In terms of practical application, the synthesized chalcones were integrated into DSSCs to assess their photovoltaic performance. The power conversion efficiencies achieved ranged from 0.05% to 0.13%, representing an advancement compared to previously reported small-molecule chalcone-based dyes. This improvement underscores the potential of the four new synthesized chalcones as viable candidates for enhancing the efficiency and stability of DSSCs, contributing to the ongoing efforts in renewable energy research.

This work was submitted and published under the title "Carboxy-substituted D- π -A arylated chalcones: Synthesis, photophysical properties and preliminary evaluation as photosensitizers for DSSCs", at *Optical Materials* journal, Volume 149, March 2024, 115039 ([10.1016/j.optmat.2024.115039](https://doi.org/10.1016/j.optmat.2024.115039)).

7. Organic light emitting diodes

The emission of light by organic materials is a study topic since the latter half of the XX century, when it was first observed luminescence in cellulose film doped with acridine orange dye and light emission in anthracene single crystal due to induction in high electric field.⁵⁸ These early observations enabled the growth of the organic luminescent compounds research, leading to the discovery of numerous fluorescent organic molecules.⁵⁹ However, the potential application of these materials in optoelectronic devices remained uncertain, and the studies primarily limited to the scientific and theoretical field.

It was in 1987 when the scientists C. Tang and S. VanSlyke developed a sandwich-type light emitting device consisting of two thin organic layers placed between an anode and cathode. For this device, it was reported light emission around 2.5 V and high luminance ($>1000 \text{ cd m}^{-2}$, obtained with under 10 V of voltage); low external quantum efficiency (EQE), 1%, and low power efficiency, 1.51 m W^{-1} .⁶⁰ Although with low general performance, the described results garnered significant attention from scientific community, marking the onset of the light-emitting organic compounds technology era, influencing both academic research and industrial applications.

In technical definition, organic light-emitting diodes (OLEDs) are devices that emit light as a response to the electric current applied to an electroluminescent organic layer.^{61,62} This type of apparatus consists, in its basic version, in a thin system of anode and cathode, electron transport layer, emissive layer and hole (positive charge) transport layer, as shown in Figure 19.⁶³

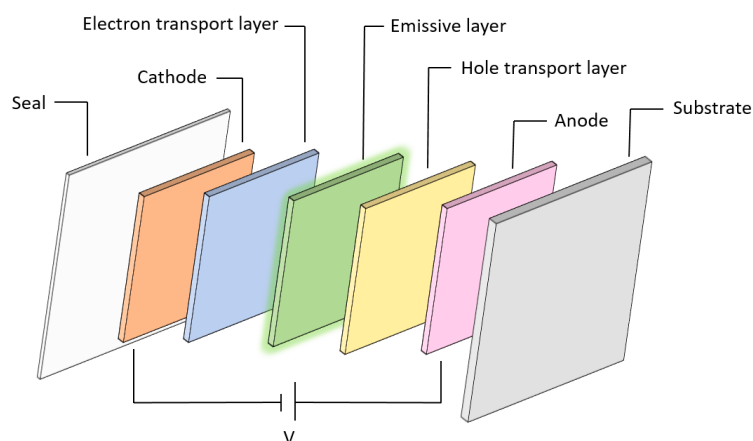


Figure 19: Schematic illustration of an OLED system.

Each represented part of the classic device pictured above can have its role described as: ^{63,64}

Seal: Layer that encapsulates the system, sealing it.

Cathode: Layer from where the electrons are injected in the system. Usually composed of aluminum.

Electron transport layer (ETL): Layer that enables the electrons flowing towards the emissive layer, blocking the holes.

Emissive layer: Layer with great capability of photon emission. Constituted of organic molecules, polymers, or metal complexes known for their high efficiency, prolonged lifespan, and color fidelity. Frequently, the emissive layer is blended within a matrix, with dopant concentrations of approximately 10% by mass, referred to as "host materials," typically resembling or identical to host molecules.

Hole transport layer (HTL): Layer that enables the injection of positive charges, promoting the recombination of these with the electron before it reaches the anode.

Anode: Layer from where the holes are injected into the system. Usually composed of indium tin oxide or indium zinc oxide.

Substrate: Layer typically composed of materials such thin metal sheets, must exhibit transparency and possess excellent conductivity, enabling the light to be emitted and shown.

With different application possibilities, OLEDs are mostly employed in displays technologies, being the substituent to liquid crystals displays (LCD) technologies in gadgets like mobiles and televisions. OLEDs offer a significant advantage over LCDs: they feature self-emitting pixel technology, meaning each pixel generates its own light. This distinction allows for a considerable reduction in display thickness and weight since no backlight is required, resulting in thinner devices (less than 1µm not including the substrate).^{65,66}

7.1. OLEDs operation

The operation of an OLED can be fundamentally described as the sequence: charge carriers injection; charge carriers transport; formation of

excitons (electron-hole pair); radiative decay and light emission. The Figure 20 elucidates the device's operation.⁶⁷

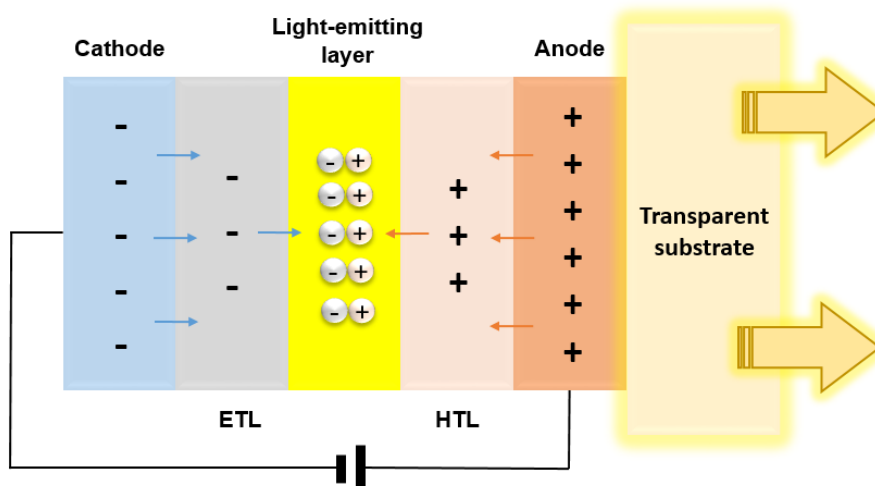


Figure 20: OLED's operation and charge internal movement.

The process initiates with the generation of positive and negative charges. Electrons are injected from the cathode into the LUMO of the compound that acts as the electron transport layer. Conversely, holes are injected from the anode into the HOMO of the compound acting as the hole transport layer. Subsequently, electrons move towards the anode while holes move towards the cathode, driven by the applied electric field and the attraction between opposite charges (Coulomb's law). During this process, recombination between holes and electrons occurs, along with various energy transfer processes, leading to the formation of electron-hole pairs in excited states within the emitting layer, promoting light emission.⁶¹

The recombination phenomenon that results in the electroluminescence forms an intermediate neutral state called exciton. These excitons have energetically distinct spin states (singlet and triplet) that are separated by a few hundred millielectronvolts (meV). Once the emissive layer compound is submitted to an electric excitation, radiative decay can happen in three different ways: fluorescence, phosphorescence and thermally activated delayed fluorescence (TADF). Figure 21 illustrates the energy diagram for the recombinations.⁶⁸

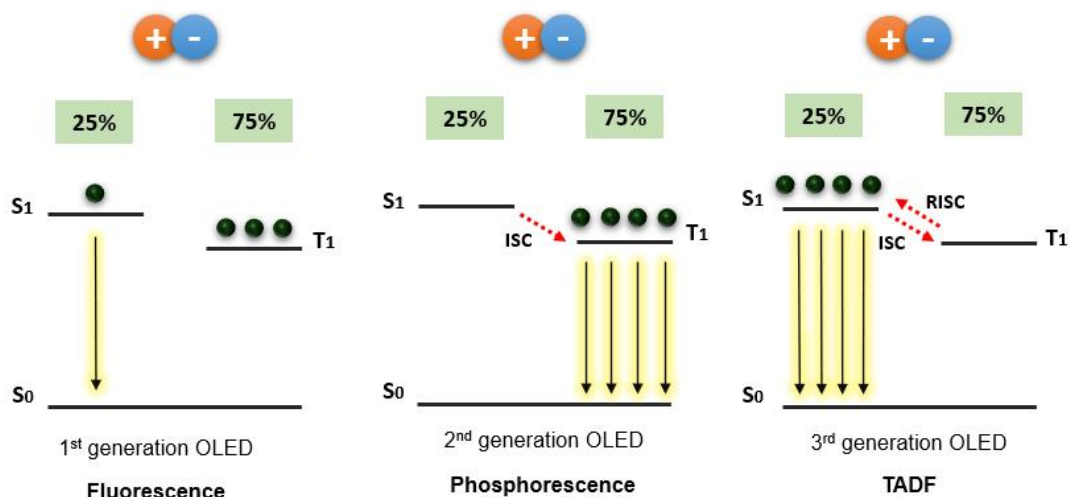


Figure 21: Energy diagrams for the 1st, 2nd and 3rd OLED generations.

For the fluorescent emission (1st generation OLEDs), the radiative decays happen from the singlet state of energy (S_1), on a nanosecond timescale, and approximately only 25% of maxima theoretical quantum efficiency (η). This occurs because the triplet state of organic compounds is triply degenerated, with three possibilities for triplets and only one for a singlet. Thus, for conventional fluorescent emitters, statistically, 75% of the excitons formed that occupy triplet states will be nonradiative, while 25% that occupy the singlet states will be free to decay emitting light. To overcome this limitation, some coordination compounds were designed for OLED's application purposes. With the introduction of metals in the structures, especially iridium, platinum and osmium complexes, new materials featuring the phosphorescence effect were developed (2nd generation OLEDs). In this case, the singlet state's population will migrate to the triplet state (T_1), a phenomenon called intersystem crossing (I_{sc}), enabling 100% of the excitons formed to occupy the T_1 and decay from this energy level, permitting a theoretical quantum efficiency of 100%. Finally, the third radiative decay possible also features a type of intersystem crossing phenomenon. In the thermally activated delayed fluorescence (TADF) compounds (3rd generation OLEDs) the energy gap between the singlet and triplet states must be considerably reduced, enabling, by thermic energy, a reverse intersystem crossing (RISC), where the T_1 population migrate back to S_1 and then decay emitting light. In this type of device, the theoretical efficiency can also reach 100%, due to the whole excitons population be concentrated at the singlet level. ⁶⁶

Highlighting the TADF molecules, one of the most important advantages that this type of OLED offers over 1st and 2nd generations is achieving good efficiency being based on metal free materials. Fluorescent OLEDs are very limited regarding internal quantum efficiency, only reaching 25%. When it comes to phosphorescent devices, in turn, generally it involves rare and expansive metals, such as iridium and platinum, as components, which turns the 2nd generation higher in cost and potentially toxic to humans and environment.⁷⁰

7.2. Time-resolved fluorescence studies

As discussed above, fluorescence and TADF emissions exhibit significantly differences when it comes to mechanism and properties. While purely fluorescent compounds emit light almost immediately after absorbing photons (in the ns scale), TADF compounds can not only emit fluorescence but also a long-lasting emission (in the scale of ms to μ s), the delayed fluorescence. In the TADF materials, the first emission arises from direct fluorescence (S_1 to S_0 decay), while the delayed emission originates from the triplet state after RISC process.⁷¹

To study the lifetime of these processes, time-resolved fluorescence spectroscopy is employed. In this technique, fluorescent decay is measured over time after an excitation pulse. For TADF materials, in the absence of O_2 (a triplet quencher), the profile of the spectrum will show a biexponential decay, referring to the prompt (τ_p) and the delayed emission (τ_d), while in conventional fluorescent compounds, a monoexponential decay will take place.⁷²

In 2019, Sharma and coworkers reported a sky-blue TADF based on a carbazole-triazine structure (CzpPhTrz), with 0.16 eV for singlet-triplet states energy difference (ΔE_{ST}), which can be considered a small value. The time-resolved fluorescence spectrum for this molecule shows a profile with two components, the prompt decay ($\tau_p = 7$ ns) and the delayed one ($\tau_d = 65$ μ s), strongly indicating that this material is a blue TADF emitter (Figure 22).⁷³

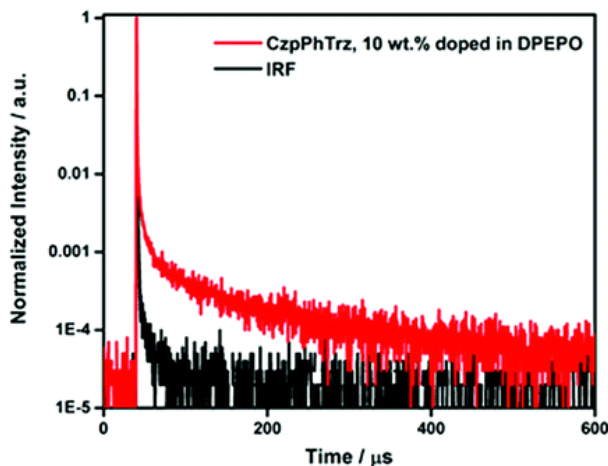


Figure 22: Time-resolved fluorescence spectrum of a TADF emitter.

7.3. Operation parameters of OLEDs

When evaluating OLEDs, some parameters are important to be determined to evaluate the device's operation and its efficiency:

Electroluminescence (EL): An optical phenomenon wherein photons are generated through the radiative recombination of electrons and holes as an electric current pass through a material. In OLED devices, the EL will be generated by the organic compound in its solid state.⁷⁴

Luminance: The brightness of light emitted from a surface per unit area in a specific direction. For the OLEDs development, this metric is quite important, because it influences directly on the observer's perception of clarity and color. It is represented by candela per square meter (cd m^{-2}).⁷⁵

Irradiance: The electromagnetic radiation incident on a surface per unit area. It is represented by watt per square meter (W m^{-2}).⁷⁶

Current efficiency: The amount of light emitted per unit of electrical current injected in the device. It indicates if the device can effectively convert electrical current into visible light.⁷⁷

External quantum efficiency (EQE): Ratio between the number of photons emitted and the electrons passing through the device. The most important metric of an OLED device, determining its yield in light emitting.⁷⁸

7.4. Emitting layer

Regarding the devices operating based on TADF, the 3rd generation of OLEDs, several structural characteristics are fundamental when planning the synthesis of a compound with potential for this mechanism of action. The molecules considered as candidates for the emissive layer of third-generation OLEDs will be those whose HOMO and LUMO exhibit low overlap between them, being located in distinct and well-defined sites along the molecular skeleton. HOMO spread over the donor group and LUMO concentrated over the acceptor unit. This structural characteristic allows for intramolecular transfer of excitons, owing to the spatial separation promoted by the donor-acceptor system (D-A), thus resulting in a reduction of the energy difference between the singlet and triplet states.⁷⁹

To promote the separation between HOMO and LUMO within a molecule, two structural strategies are considered: spiro compounds and molecules with a high dihedral angle between their donor and acceptor portions. In the former structure mentioned, the perpendicular orientation of the donor moiety with respect to the acceptor is explored. Spiro-type compounds are capable of deactivating the π - conjugations, thereby promoting non-coplanarity between HOMO and LUMO, and, hence, facilitating their optimal spatial separation.

Khan *et al.* used this strategy and synthesized a highly rigid spiro-type compound featuring a dimethyl-bridged triphenylamine group as donor (**XVII**), shown in Figure 23. The spiro conformation is due to the sp^3 hybridized carbon, which necessarily provides a tetrahedral geometry, thus guaranteeing the orthogonal position of the D-A groups. In this structure, the authors achieved a minimized singlet-triplet splitting, which was key to make the RISC event possible, resulting in a TADF molecule. The compound worked as a green emitter and achieved 16% of EQE for 10% of doping concentration in the system.⁸⁰

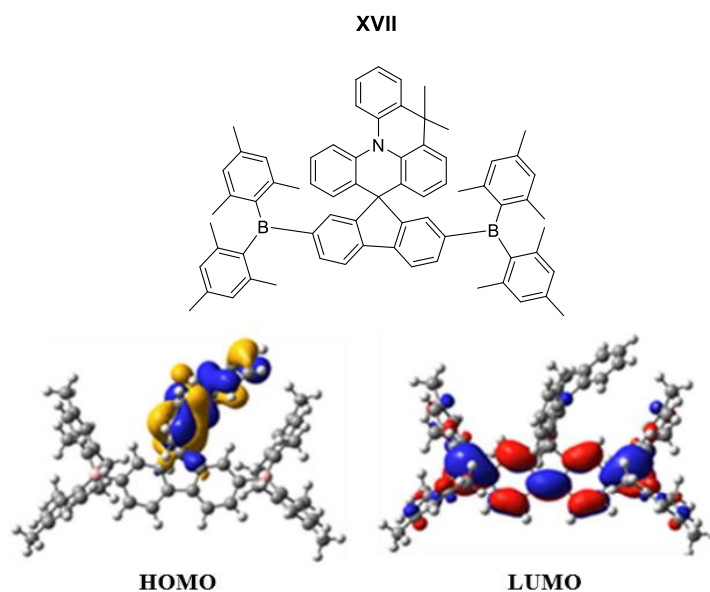


Figure 23: Triphenylamine spiro-type compound and its HOMO and LUMO regions.

For the molecules with high dihedral angle, spatial separation will occur due to the non-coplanarity between the D-A groups. The dihedral angle refers to the angle between two or more groups linked to adjacent carbon atoms.⁸¹ Hwang and coworkers used this strategy and developed a purely organic molecule with a pyridine core, as the electron-withdrawing unit, and tercarbazole moiety as electrons donor (**XVIII**), as illustrated in Figure 24. The TD-DFT analysis showed the HOMO is located at the tercarbazole region (the donor group), while the LUMO is located at the pyridine core (the acceptor unit). In this study, the authors synthesized a material with high triplet state energy, which makes possible the RISC event of the excitons to the singlet state. The structure presented a dihedral angle of 60°, which is considered a high angle, good thermal stability and 70 cd/A of current efficiency, as well as 20.27% of EQE, emitting as a green TADF.⁸²

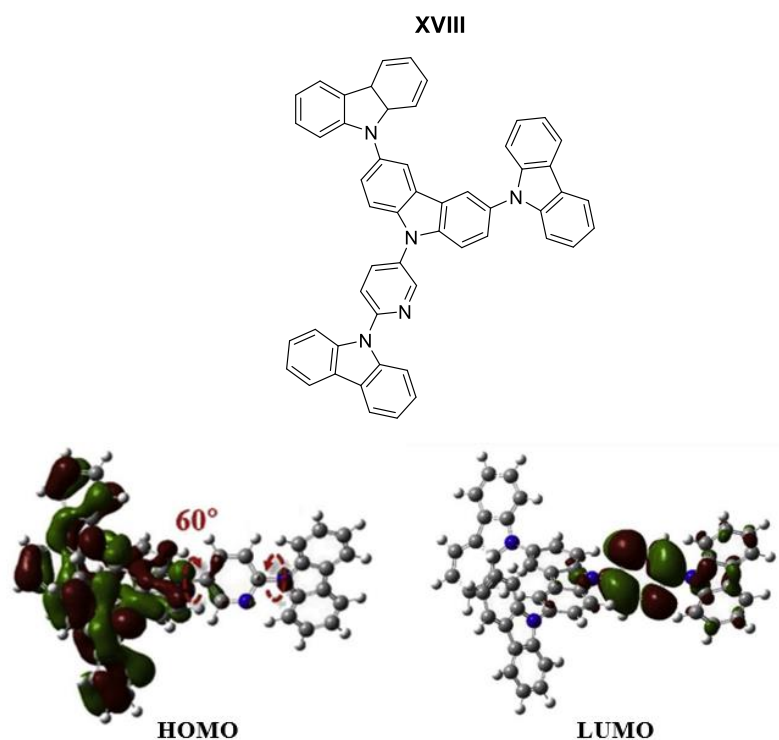


Figure 24: High dihedral angled pyridine-cored molecule and its HOMO and LUMO regions.

In this work, the high dihedral angle was the strategy chosen to create molecules whose structures had good separation of the HOMO and LUMO portions. This characteristic will enable good charge separation and the formation of a possible TADF emitter. To follow this strategy, acceptor units benzothiadiazole and dicyanopyridine were selected to compose the design and generate molecules with high dihedral angles, using a phenyl unit in between the acceptor and donor portions to achieve this goal and enable the regions to be distant from one another.

7.5. Benzothiadiazole

The 2,1,3-benzothiadiazole, BTD (**XIX**), is a nucleus with reported interesting luminescent characteristics, especially when combined with conjugated π substituents (Figure 25). It is a useful building block for donor-acceptor-type molecules (D-A), promoting the electron flow within the compound. The inclination to investigate BTD derivatives comes due to some interesting light properties of the structure, such as good stability at fundamental and excited states of energy;

high electron-withdrawing capacity, which promotes good internal charge transferring; high reduction potential and electronic affinity.^{67,83}

XIX



Figure 25: 2,1,3-benzothiadiazole structure.

Although the BTD has the structure previously presented, some variations of its original form are used when it is employed in synthetic routes. Cross-coupling reactions, such as carbon-carbon or carbon-heteroatom, can be conducted with, for example, 4,7-dibromo-BTD (**XX**) and 4,7-di(2-thienyl)-BTD (**XXI**) with metal catalysts, aiming luminescent materials production via Suzuki cross-coupling reaction (Figure 26).^{84–86}

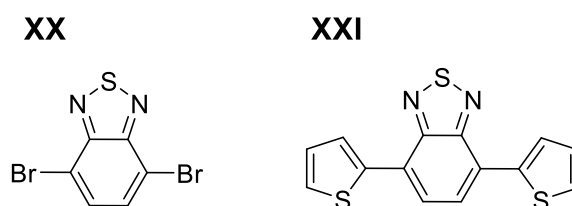


Figure 26: (XX) 4,7-dibromo-BTD and (XXI) 4,7-di(2-thienyl)-BTD structures.

Many BTD-cored molecules are reported as emissive layer compounds for OLEDs, with several different substitution groups. Some examples from literature are presented below to describe the potential of BTD derivatives for emissive layers of OLEDs (Figure 27).

Pazini *et al.* synthesized new aryl-phenoxy-BTD dyes for OLED applications. The molecules featured donor-BTD-donor and donor-BTD-acceptor architectures, with methoxyphenyl unit as donor (**XXII**) and fluorophenyl as acceptor (**XXIII**), and were synthesized via Suzuki cross-coupling reaction. The donor-BTD-donor molecule displayed better general performance with less current density, reaching $5760 \text{ L mol}^{-1} \text{ cm}^{-1}$ for molar absorptivity and 0.67 for fluorescence quantum yields. This molecule also presented better electron delocalization and

efficient internal charge transfer in the excited state, indicating the donor unit contributes more than the acceptor one to the stabilization of the excited form.⁸⁵

Liu and coworkers reported **XXIV** and **XXV** as D-A-D type TADF emitters, featuring BTB and difluoro-BTB as the acceptor cores and 9,9-dimethyl-9H-fluorene as the donor units. These emitters exhibit emission ranging from blue to green. Devices incorporating the emitters achieved maximum external quantum efficiencies of 9.13% and 8.52% to **XXIV** and **XXV**, respectively, when employed as doped emitters.⁸⁷

Ni *et al.* synthesized symmetric D-A-D type benzothiadiazole derivative (**XXVI**) featuring a dimethylacridine as the substituents on the BTB ring. The compound demonstrated TADF properties, emitting in the red region. The photoluminescence quantum yield of 0.56 when doped in a 3 wt% CBP film, achieving a maximum external quantum efficiency of 8.8%.⁸⁸

Kumsampao and colleagues synthesized D-A-D type TADF emitter featuring 5,6-dicyano[2,1,3]benzothiadiazole as the acceptor and triphenylamine as the electron-donating unit. The **XXVII** emitter molecule exhibited emission peaks at 674 nm with a photoluminescence quantum yield of 0.7. When used as the emissive layer in a device, the doped emitter achieved an external quantum efficiency of 6.57%.⁸⁹

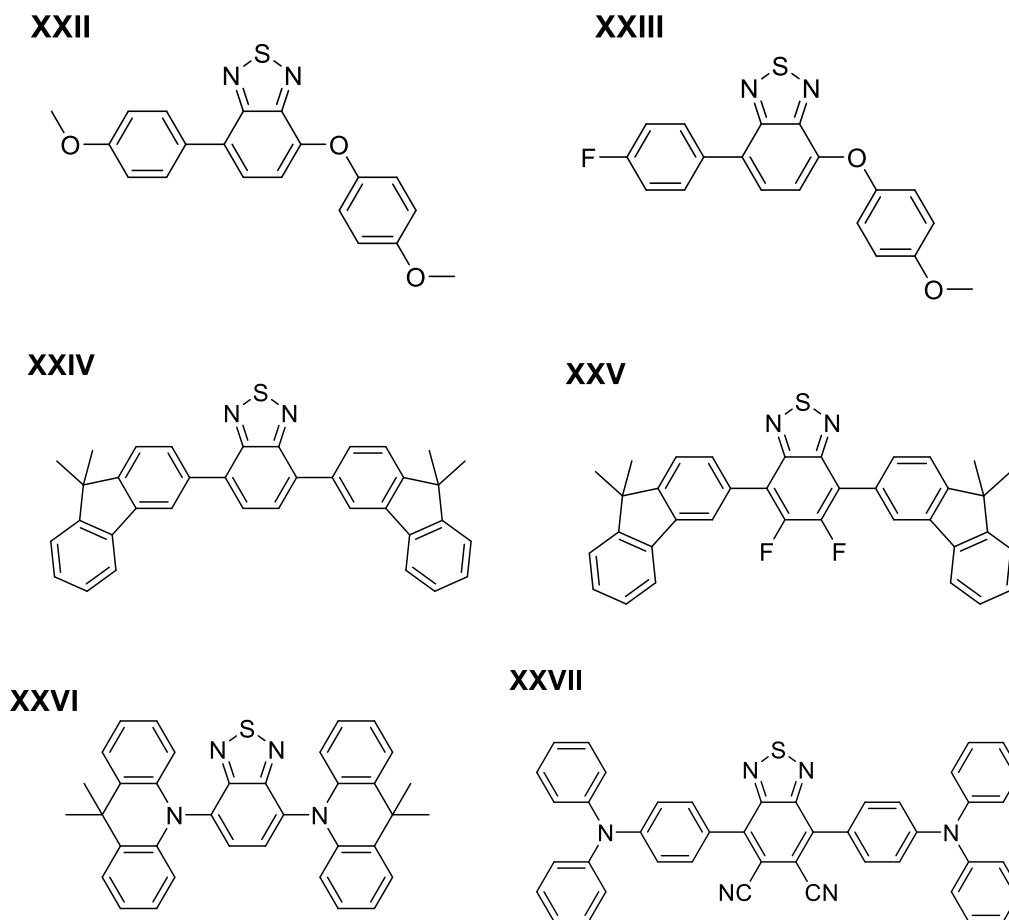


Figure 27: BTD derivatives as potential emitters, with **XXIV-XXVII** being TADF compounds.

7.6. Cyanopyridines

Cyano-substituted aromatic units structured with D-A and D- π -A architecture stand out as pivotal components in the development of candidate molecules for OLEDs. This strategic utilization stems from the profound electron-withdrawing nature inherent to the CN⁻ group, which grants an electronegative characteristic and renders it an efficient acceptor ability when integrated as a substituent in aromatic compounds.⁹⁰

As one of the cyano-compounds, pyridine-3,5-dicarbonitrile (**XXVIII**) and their derivatives (DCPs) have emerged as prominent materials, especially within the TADF research field (Figure 28). In OLEDs, these compounds serve as versatile building blocks for the fabrication of emissive layer compounds. Their electron-

deficient nature facilitates efficient electron transport within the device architecture, leading to improved charge balance and reduced energy barriers. Additionally, DCPs' inherent photoluminescence properties make them suitable candidates for OLEDs, due to their strong fluorescence emission contributing to the generation of vibrant light.⁹¹

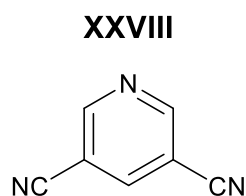


Figure 28: pyridine-3,5-dicarbonitrile molecule.

Furthermore, by incorporating electron-donating moieties into the molecular framework of DCPs, it can be engineered compounds with a small energy gap between the lowest singlet and triplet excited states, a prerequisite for efficient TADF emission. This phenomenon allows for the harvesting of both singlet and triplet excitons, thereby enhancing the efficiency of an OLED. Derivatization of DCPs offers opportunities for fine-tuning optoelectronic properties to meet specific application requirements.⁹¹ Substituent variations on the pyridine ring or the cyano groups can modulate the electronic structure and energy levels of DCP derivatives, enabling precise control over their photophysical characteristics, with potential to affect positively the performance parameters.⁹⁰ Some literature examples are addressed in the following and the respective structures are shown in Figure 29.

Liu and coworkers synthesized three new DCP derivatives featuring dimethylacridine unit as donor moiety and phenyl (**XXIX**), pyridine (**XXX**) and naphthalene (**XXXI**) units as substituents on the DCP ring. It was achieved TADF molecules due to the highly twisted structural conformations formed and suppressed non-radiative decays as a consequence of rigid geometry, resulting in blue and green emitters. The materials showed small energy gap difference from singlet and triplet states (0.3 to 0.5 eV), exhibiting two decays in time-resolved fluorescence decay and lifetimes varying from 54.6 to 36 ns and 2.5 to 0.68 μ s to fluorescent emission.⁹²

Mahesha *et al.* designed and synthesized a series of cyanopyridine derivatives via hetero cyclization, featuring thiophene (**XXXII**), chloro (**XXXIII**) and nitro (**XXXIV**) moieties. The molecules presented solid-state emission between 250

and 400 nm, in UV region, with **XXXII** and **XXXIII** showing greater fluorescence due to intramolecular charge transfer enhancement. In solution, the three evaluated materials emitted in the blue region, with the compound **XXXII** presenting the better EQE (7.75% of efficiency), which is not considered highly expressive.⁹³

New yellow TADF emitter featuring dicyanopyridine substituted with naphthyl (**XXXV**) and thienyl (**XXXVI**) acceptor units, together with a phenoxazine donor portion, were proposed by Liu and coworkers. The compounds **XXXV** and **XXXVI** presented twisted D-A design, establishing TADF processes and achieving 17,1 and 12.4% of EQE, respectively. Regarding the energy gap difference of singlet and triplet states, molecules presented small ΔE_{st} , which allows the RISC phenomenon.⁹⁴

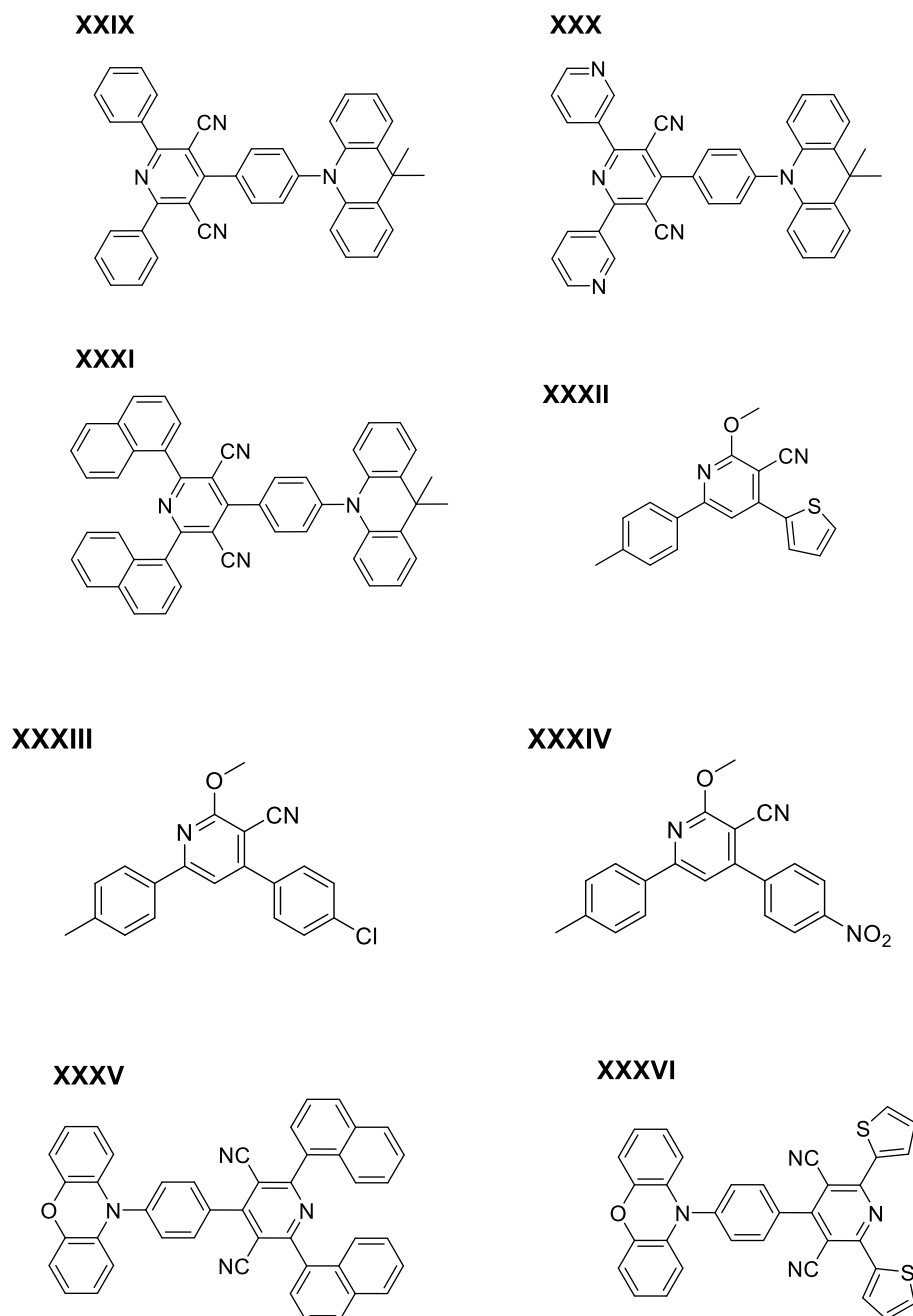


Figure 29: Cyanopyridine derivatives molecules with TADF emission.

7.7. Carbazole and triphenylamino groups

In both cases, for the aryloxy-BTD and DCP molecules, the strategy was to vary the donor unit from what was previously synthesized and tested in our research group. Considering the literature produced by the group, donor units such as phenoxy, simple aryl groups and acridine has already been tested composing the structures of the potential emitters. In order to produce new stable and highly

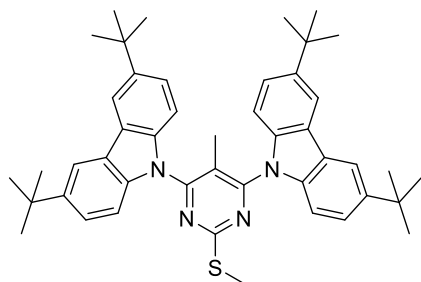
emissive TADF candidates with different donor portions, the units carbazole and triphenylamine were selected.

Many organic molecules featuring carbazole group are reported as TADF emitters (Figure 30). Serevicius *et al.* synthesized a carbazole-pyrimidine compound (**XXXVII**) with potential TADF properties and deep-blue emission. Besides contributing to the stability of the compound, the carbazole unit influenced on twisting the D-A angle of the molecule, showing electroluminescence with 8.7% external quantum efficiency.⁹⁵

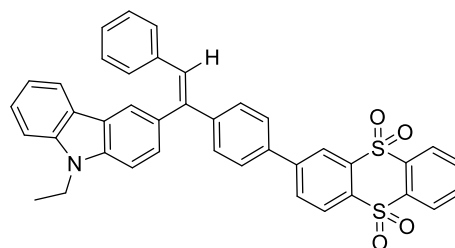
Duan and coworkers reported potential AIE and TADF emitters with carbazole group as donor and thianthrene-tetraoxide as acceptor moieties (**XXXVIII** and **XXXIX**). The molecules presented small ΔE_{st} (0.0514 and 0.0380 eV) and the same order of magnitude for both values, which is consistent with a small overlapping of HOMO and LUMO, due to carbazole and thianthrene-tetraoxide groups contribution to twisted conformation.⁹⁶

Kang, in 2019, reported a high-efficiency carbazole-triazine-based (**XL**) blue OLEDs with TADF emission. The molecule presented high rate of RISC due to small ΔE_{st} (0.037 eV) and good OLED performance, with 22,3% of maximum external quantum efficiency. It is attributed to the presence of two carbazole in the structure the good hole-transport ability of the compound.⁹⁷

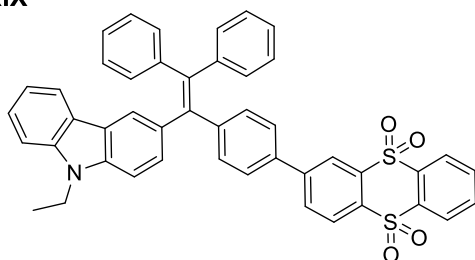
XXXVII



XXXVIII



XXXIX



XL

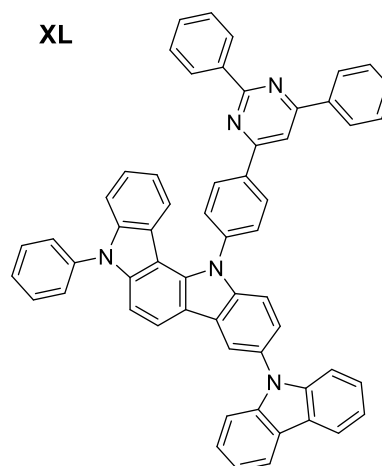


Figure 30: Carbazole-substituted TADF compounds.

Molecules featuring a triphenylamine portion are also synthesized and reported as TADF emitters in literature. In many studies, the triphenylamine unit is combined with carbazole to create new species with suitable properties for OLED application (Figure 31). Ma *et al.* designed an AIE-active TADF material based on a triphenylamine as donor and phenyl-ketone as acceptor groups (**XLI**). The compound showed improved K_{risc} and good luminescence efficiency, due to intramolecular motion suppression, showing an EQE value of 13.3%.⁹⁸

Wu and coworkers synthesized a triphenylamine-tetracarbonitrile-based fluorophore (**XLII**) with TADF emission and AIE property. The compound exhibited good thermal stability and excellent electroluminescence performance, showing 17.2% of EQE and emission peak at 548 nm, corresponding to a bright green color.⁹⁹

Shi and collaborators reported a diphenylaminocarbazole-based material (**XLIII**) with enhanced K_{risc} and efficiency stability. The TADF potential of the molecule and the steric hindrance are attributed to the presence of the

diphenylaminocarbazole group. The OLED exhibited EQE of 17.8%, pale yellow emission and $\Delta E_{st} = 0.03$ eV.¹⁰⁰

Chen *et al.* designed an acylimine-based molecule featuring a triphenylamino as donor unit, with orange TADF emission and EQE value of 11.3%. The molecule presents high stability and photoluminescence quantum yields, as well as a large dihedral angle, which resulted in a twisted conformation and good separation between HOMO and LUMO portions.¹⁰¹

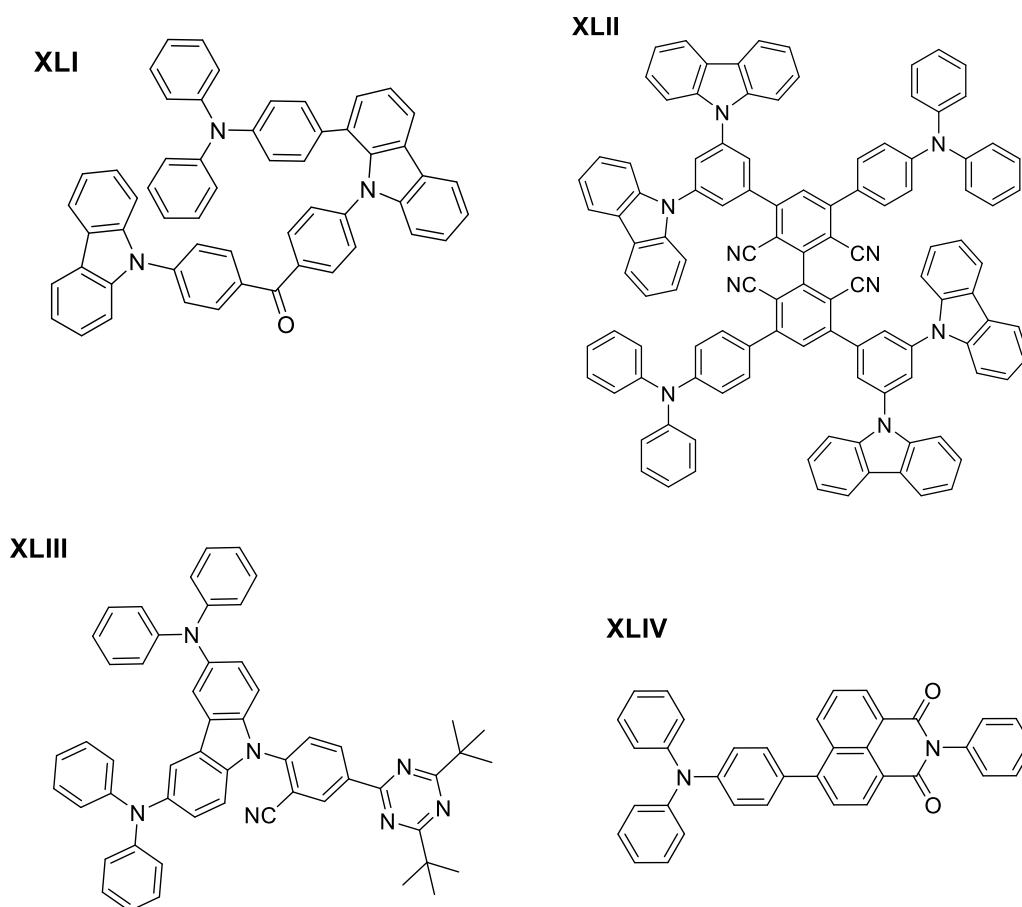


Figure 31: Triphenylamine-substituted TADF compounds.

In summary, with all the discussed above, the exploration of new purely organic designs has unveiled significant opportunities and advancements within the OLEDs field. This dissertation seeks to address the challenges of synthesizing and evaluating aryloxy-BTD and DCP derivatives featuring strong donor units (triphenylamine and carbazole). The forthcoming sections will detail the objective

and the selected pathway to achieve these structures, as well as their characterization and properties evaluation.

8. Objectives

In this study, the focus was on designing, synthesizing, and characterizing novel luminescent compounds based on benzothiadiazole (BTD) and 2,6-diphenylpyridine-3,5-dicarbonitrile (DCP) acceptor units, introducing a phenyl unit between the donor and acceptor. Our goal is to create highly emissive materials with TADF and AIE properties featuring triphenylamino (TF) and carbazole (CB) as donor units.

The specific objectives set for this project are as follows:

- To plan and synthesize novel BTDs and DCP derivatives through cross-coupling reactions.
- To perform photophysical and electrochemical characterization of the new luminescent compounds, measuring absorption and emission maxima, band gap, Stokes shift, and fluorescence quantum yield in both solution and solid state.
- To investigate how the compounds behave in aggregate state, presenting AIE (aggregation-induced emission) or AIEE (aggregation-induced emission enhancement) and correlate with their molecular structures.
- To perform electrochemical characterization of the dyes via cyclic voltammetry, determining oxidation and reduction energies, HOMO and LUMO and band gap energy.

9. Methodology

The chemicals and solvents employed in this investigation were procured from commercial suppliers and used without additional purification unless otherwise stated. Solvents utilized in cross-coupling reactions were previously degassed using a nitrogen stream.

All newly synthesized molecules for this project underwent characterization through ^1H and ^{13}C NMR spectroscopy using a Bruker Advance III HD 400 MHz spectrometer. NMR analyses were conducted at the Analytical Facilities "Pe. Leopoldo Hainberger" of the Chemistry Department at PUC-Rio (CAPLH PUC-Rio).

The final products underwent characterization using the techniques outlined below:

UV-Vis absorption spectra were acquired using a Shimadzu UV-1900i spectrophotometer equipped with a 1.0 cm optical path quartz cuvette. Photoluminescence measurements were conducted on a Shimadzu RF-6000 spectrofluorometer, employing four clear-faced 1.0 cm quartz cuvettes, a scanning rate of 6000 nm min^{-1} , and a spectral bandpass of 5.0 nm. Absorption and emission measurements were performed at solid-state and in solutions with concentrations approximately around 10^{-5} and $10^{-6}\text{ mol L}^{-1}$, respectively, for both BTD and dicyanopyridine derivatives.

Fluorescence quantum yield assessments were also conducted in the Shimadzu RF-6000, utilizing the same quartz cuvettes of the photoluminescence studies described above. The spectrofluorometer operated at a scan rate of 1000 nm min^{-1} with spectral excitation and emission bandpasses set at 10.0 nm. Quinine sulphate and fluoresceine was used as standard solutions.

Aggregation induced emission qualitative experiments were performed in THF/water solvent mixture, with $7.5 \times 10^{-6}\text{ mol L}^{-1}$ concentration and varying the proportion of water in the medium. The fluorescence emission of these solutions was conducted likewise the photoluminescence measurements described previously.

Electrochemical studies were conducted using a potentiostat/galvanostat (μ -AUTOLAB Type III, Metrohm, The Netherlands) connected to a computer and operated in cyclic voltametric mode. The working electrode was made of glassy carbon, with an Ag|AgCl (KCl(sat)) electrode serving as the reference and a platinum wire as the auxiliary electrode. The electrochemical cell consisted of Pyrex glass with a Teflon cap featuring openings for electrode insertion. Cyclic voltammetry experiments were carried out at a scan rate of 50 mV/s at room temperature under a nitrogen atmosphere. The electrolyte used was a 0.04 M solution of tetrabutylammonium hexafluorophosphate (TBAPF₆) in acetonitrile, with ferrocene employed as the internal standard for calibration.

9.1. Synthesis of the intermediates

9.1.1. Aryloxy-BTD

The synthesis of the aryloxy-BTD intermediate was performed accordingly to described by Pazini *et al.*⁸⁵

In a Schlenk flask, it was added 0.601 g (2.05 mmol) of 4,7-dibromo-BTD (compound 8), 0.559 g (4.51 mmol) of 4-metoxyphenol (compound 9), 0.874 g (6.3 mmol) of K₂CO₃ and 13 mL of DMF as solvent. Under 100 °C and after 24 h of reaction, the mixture was allowed to cool down until it was primary treated via liquid-liquid extraction with H₂O and ethyl acetate (2:1). The organic fraction was then collected and submitted to rotatory evaporation. The crude product was purified via silica column chromatography, with hexane and ethyl acetate (9:1) eluent.

9.1.2. Pyridine-3,5-carbonitrile derivative (DCP)

The synthesis of the DCP intermediate was performed accordingly to described by Vesga-Hernández *et al.*¹⁰²

For the first step of this synthesis, a mixture with 0.129 g (0.7 mmol) of 4-bromobenzaldehyde (compound 12), 0.259 g (1.8 mmol) of benzoylacetone nitrile (compound 13), 0.444 g (5.8 mmol) of CH₃COONH₄ was added in a Schlenk flask. A volume of 17.5 mL of CH₃COOH 100% as solvent was incorporated after 40 min submitted to N₂ atmosphere. The system underwent a 12 h reaction at 120 °C.

For the second step, past 12 h reaction, the system was allowed to cool down to 66 °C, and 0.484 g (7.0 mmol) of NaNO₂ was gradually added in the flask. After 1 h under temperature, the reaction was ceased, and the crude was poured into a beaker with 400 mL of water and ice. To neutralize the acid, 22.4 mL of NH₄OH was gradually added, and the precipitate was vacuum filtered with ethanol/toluene (1:1) mixture as cleansing solvent.

9.2. Synthesis of the luminophores

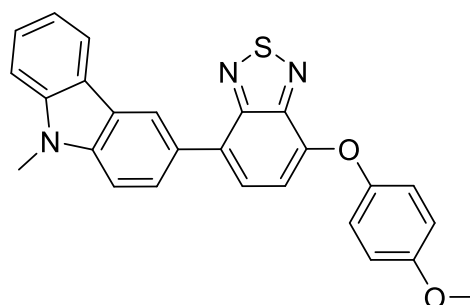
It was synthesized four new luminophores: two benzothiadiazole derivatives and two dicyanopyridine derivatives. A reaction environment containing palladium acetate (0.01 mmol, 0.0023 g), PPh₃ (0.02 mmol, 0.005 g), potassium carbonate (0.4 mmol, 0.055 g) and 6 mL of toluene/ethanol mixture (1:1) as solvent, common to the four syntheses. The Schlenk flask used was previously purged at vacuum and nitrogen alternated atmosphere. All the reactions were conducted under 100°C and, after 18 hours, the brute was primary treated via liquid-liquid extraction with water/ethyl acetate (4:1) and the final interest product was purified via chromatographic column, using silica, and hexane/ethyl acetate (10:1) as eluent.

The luminophores described below were synthesized and purified strictly according to the conditions described above. For each synthetic route, it was used a combination of two raw materials.

9.2.1. Carbazole-benzothiadiazole (CB-BTD)

Aryloxy-BTD (0.21 mmol, 0.073 g) and 9-methyl-9H-carbazole-3-boronic acid pinacol ester (0.25 mmol, 0.077 g).

4-(4-methoxyphenoxy)-7-(9-methyl-9H-carbazol-3-yl)benzo[c][1,2,5]thiadiazole (**CB-BTD**): Orange solid; Yield: 57%; mp: 154-158 °C. ¹H NMR (400 MHz, CDCl₃) δ 8.59 (d, *J* = 1.3 Hz, 1H), 8.16 (d, *J* = 7.4 Hz, 1H), 8.03 (dd, *J* = 8.5, 1.8 Hz, 1H), 7.64 (d, *J* = 7.8 Hz, 1H), 7.57 – 7.48 (m, 2H), 7.44



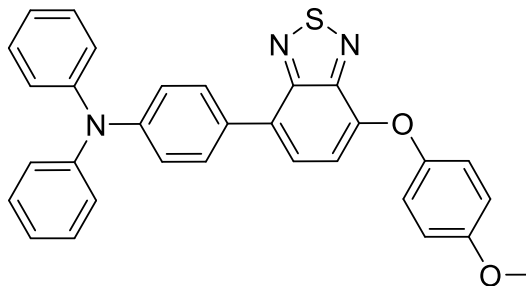
(d, *J* = 8.2 Hz, 1H), 7.31 – 7.24 (m, 1H), 7.23 – 7.17 (m, 2H), 7.02 – 6.95 (m, 2H), 6.88 (dd, *J* = 7.9, 2.1 Hz, 1H), 3.92 (s, 3H), 3.86 (s, 3H). ¹³C NMR (101 MHz, CDCl₃) δ 156.87, 155.42, 149.41, 149.03, 148.90, 141.62, 140.95, 129.58, 128.43, 128.05, 127.11, 126.09, 123.30, 123.11, 121.66, 121.08, 120.66, 119.27, 115.21, 111.94, 108.77, 108.63, 55.83, 29.39.

9.2.2. Triphenyl-benzothiadiazole (TF-BTD)

Aryloxy-BTD (0.19 mmol, 0.069 g) and 4-(diphenylamino)phenyl boronic acid pinacol ester (0.19 mmol, 0.073 g).

4-(7-(4-methoxyphenoxy)benzo[c][1,2,5]thiadiazol-4-yl)-N,N-diphenylaniline (**TF-BTD**): Dark orange solid; Yield: 46%; mp: 75-80 °C. ¹H NMR (400 MHz, CDCl₃) δ 7.81 – 7.75 (m, 2H), 7.51 (d, *J* = 7.9 Hz, 1H), 7.31 – 7.26 (m, 4H), 7.21 – 7.14 (m, 8H), 7.05 (t, *J* = 7.3 Hz, 2H), 6.99 – 6.94 (m, 2H), 6.80 (d, *J* = 7.9 Hz, 1H), 3.85 (s,

3H). ¹³C NMR (101 MHz, CDCl₃) δ 156.94, 154.94, 149.71, 148.82, 148.79, 147.81, 147.68, 131.09, 129.75, 129.47, 128.00, 127.72, 124.91, 123.33, 123.28, 121.76, 115.22, 111.57, 55.82.

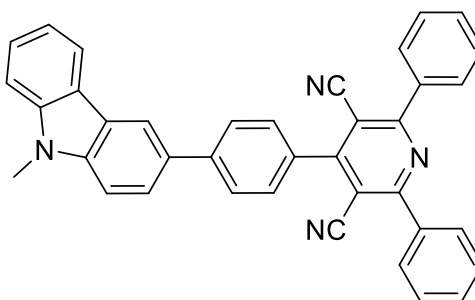


9.2.3. Carbazole-dicyanopyridine (CB-DCP)

Bromo-dicyanopyridine (0.23 mmol, 0.10 g) and 9-methyl-9H-carbazole-3-boronic acid pinacol ester (0.22 mmol, 0.0676 g).

4-(4-(9-methyl-9H-carbazol-3-yl)phenyl)-2,6-diphenylpyridine-3,5-dicarbonitrile (**CB-DCP**): Pale yellow solid. Yield: 73%; mp: 279-282 °C. ¹H NMR (400 MHz, CDCl₃) δ 8.43 (d, *J* = 1.5 Hz, 1H), 8.18 (d, *J* = 7.7 Hz, 1H), 8.13 – 8.07 (m, 4H), 7.99 – 7.95 (m, 2H), 7.83 (dd, *J* = 8.5, 1.8 Hz, 1H), 7.79 – 7.74 (m, 2H), 7.59 (tt, *J* = 4.2, 2.0 Hz, 6H), 7.51 (dd, *J* = 4.9, 3.7 Hz, 2H), 7.44 (d, *J* = 8.2 Hz, 1H), 7.33 – 7.27 (m, 1H), 3.91 (s, 3H). ¹³C NMR (101

MHz, CDCl₃) δ 163.57, 160.41, 145.10, 141.64, 141.11, 136.66, 131.48, 131.38, 130.89, 129.73, 129.71, 128.93, 127.90, 126.20, 125.39, 123.54, 123.01, 120.58, 119.39, 119.34, 116.28, 109.03, 108.82, 106.04, 29.37.

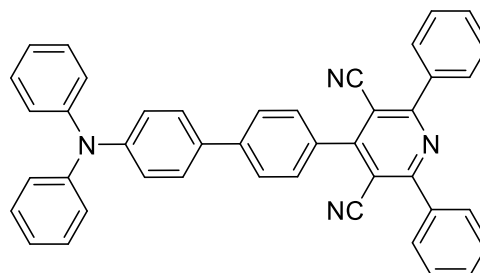


9.2.4. Triphenyl-dicyanopyridine (TF-DCP)

Bromo-dicyanopyridine (0.23 mmol, 0.10 g) and 4-(diphenylamino)phenyl boronic acid pinacol ester (0.22 mmol, 0.082 g).

4-(4'-(diphenylamino)-[1,1'-biphenyl]-4-yl)-2,6-diphenylpyridine-3,5-dicarbonitrile (TF-DCP): Yellow solid. Yield: 64%; mp:

216-220 °C. ¹H NMR (400 MHz, CDCl₃) δ 8.13 – 8.05 (m, 4H), 7.84 – 7.79 (m, 2H), 7.73 – 7.68 (m, 2H), 7.61 – 7.54 (m, 8H), 7.33 – 7.27 (m, 4H), 7.21 – 7.12 (m, 6H), 7.10 – 7.03 (m, 2H).



10. Results and Discussion

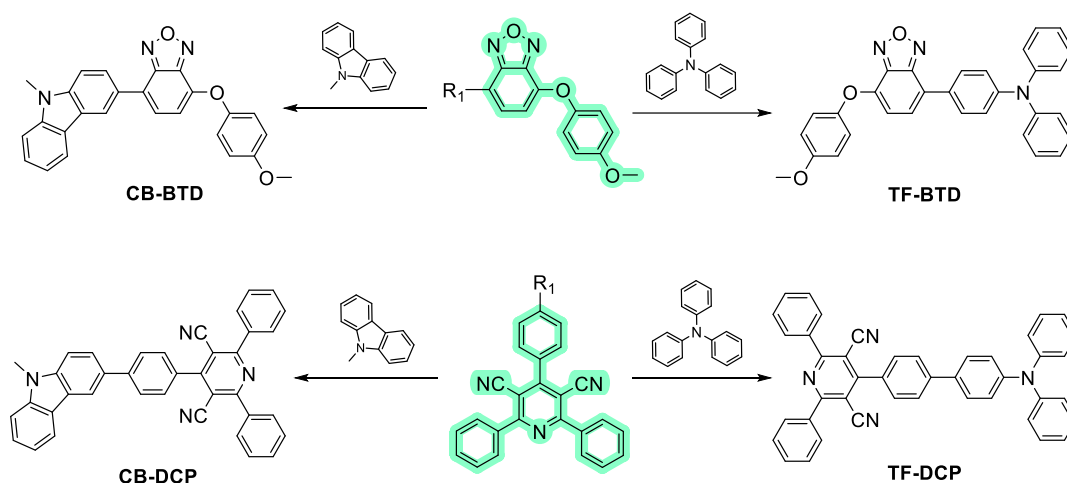
10.1. Design and synthesis

Four novel molecules featuring either BTD or DCP acceptor units were designed to be studied as potential emitters for OLEDs. The strategy used in the molecular design was to combine good electron injectors with BTD or DCP to create the new structures. Therefore, the groups triphenylamino and carbazole were selected as the donor moieties. To synthesize molecules with high dihedral angle, the incorporation of a phenyl unit as a spacer in the central portion of the molecule was employed to create a more efficient separation of the donor and acceptor parts, promoting better delimitation of the HOMO and LUMO regions. The proposed designs are depicted in Scheme 5.

First described and reported by Pazini *et al.*, aryloxy-BTD derivatives have presented good characteristics to be applied as emissive layers in OLEDs.⁸⁵ With the methoxy group possessing an electron donor character and the BTD as an acceptor unit, the goal was to create a D-A-D structure by adding another donor unit on the other side of the BTD core. Furthermore, the insertion of an aryloxy group enables the molecules to present aggregation induced emission (AIE) or aggregation induced enhanced emission (AIEE), due to the limitation of the intermolecular rotation of the methoxy group. This characteristic was demonstrated

in previous works of our group and will be thoroughly discussed throughout the text.

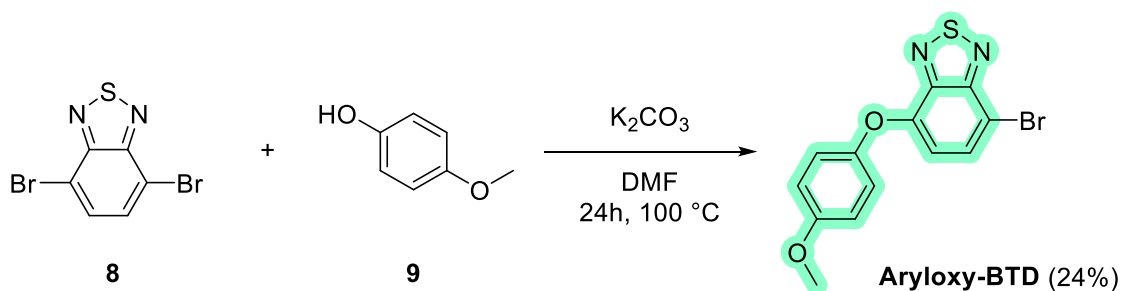
Regarding the dicyanopyridine nucleus and its variations, this structure was chosen as the acceptor unit due to its capacity to produce TADF molecules. More specifically, 2,6-diphenylpyridine-3,5-dicarbonitrile (DCP) structure was also studied by our group in previous works, demonstrating the capacity to generate good and stable fluorophores presenting aggregation-induced emission.¹⁰²



Scheme 5: Aryloxy-BTD and DCP derivatives with D-A-D structure.

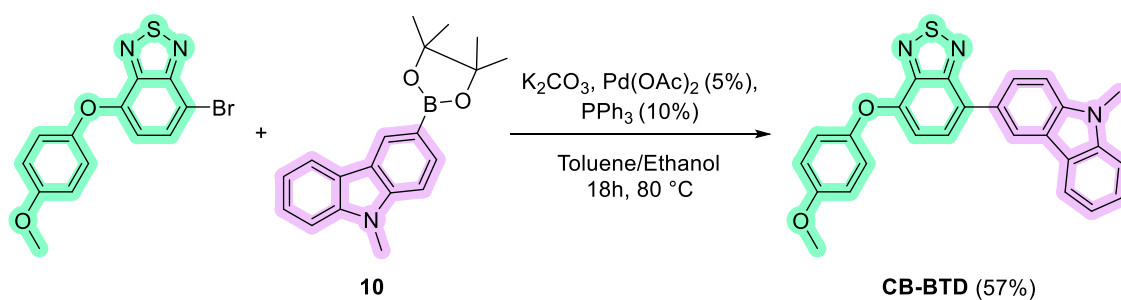
In order to synthesize the new BTD-based fluorophores, initially, 4-methoxyphenol (**9**) was reacted with dibromobenzothiadiazole (**8**), in a protocol previously described by our group,⁸⁵ leading to the intermediate 4-bromo-7-(4-methoxyphenoxy)benzo[*c*][1,2,5]thiadiazole molecule (aryloxy-BTD) in 24% yield, as illustrated in scheme 6.

Taking into consideration the BTD core as an electron deficient nucleus and the potential nucleophilicity of the compound **9**, in a basic medium, it is suggested that the reaction occurs through an aromatic nucleophilic substitution mechanism, with the bromide as a good leaving group. The step of incorporating the aryloxy group is of great importance to guarantee the final molecules the ability to still emit light or even enhance the light emission in aggregated state.

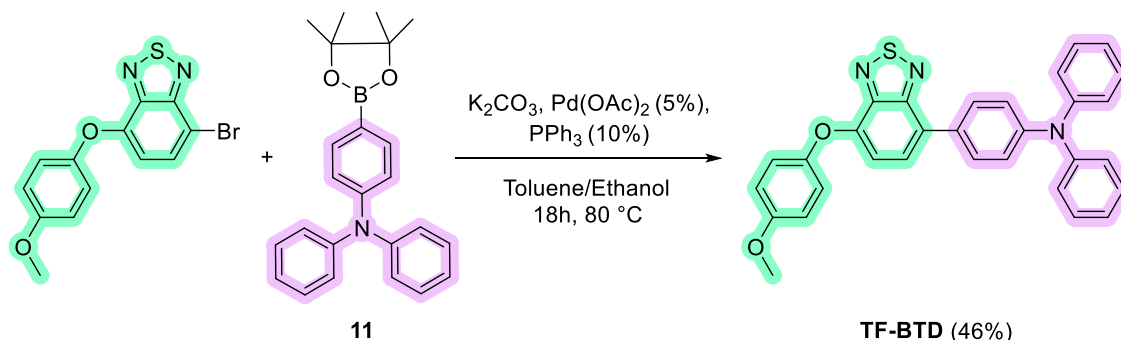


Scheme 6: Synthesis of the intermediate aryloxy-BTD.

The schemes 7 and 8 show the synthetic routes of the aryloxy-BTD derivatives TF-BTD and CB-BTD. The TF and CB donor units were inserted via Pd-catalyzed Suzuki cross coupling, using the boronic acids pinacol esters 10 and 11, in a system containing $Pd(OAc)_2$, PPh_3 , and $NaOH$, with the bromated aryloxy-BTD intermediate. After 18h of reaction, the final products, a carbazole and a triphenylamine linked to an aryloxy-BTD, were obtained in 57 and 46% yield, respectively.



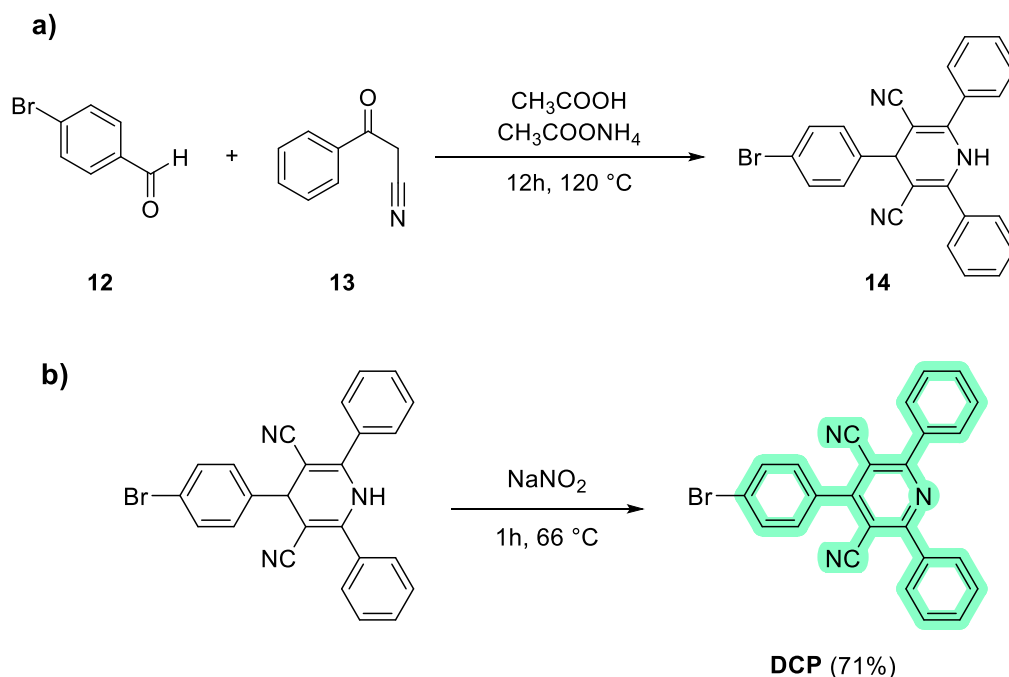
Scheme 7: Synthesis of the final BTD-cored compound with a carbazole as donor unit.



Scheme 8: Synthesis of the final BTD-cored compound with a carbazole as donor unit.

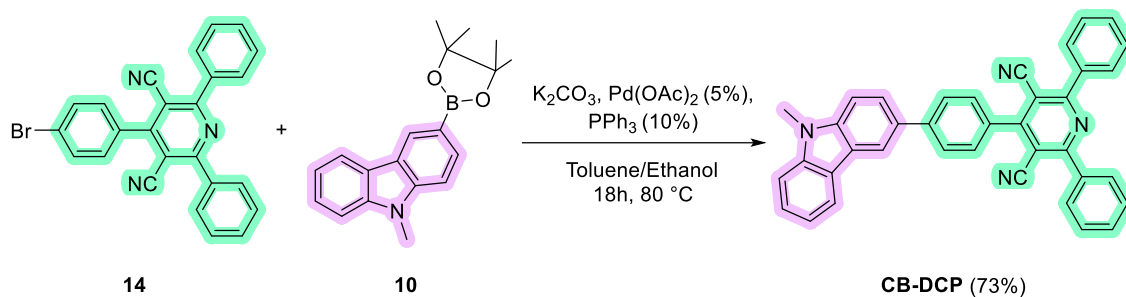
To produce the desired intermediate, the DCP, the compounds 12 and 13 were reacted via Hantzsch multicomponent mechanism, enabling the incorporation of different groups in the pyridine ring. Scheme 9 (a) shows the formation of the

dihydropyridine in a medium with acetic acid as solvent and (b) shows the oxidation of the N and the pyridine ring formation. From this reaction, the intermediate 2,6-diphenylpyridine-3,5-dicarbonitrile was formed with 71% yield.

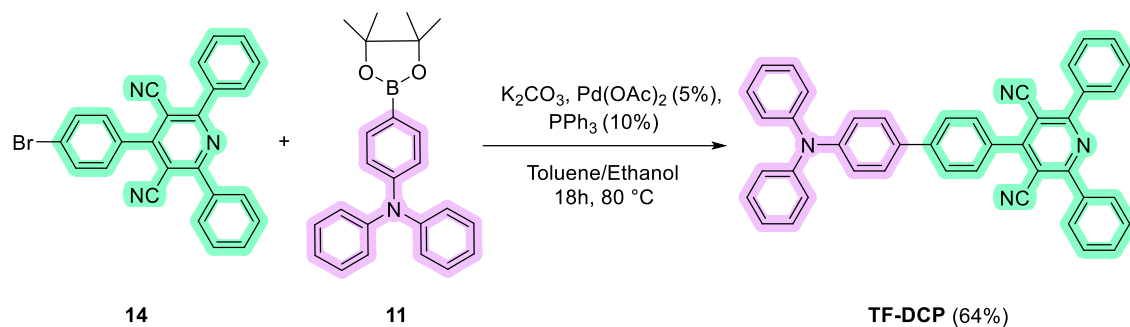


Scheme 9: (a) Synthesis of the dicyanopyridine ring via Hantzsch reaction, (b) pyridine ring formation.

Following the same strategy applied for the aryloxy-BTD derivatives, the donor groups carbazole and triphenylamine were incorporated with the DCP electron withdrawing unit to produce the target DCP derivatives structures. The schemes 10 and 11 show the reactions' conditions. Likewise the BTD reactions, both carbazole and triphenylamine were in their boronic acid pinacol ester form to react via Suzuki cross coupling mechanism under the exact same conditions. After 18 h, the final molecules, CB-DCP and TF-DCP, yielded 73 and 64%, respectively.



Scheme 10: Synthesis of the final DCP derivative compound with carbazole as donor unit.



Scheme 11: Synthesis of the final DCP derivative compound with triphenylamino as donor unit.

The structural characterization of the four final compounds were performed by ^1H and ^{13}C NMR. These spectra are provided in the Appendix section figures A35-42. To illustrate the structural characterization of these compounds, CB-BTD ^1H NMR spectrum is shown in Figure 32. The two singlets integrating for 3Hs at 2.93 ppm and 3.30 ppm refer to the CH_3 of the methoxy group and to the carbazole, respectively. Coupled doublets at 7.63 and 6.87 ppm, integrating for 1H, refer to the hydrogens of the BTD core. Coupled doublets at 7.22 and 6.99 ppm are related to the hydrogens of the 4-methoxyphenol group. The aromatic hydrogens present in the carbazole portion are depicted in 8.73 and 8.46 ppm.

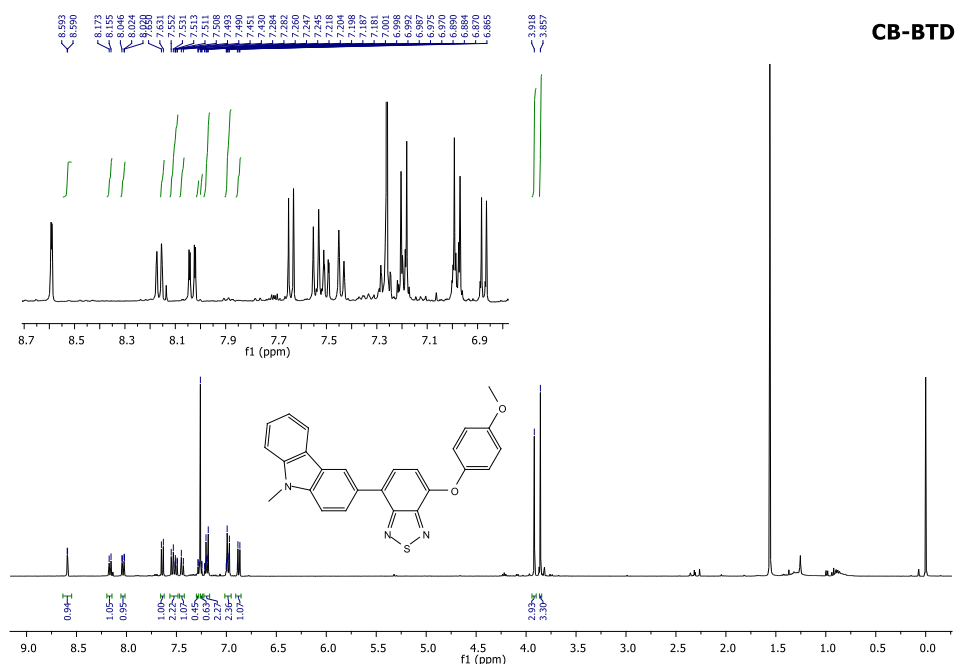


Figure 32: ^1H NMR spectrum for CB-BTD (400 MHz, CDCl_3).

10.2. Photophysical properties

Initially, the photophysical properties of the Aryloxy-BTD and DCP derivatives were evaluated via UV-Vis spectroscopy in five solvents with different polarities (acetonitrile, ethanol, chloroform, acetone or THF and toluene). The correspond absorbance vs wavelength spectra of the four compounds are shown in Figure 33 and the relevant absorbance data is depicted in Table 4. Regarding the aryloxy-BTD molecules, CB-BTD solutions presented more intense absorptions than TF-BTD solutions in the visible region, with λ_{abs} maxima ranging from 415 to 423 nm and 423 to 438 nm, respectively, both related to their π - π^* transitions. The redshifted absorption of TF-BTD compared to CB-BTD can be related to the higher donor capacity of TF, compared to carbazole, since for the latter the nitrogen electron pair is compromised with the aromaticity of the 5-membered ring. A better donor groups tends to increase HOMO energy, decreasing the band-gap and consequently leading to less-energetic redshifted absorption. In terms of solvatochromic effect on the absorption, the increase in the polarity of the medium promotes a better interaction between the solvent and the polarized excited state of the compound, stabilizing it and redshifting the absorption energy.

DCP derivatives presented absorptions from UV to blue region, with λ_{abs} maxima ranging from 346 to 353 nm and 355 to 385 nm for CB-DCP and TF-DCP, respectively. Again, the TF-substituted compound presented redshifted absorption compared to CB. Moreover, compared to their BTD compounds presented less-defined absorption bands, especially in the case of CB-DCP, indicating the existence of different electronic transitions on this compound. It is also important to highlight the considerable solvatochromic effect observed for TF-DCP ($\Delta\lambda_{\text{abs}} = 35$ nm), indicating a higher degree of charge formation in the ground state for this compound.

Comparing the donor portions, absorption maxima on less energetic wavelengths may indicate that the triphenylamine group can promote better charge injection within the molecule. Analyzing both carbazole and triphenylamine structures, the lone pair of electrons on the N atoms have different availability. On the carbazole unit, these electrons are compromised with the aromaticity of the structure, making it harder to donate them due to loss of stability. On triphenylamine unit, the lone pair of electrons is free to be donated by resonance. This characteristic of the TF-substituted molecules will promote a better charge

distribution, which will result in a more intense dipolar moment, explaining the positive solvatochromism observed in the spectra.

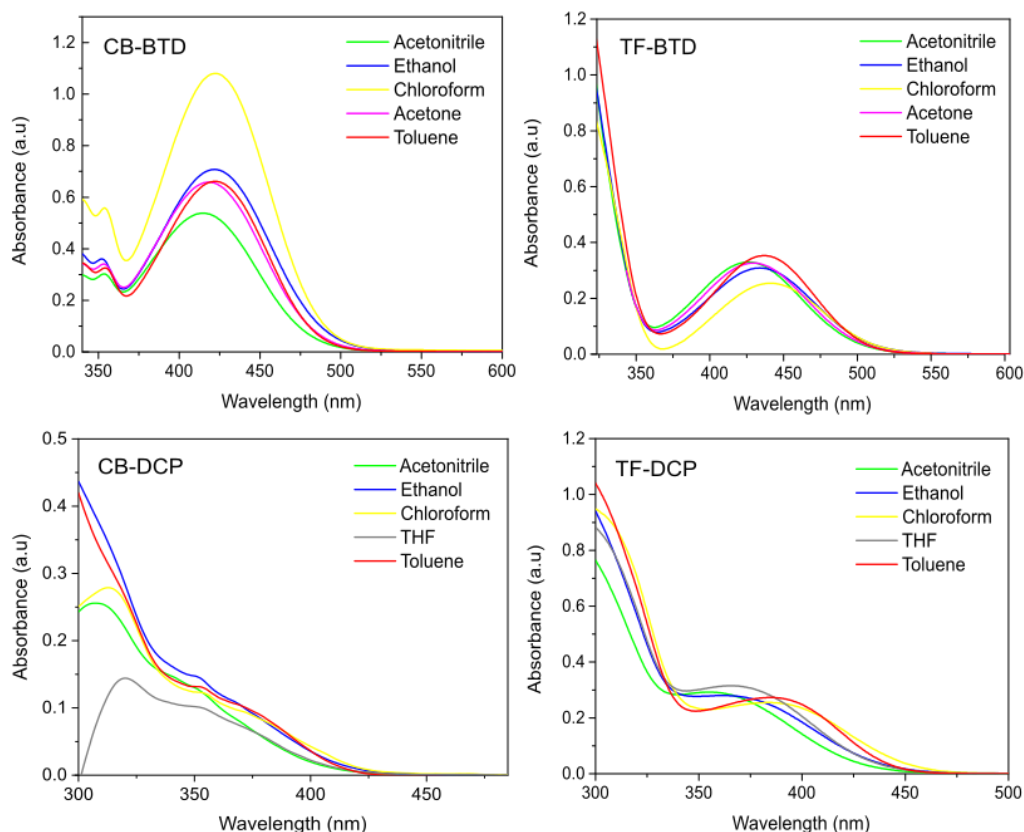


Figure 33: BTD and DCP derivatives' absorption spectra in different solvents.

Fluorescence intensity measurements were performed using the same solvents, with the solutions being excited at the respective absorption maxima wavelength of each solvent. The obtained spectra are depicted in Figure 34 and the emission data are summarized in Table 4. All compounds presented fluorescence in solution. CB-BTD and TF-BTD presented emission maxima ranging from 569 to 634 nm and 623 to 697 nm, respectively, which corresponds to the yellow to red region. For the DCPs, the carbazole and triphenylamino derivatives had their emission ranging from 496 to 625 nm and 461 to 625 nm, respectively, corresponding to the green to orange region. In all cases, the solution with toluene resulted in the most intense and blue-shifted emission recorded; while for acetonitrile and ethanol, the compounds presented a bathochromic shift, with smaller or inexpressive emission intensity compared to the other solutions. Due to a very polarized excited state of the compounds, polar solvents will better stabilize the molecule, shifting the fluorescence emissions to red and, in many cases,

deactivating it due to non-radiative decay processes promoted by strong solvent-fluorophore interaction.

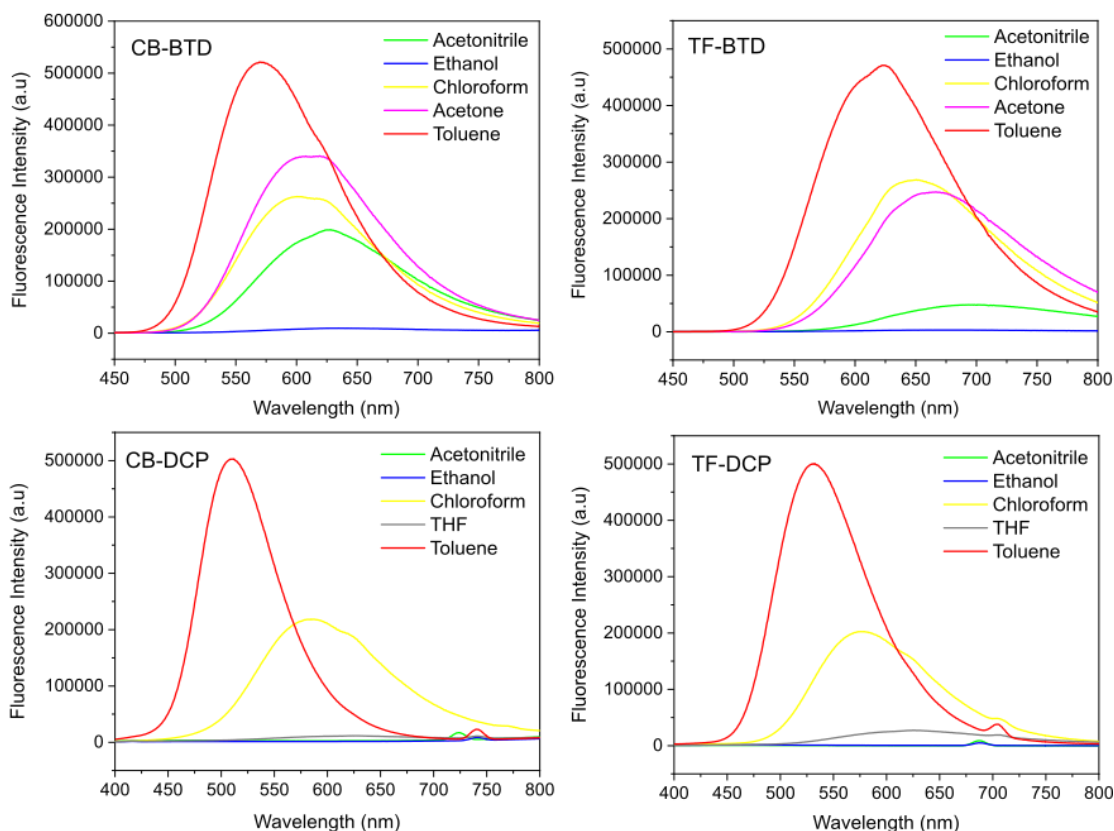


Figure 34: BTD and DCP derivatives' fluorescence emission spectra in different solvents.

From the photophysical characterization, moderate to large Stokes shifts were observed for all the fluorophores, which indicates good general stabilization of the compounds in the excited state. For both aryloxy-BTD derivatives and CB-DCP, an expressive Stokes shift especially in acetonitrile medium (210, 274 and 279 nm) was observed, showing better stabilization in polar environments. The TF-DCP molecule, however, showed its largest shift for the THF medium (260 nm).

Fluorescence quantum yields were determined for all the compounds in toluene and values between 0.63 and 0.41 were obtained, with the aryloxy-BTD derivatives presenting higher ϕ_{FL} . It was observed that the change in the donor group did not influence significantly on the ϕ_{FL} value, since the variations for the BTD and DCP derivatives were small.

Table 4: Photophysical data of the BTD and DCP derivatives, where ϵ ($10^4 \text{ mol L}^{-1} \text{ cm}^{-1}$) is the molar absorptivity coefficient, λ_{abs} and λ_{em} (nm) are the absorption and emission maxima, respectively, E_g (eV) is the optical bandgap energy, $\Delta\lambda_{\text{ST}}$ is the Stokes shift (nm) and ϕ_{FL} is the fluorescence quantum yield.

Dye	Solvent	λ_{abs}	ϵ	E_g	λ_{em}	$\Delta\lambda_{\text{ST}}$	ϕ_{FL}
CB-BTD	Acetonitrile	415	10.8	2.57	625	210	0.63 ^a
	Ethanol	422	14.2	2.53	634	212	
	Chloroform	423	22.0	2.54	600	177	
	Acetone	419	13.2	2.56	619	200	
	Toluene	422	13.2	2.55	569	147	
TF-BTD	Acetonitrile	423	6.6	2.48	697	274	0.60 ^a
	Ethanol	430	6.2	2.46	690	260	
	Chloroform	438	5.0	2.44	652	214	
	Acetone	426	6.6	2.49	666	240	
	Toluene	435	7.0	2.48	623	188	
CB-DCP	Acetonitrile	346	9.3	3.02	625	279	0.41 ^b
	Ethanol	351	10.0	2.98	511	160	
	Chloroform	353	8.0	2.92	585	232	
	THF	350	6.7	2.97	478	128	
	Toluene	352	8.7	2.95	476	124	
TF-DCP	Acetonitrile	355	20.0	2.89	461	106	0.44 ^b
	Ethanol	359	20.0	2.81	463	104	
	Chloroform	384	16.9	2.73	579	195	
	THF	365	21.0	2.85	625	260	
	Toluene	385	18.0	2.78	530	145	

^a with fluoresceine as standard

^b with quinine sulfate as standard

The photophysics of these compounds was also studied in solid state through absorption (DRUV), excitation and fluorescence measurements (Figure 35). For the absorption assays (Figure 35a), CB-BTD and TF-BTD had their absorption maxima ranging from 400 and 450 nm (blue region). CB-DCP and TF-DCP, in turn, were both blue-shifted, having their maxima concentrated between 350 and 425 nm, which corresponds to the violet to blue region, with a sharp absorption decrease at wavelengths higher than 430 nm.

A similar pattern was observed for the fluorescence emission studies. For the test with the emission wavelength (Figure 35b), the aryloxy-BTDs presented

fluorescence intensity maxima redshifted in relation to the DCPs, with the peaks ranging from 575 to 650 nm and 525 to 600 nm, respectively, emitting in yellow to orange region. The test with excitation wavelength, likewise the UV-Vis absorption spectroscopy, presented peaks around 400 and 475 nm for the BTDs fluorophores and 375 and 425 nm for the DCPs ones.

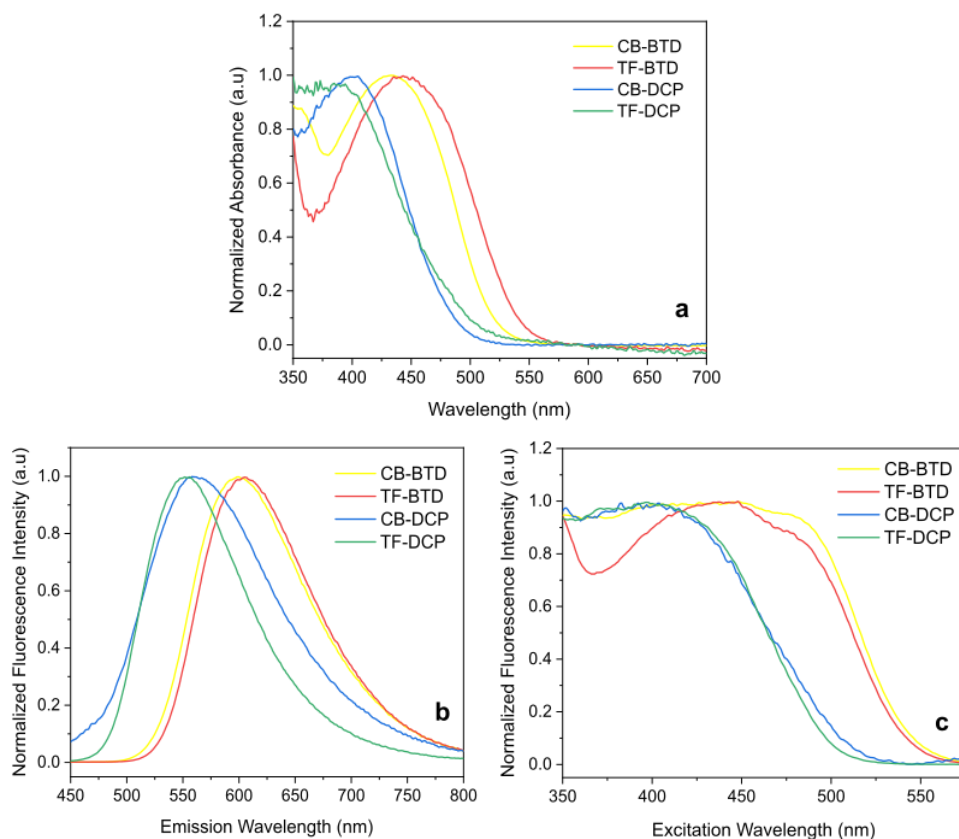


Figure 35: (a) Absorption, (b) emission fluorescence and (c) excitation fluorescence of the compounds in solid state.

10.3. Aggregation induced emission experiments

To verify whether the molecules still emit in forced aggregation environments, AIE experiments were conducted in mixtures of water/acetone for BTD-based molecules, and water/THF for DCP derivatives. Changing the proportions, the solutions started at 0% of water (fluorophore molecularly dissolved) and gradually increasing the water fraction (f_w) until 99%. In these conditions, with high water content, compound's aggregation is forced.

Initially, visual tests were performed, and the results are depicted in Figure 36. A similar trend was observed for all compounds: considerable emission in pure

organic solvent, followed by quenching of luminescence and finally sharp increase in fluorescence. This later can be related to aggregation-induced enhanced emission.

Regarding the aryloxy-BTD derivatives, both compounds showed luminescence in the most polar environments. It can be noticed progressive emission decreasing on the solutions with 20, 40, 50, 60 and 70% f_w (second to seventh flasks), with CB-BTD recovering the luminescence at 80% f_w (eightieth flask). TF-BTD, in turn, had its emission recovered at 70% f_w , with the luminescence returning with even higher visual intensity. It can also be seen a difference in the color of the TF-BTD solutions, from an intense to a yellowish orange. Bearing in mind the aryloxy-BTD structure, it is expected that luminescence will return in higher f_w due to a limitation on the free rotation of the aryloxy group, imposed by the aggregation condition. With the intramolecular rotation limited, the relaxation can occur through radiative decay. Moreover, bulky substituents, such as the carbazole and triphenylamino units, decrease π - π stacking interactions by avoiding planarity, which also contributes to the AIE effect. Regarding the color change, TF-BTD presented the hypsochromic shift after aggregation. This event occurs because the nano-aggregates restrict the access of the solvent, destabilizing the excited state, and thus blue-shifting the emission.

For the DCP derivatives, a similar behavior was observed. Both CB and TF-DCP had their luminescence quenched from 20 to 70% f_w , then recovering it at 80%. The solutions presented a light orangish emission at 100% acetone and, in more polar environments, showed a more intense and yellow color. Analyzing DCP's structure, the bulky character of the molecule promoted by the two phenyl groups, as well as the CN units, increases the steric hindrance of the compound. Likewise the aryloxy-BTD, when in aggregation, the intramolecular rotations of the DCP become restricted, promoting radiative decays. As well as in TF-BTD, the DCP derivatives also presented the hypsochromic shift, indicating the formation of less solvent-accessible nano-aggregates.

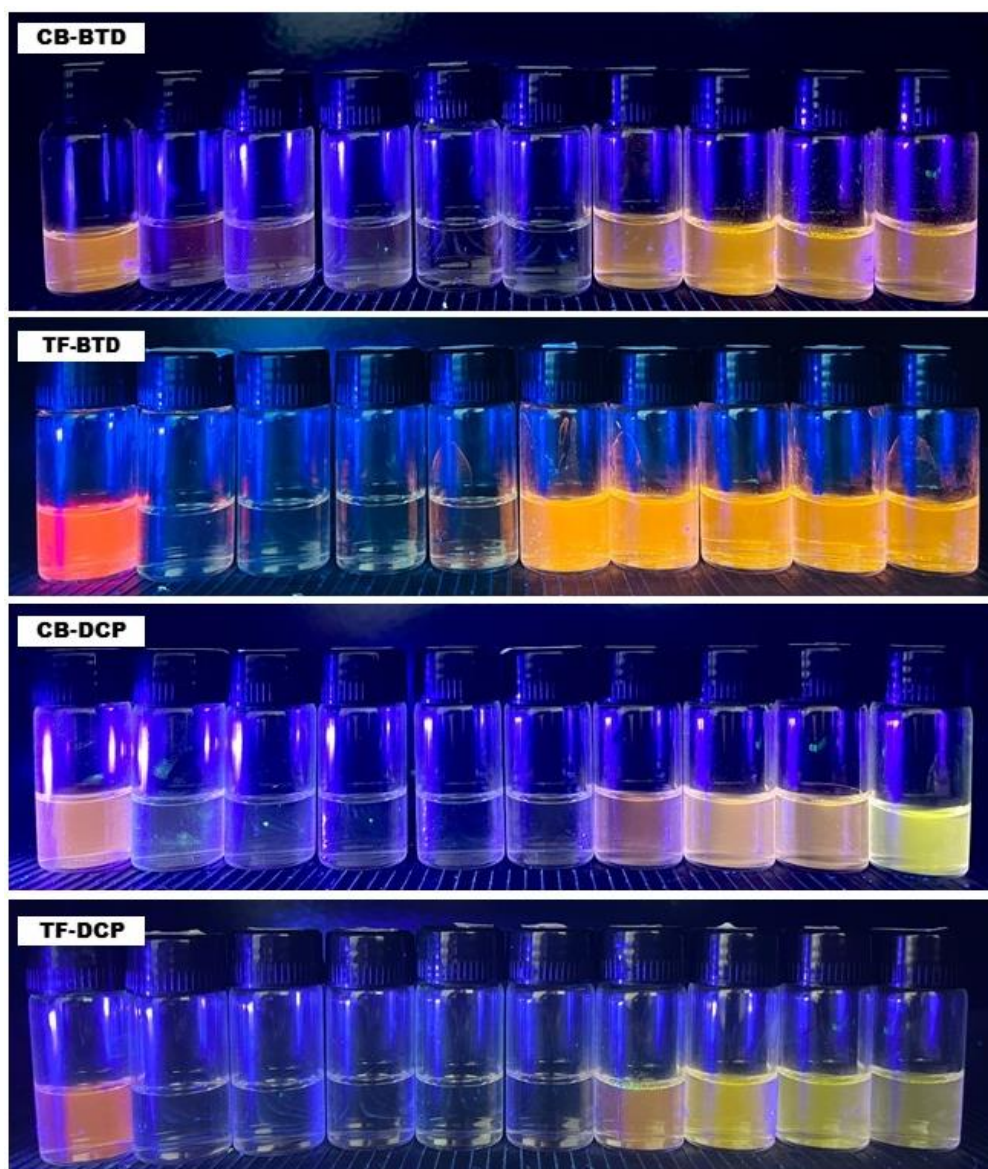


Figure 36: Aryloxy-BTD and DCP derivatives AIEE experiments under UV light, with 0, 20, 40, 50, 60, 70, 80, 90, 95 and 99% of water concentration in the solutions.

Fluorescence measurements were conducted using the same acetone/water or THF/water mixtures (Figure 37). Overall, the results supported the visual observations obtained previously. For all compounds, an increase in f_w led to a decrease in fluorescence. This reduction was attributed to the inhibition of the internal charge transfer process in the excited states, caused by the increasing polarity of the medium. As the solutions reached their critical point and aggregates began to form, a significant increase in fluorescence intensity was observed. To illustrate this effect more clearly, the relative intensity (I/I_0) was plotted against the water fraction (Figure 37, right).

For CB-BTD, the two first solutions (0 and 20% *fw*) presented their emission maxima around 625 and 650 nm, while the 80, 90, 95 and 99% *fw* solutions were slightly blue shifted (around 575 and 600 nm), although producing an unperceptive change in color. The (I/I_0) vs water fraction profile demonstrates the decline in emission and posterior aggregation-induced emission. The mixture containing 95% *fw* restored almost 60% of its relative intensity. TF-BTD, in turn, presented emission maxima ranging from 572 to 625 nm for the most polar solutions, and around 675 nm to the pure acetone solution. It can be observed an enhancement on the fluorescent emission for the last concentrations. The profiles shown in Figure 38 for TF-BTD demonstrate that the critical point of aggregation starts around 70%, improving 1.6-fold the relative fluorescence intensity.

For CB-DCP, a similar behavior to CB-BTD was observed, with the most polar media leading to a slight hypsochromic shift, but not enough to notice a color change. The (I/I_0) vs water fraction graph demonstrated an enhanced fluorescent emission from the 80% *fw* solution on, with 90% *fw* solution showing a relative intensity 6.5-fold improvement. In turn, TF-DCP presented emission maxima around 550 to 600 nm in polar media, and 600 to 650 nm in pure THF. For this compound, a more expressive hypsochromic shift resulted in a perceptible color change. The relative intensity profile also showed an enhancement on the emission for the more aggregated solutions, achieving a 3-fold relative intensity improvement.

Revisiting what was previously discussed, the bulky and non-planar structures of the molecules contribute to the formation of the emissive nano-aggregates. The donor groups, especially the triphenylamine unit, as well as the centered phenyl, increase the twisting angles on the D and A portions, positively influencing the AIE/AIEE properties, by deactivating the non-radiative relaxation.

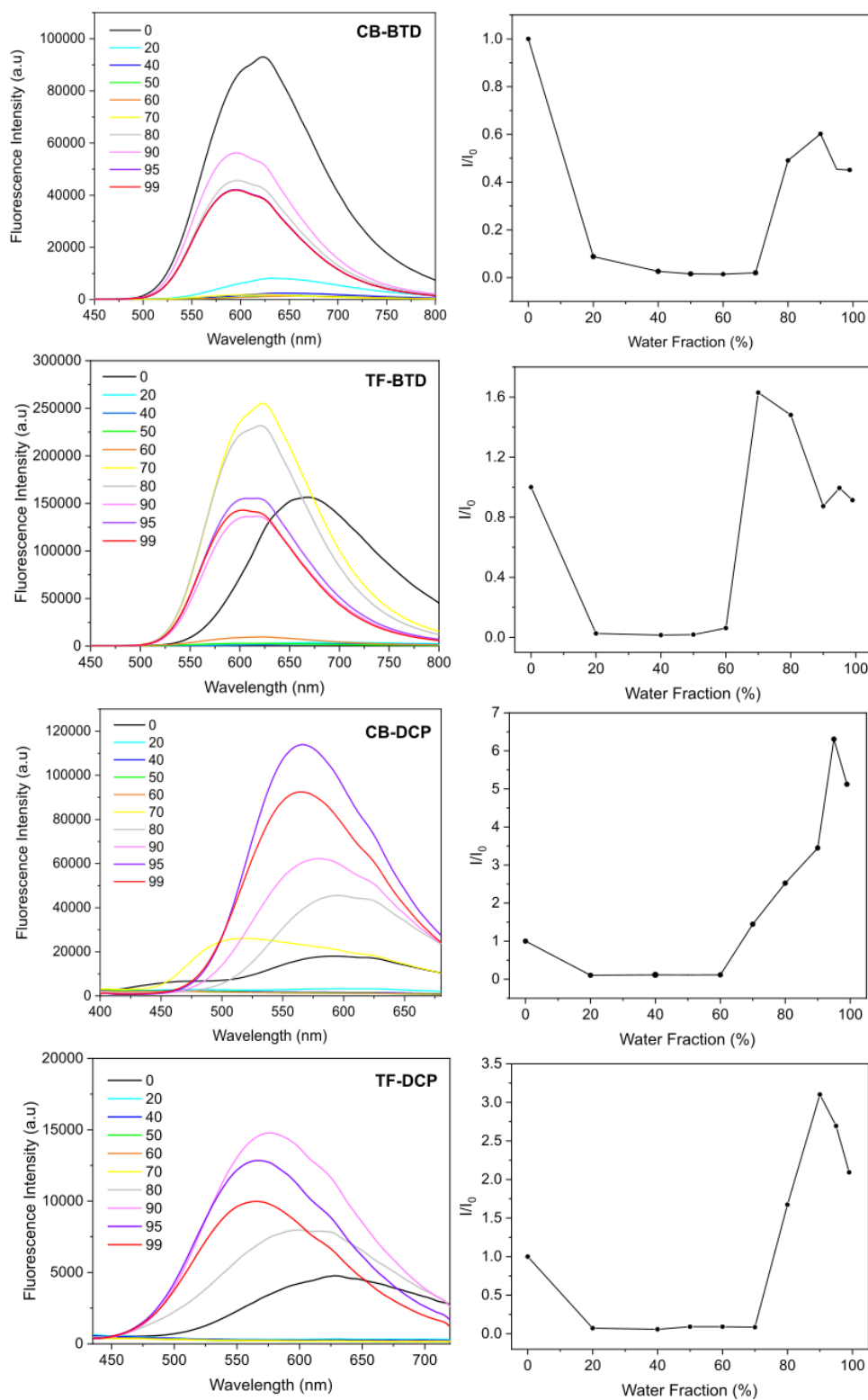


Figure 37: AIE fluorescence intensity spectroscopy in different solvents proportions and relative intensity (I/I_0) vs the water fraction of the four fluorophores.

10.4. Electrochemical evaluation

The electrochemical properties of the compounds were evaluated via cyclic voltammetry in dichloromethane medium. Table 5 summarizes the obtained data and the voltammograms are depicted in Appendix section (A43-46). As a result, the compounds presented oxidation peaks ranging from 0.87 to 1.16 V and reduction peaks, from -1.35 to -1.05 V. For HOMO and LUMO orbitals, with energy values around -5.23 and -5.52 eV and -3.01 and -3.31 eV, respectively, the energy gaps ranged from 2.09 to 2.43 eV. Associating the oxidation energy to the donor unit of the molecules, since the triphenylamino group is a stronger electron donor when compared to the carbazole, TF-BTD and TF-DCP will present smaller values of E^{ox} . Thus, it is also expected that the HOMO of the TF-substituted molecules will be more energetic, with more easily donating electrons. Analyzing the LUMO energy, the less energetic and most suitable to receive electrons was the BTD, when it is associated with the carbazole group. However, the HOMO of CB-BTD is relatively low (-5.44 eV) and the band gap becomes larger, thus more energetic. The best HOMO-LUMO combination formed was in TF-BTD molecule. Although the LUMO for this molecule was not the less energetic, the HOMO high energy compensates it, generating the smallest band gap obtained ($E_{\text{gap}} = 2.09$ eV).

Table 5: Electrochemical properties of the fluorophores, with oxidation and reduction energies (V), HOMO and LUMO (eV) and band gap (eV).

Dye	E^{ox} onset	E^{red} onset	HOMO	LUMO	E_{gap}
CB-BTD	1.08	-1.35	-5.44	-3.01	2.43
TF-BTD	0.87	-1.22	-5.23	-3.14	2.09
CB-DCP	1.16	-1.05	-5.52	-3.31	2.21
TF-DCP	0.99	-1.29	-5.35	-3.07	2.28

11. Conclusions

In this work, four novel organic dyes have successfully been synthesized with potential applications in OLEDs, featuring benzothiadiazole and dicyanopyridine as electron-accepting units and carbazole and triphenylamine as electron-donating units. Absorption maxima for the synthesized dyes ranged from 346 to 438 nm, while emission maxima varied significantly. CB-BTD and TF-BTD molecules demonstrated emission maxima from 569 to 697 nm, while CB-DCP and TF-DCP emitted from 461 to 625 nm, showcasing a range of vibrant colors suitable for OLED applications.

The AIE studies revealed that both aryloxy-BTD derivatives exhibited strong luminescence in polar environments, with TF-BTD showing a noticeable color shift from intense to yellowish-orange upon aggregation. This behavior is attributed to restricted intramolecular rotation due to the aggregation-induced rigidity, which enhances radiative decay. Similarly, the DCP derivatives displayed a complex emission profile with luminescence quenching and recovery, highlighting their sensitivity to aggregation and solvent polarity, and showing AIEE properties. The observed hypsochromic shift in both TF-BTD and DCP derivatives further supports the formation of less accessible nano-aggregates, contributing to the distinctive emission characteristics.

Electrochemical and computational studies provided insights into the electronic properties of the dyes. The cyclic voltammetry results indicated oxidation peaks ranging from 0.87 to 1.16 V and reduction peaks from -1.35 to -1.05 V, with energy gaps between 2.09 and 2.43 eV. DFT calculations corroborated these findings, with HOMO and LUMO energies revealing effective charge separation and promising potential for TADF applications, particularly for TF-DCP. This research demonstrates that the strategic combination of electron-donating and -accepting units in these organic dyes can yield materials with advantageous optical and electronic properties, paving the way for their future development and application in advanced OLED technologies.

Time-resolved fluorescence studies and OLED fabrication are currently underway in our research group. These forthcoming experiments will offer valuable insights into the fluorescence mechanism of the synthesized dyes and their potential performance in practical OLED applications. The continued exploration of

these molecules will provide us a more comprehensive understanding of the compound's photophysics and photovoltaic behavior.

Bibliography

1. Karunathilake, H. & Witharana, S. Fossil Fuels and Global Energy Economics. in *Encyclopedia of Renewable Energy, Sustainability and the Environment* 107–120 (Elsevier, 2024). doi:10.1016/B978-0-323-93940-9.00050-5.
2. Wang, J. & Azam, W. Natural resource scarcity, fossil fuel energy consumption, and total greenhouse gas emissions in top emitting countries. *Geoscience Frontiers* **15**, 101757 (2024).
3. Statistical Review of World Energy. *Energy Institute* (2024).
4. Lile, D. L. Optoelectronic Devices. in *Handbook of Compound Semiconductors* 813–865 (Elsevier, 1995). doi:10.1016/B978-081551374-2.50018-1.
5. Zhang, X. *et al.* A review on optoelectronic device applications of 2D transition metal carbides and nitrides. *Mater Des* **200**, 109452 (2021).
6. Lincot, D. The new paradigm of photovoltaics: From powering satellites to powering humanity. *C R Phys* **18**, 381–390 (2017).
7. Pan, A. & Zhu, X. Optoelectronic properties of semiconductor nanowires. in *Semiconductor Nanowires* 327–363 (Elsevier, 2015). doi:10.1016/B978-1-78242-253-2.00012-8.
8. El Chaar, L. Photovoltaic System Conversion. in *Alternative Energy in Power Electronics* 155–175 (Elsevier, 2011). doi:10.1016/B978-0-12-416714-8.00003-2.
9. Sharma, D., Mehra, R. & Raj, B. Comparative analysis of photovoltaic technologies for high efficiency solar cell design. *Superlattices Microstruct* **153**, 106861 (2021).
10. Bailey, S. & Raffaele, R. Operation of Solar Cells in a Space Environment. in *McEvoy's Handbook of Photovoltaics* 987–1003 (Elsevier, 2012). doi:10.1016/B978-0-12-809921-6.00027-6.
11. Yin, H., Zadshir, M. & Pao, F. Fundamentals of BIPVT design and integration. in *Building Integrated Photovoltaic Thermal Systems* 45–129 (Elsevier, 2022). doi:10.1016/B978-0-12-821064-2.00003-1.
12. Di Sabatino, M., Hendawi, R. & Garcia, A. S. Silicon Solar Cells: Trends, Manufacturing Challenges, and AI Perspectives. *Crystals (Basel)* **14**, 167 (2024).
13. Ember (2024); Energy Institute - Statistical Review of World Energy (2024) – with major processing by Our World in Data. (2024).
14. Lee, J.-K. & Yang, M. Progress in light harvesting and charge injection of dye-sensitized solar cells. *Materials Science and Engineering: B* **176**, 1142–1160 (2011).
15. Holkar, C. R., Jain, S. S., Jadhav, A. J. & Pinjari, D. V. Scale-Up Technologies for Advanced Nanomaterials for Green Energy. in *Nanomaterials for Green Energy* 433–455 (Elsevier, 2018). doi:10.1016/B978-0-12-813731-4.00014-X.

16. Zheng, D. *et al.* Revolutionizing dye-sensitized solar cells with nanomaterials for enhanced photoelectric performance. *J Clean Prod* **464**, 142717 (2024).
17. Ilic, S. & Paunovic, V. Characteristics of curcumin dye used as a sensitizer in dye-sensitized solar cells. *Facta universitatis - series: Electronics and Energetics* **32**, 91–104 (2019).
18. Marques, A. dos S., da Silva, V. A. S., Ribeiro, E. S. & Malta, L. F. B. Dye-Sensitized Solar Cells: Components Screening for Glass substrate, Counter-Electrode, Photoanode and Electrolyte. *Materials Research* **23**, (2020).
19. Moreira, J. *et al.* DYE-SENSITIZED SOLAR CELLS (DSSC): AN APPROACH TO PRACTICE IN UNDERGRADUATE TEACHING. *Quim Nova* (2024) doi:10.21577/0100-4042.20230133.
20. Hagfeldt, A., Boschloo, G., Sun, L., Kloo, L. & Pettersson, H. Dye-Sensitized Solar Cells. *Chem Rev* **110**, 6595–6663 (2010).
21. Grätzel, M. Solar Energy Conversion by Dye-Sensitized Photovoltaic Cells. *Inorg Chem* **44**, 6841–6851 (2005).
22. Tachibana, Y., Haque, S. A., Mercer, I. P., Durrant, J. R. & Klug, D. R. Electron Injection and Recombination in Dye Sensitized Nanocrystalline Titanium Dioxide Films: A Comparison of Ruthenium Bipyridyl and Porphyrin Sensitizer Dyes. *J Phys Chem B* **104**, 1198–1205 (2000).
23. Sonai, G. G., Melo Jr., M. A., Nunes, J. H. B., Megiatto Jr., J. D. & Nogueira, A. F. SOLAR CELLS SENSITIZED WITH NATURAL DYES: AN INTRODUCTORY EXPERIMENT ABOUT SOLAR ENERGY FOR UNDERGRADUATE STUDENTS. *Quim Nova* (2015) doi:10.5935/0100-4042.20150148.
24. O’Kane, M. Solar Cell Characterization and Testing.
25. Kumara, N. T. R. N., Lim, A., Lim, C. M., Petra, M. I. & Ekanayake, P. Recent progress and utilization of natural pigments in dye sensitized solar cells: A review. *Renewable and Sustainable Energy Reviews* **78**, 301–317 (2017).
26. Devadiga, D., Selvakumar, M., Shetty, P. & Santosh, M. S. The integration of flexible dye-sensitized solar cells and storage devices towards wearable self-charging power systems: A review. *Renewable and Sustainable Energy Reviews* **159**, 112252 (2022).
27. Tomar, N., Agrawal, A., Dhaka, V. S. & Surolia, P. K. Ruthenium complexes based dye sensitized solar cells: Fundamentals and research trends. *Solar Energy* **207**, 59–76 (2020).
28. Najm, A. S., Alwash, S. A., Sulaiman, N. H., Chowdhury, M. S. & Techato, K. N719 dye as a sensitizer for dye-sensitized solar cells (DSSCs): A review of its functions and certain rudimentary principles. *Environ Prog Sustain Energy* **42**, (2023).
29. Cerda, B., Sivakumar, R. & Paulraj, M. Natural dyes as sensitizers to increase the efficiency in sensitized solar cells. *J Phys Conf Ser* **720**, 012030 (2016).

30. Mariotti, N. *et al.* Recent advances in eco-friendly and cost-effective materials towards sustainable dye-sensitized solar cells. *Green Chemistry* **22**, 7168–7218 (2020).
31. Yen, Y.-S., Chou, H.-H., Chen, Y.-C., Hsu, C.-Y. & Lin, J. T. Recent developments in molecule-based organic materials for dye-sensitized solar cells. *J Mater Chem* **22**, 8734 (2012).
32. Siddiqui, A., Islavath, N., Swetha, T. & Singh, S. P. D– π –A organic dyes derived from the indacenodithiophene core moiety for efficient dye-sensitized solar cells. *Energy Advances* **2**, 1045–1050 (2023).
33. Ren, Z., Cao, Y., Shang, C. & Sun, C. Evaluating the photoelectric performance of D– π –A dyes with different π -conjugated bridges for DSSCs. *Chem Phys Lett* **806**, 140035 (2022).
34. Cai, K. *et al.* Molecular engineering of the fused azacycle donors in the D–A– π –A metal-free organic dyes for efficient dye-sensitized solar cells. *Dyes and Pigments* **197**, 109922 (2022).
35. Yang, W. *et al.* Dye-sensitized solar cells based on (D– π –A)₃L₂ phenothiazine dyes containing auxiliary donors and flexible linkers with different length of carbon chain. *Electrochim Acta* **283**, 1732–1741 (2018).
36. Thapa, P. *et al.* Chalcone and its analogs: Therapeutic and diagnostic applications in Alzheimer's disease. *Bioorg Chem* **108**, 104681 (2021).
37. Zhang, Y. *et al.* Chalcones. in *Privileged Scaffolds in Drug Discovery* 21–39 (Elsevier, 2023). doi:10.1016/B978-0-443-18611-0.00028-0.
38. Cazarolli, L. H. *et al.* Natural and Synthetic Chalcones. in 47–89 (2013). doi:10.1016/B978-0-444-62615-8.00002-3.
39. Saadullah, M., Rashad, M., Asif, M. & Shah, M. A. Biosynthesis of phytonutrients. in *Phytonutrients and Neurological Disorders* 57–105 (Elsevier, 2023). doi:10.1016/B978-0-12-824467-8.00003-6.
40. Lee, S.-C. *et al.* Development of a fluorescent chalcone library and its application in the discovery of a mouse embryonic stem cell probe. *Chemical Communications* **48**, 6681 (2012).
41. Wang, K.-P. *et al.* The coumarin conjugate: synthesis, photophysical properties and the ratiometric fluorescence response to water content of organic solvent. *Dyes and Pigments* **151**, 233–237 (2018).
42. Song, Z. *et al.* A Ratiometric Fluorescent Probe Based on ESIPT and AIE Processes for Alkaline Phosphatase Activity Assay and Visualization in Living Cells. *ACS Appl Mater Interfaces* **6**, 17245–17254 (2014).
43. da Costa, R. G. M. *et al.* Synthesis, photophysical properties and aggregation-induced enhanced emission of bischalcone-benzothiadiazole and chalcone-benzothiadiazole hybrids. *J Lumin* **239**, 118367 (2021).

44. Sachdeva, T. & Milton, M. D. AIEE active novel red-emitting D- π -A phenothiazine chalcones displaying large Stokes shift, solvatochromism and “turn-on” reversible mechanofluorochromism. *Dyes and Pigments* **181**, 108539 (2020).
45. Teo, K. Y. *et al.* The influence of the push-pull effect and a π -conjugated system in conversion efficiency of bis-chalcone compounds in a dye sensitized solar cell. *J Mol Struct* **1143**, 42–48 (2017).
46. Anandkumar, D., Ganesan, S., Rajakumar, P. & Maruthamuthu, P. Synthesis, photophysical and electrochemical properties and DSSC applications of triphenylamine chalcone dendrimers via click chemistry. *New Journal of Chemistry* **41**, 11238–11249 (2017).
47. Teo, K. Y. *et al.* The influence of the push-pull effect and a π -conjugated system in conversion efficiency of bis-chalcone compounds in a dye sensitized solar cell. *J Mol Struct* **1143**, 42–48 (2017).
48. Anizaim, A. H., Zaini, M. F., Razak, I. A. & Arshad, S. Insight into the impact of the substituent modification on the photovoltaic performance of ferrocenyl chalcones based DSSCs. *J Solid State Chem* **304**, 122551 (2021).
49. Mohd Nizar, S. N. A. *et al.* The Photovoltaic Performance of Sensitizers for Organic Solar Cells Containing Fluorinated Chalcones with Different Halogen Substituents. *Crystals (Basel)* **11**, 1357 (2021).
50. Karaca, H. *et al.* Thiochalcone substituted phthalocyanines for dye-sensitized solar cells: Relation of optical and electrochemical properties for cell performance. *J Coord Chem* **71**, 1606–1622 (2018).
51. Rajakumar, P., Thirunarayanan, A., Raja, S., Ganesan, S. & Maruthamuthu, P. Photophysical properties and dye-sensitized solar cell studies on thiadiazole–triazole–chalcone dendrimers. *Tetrahedron Lett* **53**, 1139–1143 (2012).
52. Levitus, M. Tutorial: measurement of fluorescence spectra and determination of relative fluorescence quantum yields of transparent samples. *Methods Appl Fluoresc* **8**, 033001 (2020).
53. Aminabhavi, T. & Banerjee, K. Density, viscosity, refractive index, and speed of sound in binary mixtures of dimethyl carbonate with methanol, chloroform, carbon tetrachloride, Cyclohexane, and Dichloromethane in the Temperature Interval (298.15–308.15) K. *J Chem Eng Data* **43**, 1096–1011 (1998).
54. Bloking, J. T. *et al.* Solution-Processed Organic Solar Cells with Power Conversion Efficiencies of 2.5% using Benzothiadiazole/Imide-Based Acceptors. *Chemistry of Materials* **23**, 5484–5490 (2011).
55. Bredas, J. L., Silbey, R., Boudreaux, D. S. & Chance, R. R. Chain-length dependence of electronic and electrochemical properties of conjugated systems: polyacetylene, polyphenylene, polythiophene, and polypyrrole. *J Am Chem Soc* **105**, 6555–6559 (1983).
56. Yahya, M., Bouziani, A., Ocak, C., Seferoğlu, Z. & Sillanpää, M. Organic/metal-organic photosensitizers for dye-sensitized solar cells (DSSC): Recent

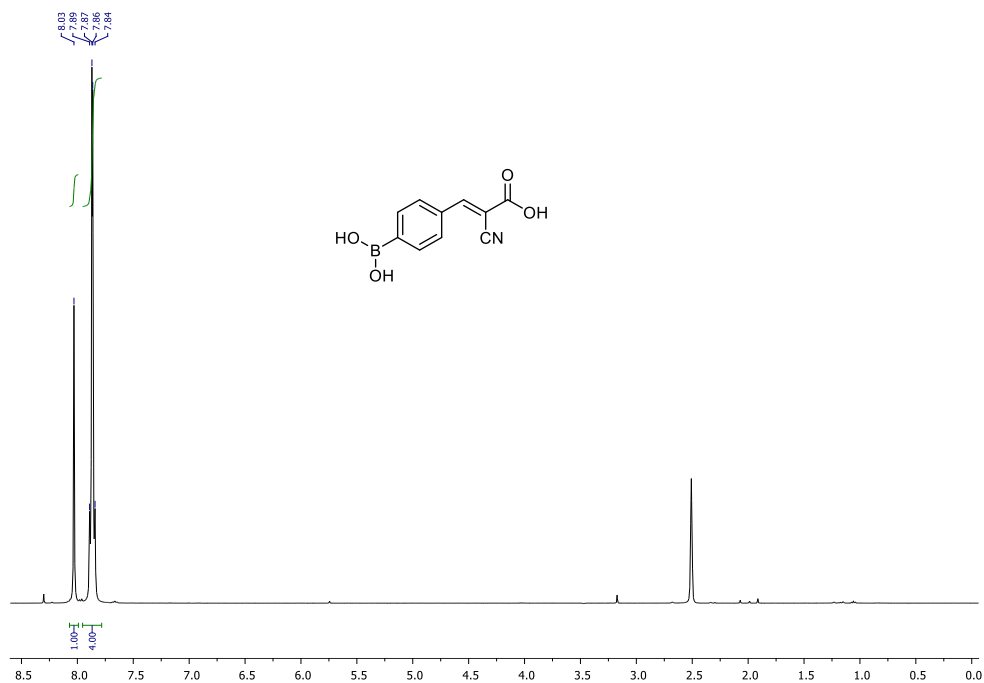
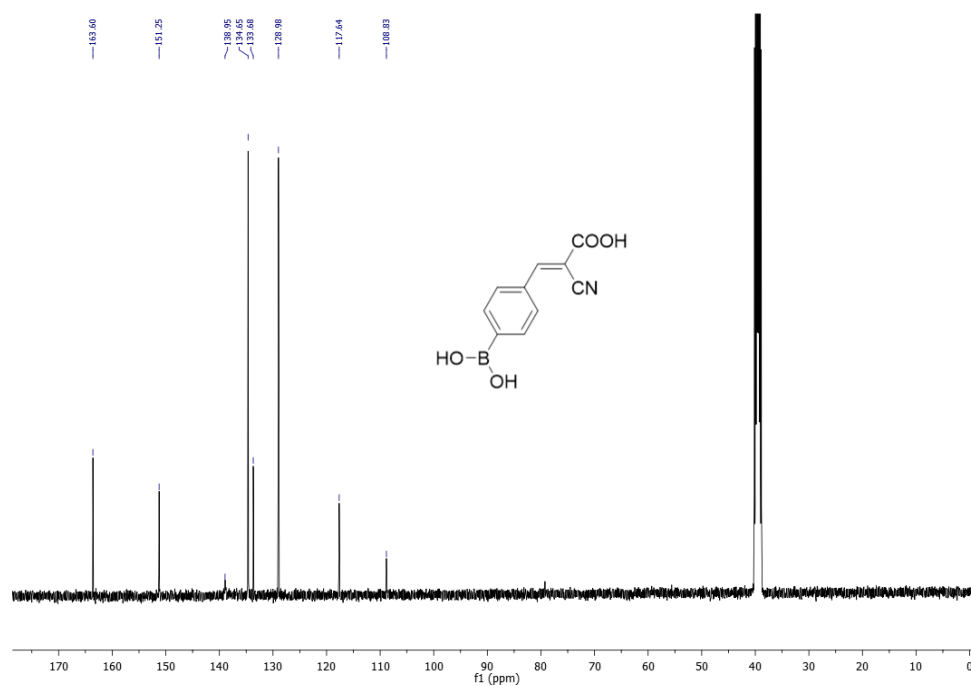
- developments, new trends, and future perceptions. *Dyes and Pigments* **192**, 109227 (2021).
57. Lee, C.-P., Li, C.-T. & Ho, K.-C. Use of organic materials in dye-sensitized solar cells. *Materials Today* **20**, 267–283 (2017).
 58. Bernanose, A., Comte, M. & Vouaux, P. Sur un nouveau mode d'émission lumineuse chez certains composés organiques. *Journal de Chimie Physique* **50**, 64–68 (1953).
 59. Pope, M., Kallmann, H. P. & Magnante, P. Electroluminescence in Organic Crystals. *J Chem Phys* **38**, 2042–2043 (1963).
 60. Tang, C. W. & VanSlyke, S. A. Organic electroluminescent diodes. *Appl Phys Lett* **51**, 913–915 (1987).
 61. Volz, D. *et al.* From iridium and platinum to copper and carbon: new avenues for more sustainability in organic light-emitting diodes. *Green Chemistry* **17**, 1988–2011 (2015).
 62. Zou, S.-J. *et al.* Recent advances in organic light-emitting diodes: toward smart lighting and displays. *Mater Chem Front* **4**, 788–820 (2020).
 63. Thejo Kalyani, N. & Dhoble, S. J. Organic light emitting diodes: Energy saving lighting technology—A review. *Renewable and Sustainable Energy Reviews* **16**, 2696–2723 (2012).
 64. Nayak, D. & Choudhary, R. B. A survey of the structure, fabrication, and characterization of advanced organic light emitting diodes. *Microelectronics Reliability* **144**, 114959 (2023).
 65. Liu, S., Xie, W. & Lee, C.-S. Organic light-emitting diodes, what's next? *Next Nanotechnology* **1**, 100003 (2023).
 66. Chen, H.-W., Lee, J.-H., Lin, B.-Y., Chen, S. & Wu, S.-T. Liquid crystal display and organic light-emitting diode display: present status and future perspectives. *Light Sci Appl* **7**, 17168–17168 (2017).
 67. Neto, B. A. D., Lapis, A. A. M., da Silva Júnior, E. N. & Dupont, J. 2,1,3-Benzothiadiazole and Derivatives: Synthesis, Properties, Reactions, and Applications in Light Technology of Small Molecules. *European J Org Chem* **2013**, 228–255 (2013).
 68. Swartzfager, J., Chen, G., Francese, T., Galli, G. & Asbury, J. Interplay of Molecular Dynamics and Radiative Decay of a TADF Emitter in a Glass-Forming Liquid. *Physical Chemistry Chemical Physics* (2022).
 69. Sheng, H. Study on Working Principle, Structure, Enhancement Technology, and Applications of Organic Light-emitting Diodes. *Highlights in Science, Engeneering and Technology* **27**, 302–310 (2022).
 70. Yin, X. *et al.* Recent Advances in Thermally Activated Delayed Fluorescent Polymer—Molecular Designing Strategies. *Front Chem* **8**, (2020).

71. Nasiri, S. *et al.* What is TADF (thermally activated delayed fluorescence) compared to the mechanisms of FL (fluorescence), PH (phosphorescence), and TTA (triplet–triplet annihilation) based on a novel naphthalimide sulfonylphenyl derivative as a host? *J Photochem Photobiol A Chem* **447**, 115289 (2024).
72. Arnaut, L. Experimental methods. in *Chemical Kinetics* 37–91 (Elsevier, 2021). doi:10.1016/B978-0-444-64039-0.00004-2.
73. Sharma, N. *et al.* Turn on of sky-blue thermally activated delayed fluorescence and circularly polarized luminescence (CPL) *via* increased torsion by a bulky carbazolophane donor. *Chem Sci* **10**, 6689–6696 (2019).
74. Mueller-Mach, R. & Mueller, G. O. Chapter 2 Thin Film Electroluminescence. in 27–105 (1999). doi:10.1016/S0080-8784(08)62605-8.
75. Lister, G. G. & Waymouth, J. F. Light Sources. in *Encyclopedia of Physical Science and Technology* 557–595 (Elsevier, 2003). doi:10.1016/B0-12-227410-5/00378-1.
76. Meyer, R., Schlecht, M. & Chhatbar, K. Solar resources for concentrating solar power (CSP) systems. in *Concentrating Solar Power Technology* 68-e2 (Elsevier, 2012). doi:10.1533/9780857096173.1.68.
77. Li, S. Introduction to Electrochemical Reaction Engineering. in *Chemical Reaction Engineering* 599–651 (Elsevier, 2017). doi:10.1016/B978-0-12-410416-7.00013-6.
78. Sadhukhan, S. *et al.* Evolution of high efficiency passivated emitter and rear contact (PERC) solar cells. in *Sustainable Developments by Artificial Intelligence and Machine Learning for Renewable Energies* 63–129 (Elsevier, 2022). doi:10.1016/B978-0-323-91228-0.00007-0.
79. Zhang, Q. *et al.* Design of Efficient Thermally Activated Delayed Fluorescence Materials for Pure Blue Organic Light Emitting Diodes. *Journal of American Chemical Society* **134**, 14706–14709 (2012).
80. Khan, A. *et al.* Donor-spiro-acceptor architecture for green thermally activated delayed fluorescence (TADF) emitter. *Org Electron* **77**, 105520 (2020).
81. Karnik, A. V. & Hasan, M. Basic concepts of structure and stereochemistry. in *Stereochemistry* 3–23 (Elsevier, 2021). doi:10.1016/B978-0-12-821062-8.00011-9.
82. Hwang, J. *et al.* Structural isomers of 9-(pyridin-2-yl)-9H-carbazole in combination with 9'H-9,3':6',9''-tercarbazole and their application to high efficiency solution processed green TADF OLEDs. *Dyes and Pigments* **179**, 108403 (2020).
83. Neto, B. A. D., Correa, J. R. & Spencer, J. Fluorescent Benzothiadiazole Derivatives as Fluorescence Imaging Dyes: A Decade of New Generation Probes. *Chemistry – A European Journal* **28**, (2022).
84. Zhang, Y., Song, J., Qu, J., Qian, P.-C. & Wong, W.-Y. Recent progress of electronic materials based on 2,1,3-benzothiadiazole and its derivatives: synthesis and their application in organic light-emitting diodes. *Sci China Chem* **64**, 341–357 (2021).

85. Pazini, A. *et al.* Phenoxy-benzothiadiazole dyes: Synthesis, photophysical properties and preliminary application in OLEDs. *Tetrahedron Lett* **59**, 2994–2999 (2018).
86. DaSilveira Neto, B. A. *et al.* Photophysical and electrochemical properties of π -extended molecular 2,1,3-benzothiadiazoles. *Tetrahedron* **61**, 10975–10982 (2005).
87. Liu, J. *et al.* Experimental Evidence for “Hot Exciton” Thermally Activated Delayed Fluorescence Emitters. *Adv Opt Mater* **7**, (2019).
88. Ni, F. & *et al.* Teaching an old acceptor new tricks: rationally employing 2,1,3-benzothiadiazole as input to design a highly efficient red thermally activated delayed fluorescence emitter. *J Mater Chem C Mater* **5**, 1363–1368 (2017).
89. Kumsampao, J. *et al.* A Simple and Strong Electron-Deficient 5,6-Dicyano[2,1,3]benzothiadiazole-Cored Donor-Acceptor-Donor Compound for Efficient Near Infrared Thermally Activated Delayed Fluorescence. *Chem Asian J* **15**, 3029–3036 (2020).
90. Cao, X., Zhang, D., Zhang, S., Tao, Y. & Huang, W. CN-Containing donor–acceptor-type small-molecule materials for thermally activated delayed fluorescence OLEDs. *J Mater Chem C Mater* (2017).
91. Chen, Z. *et al.* Emitters with a pyridine-3,5-dicarbonitrile core and short delayed fluorescence lifetimes of about 1.5 μ s: orange-red TADF-based OLEDs with very slow efficiency roll-offs at high luminance. *J Mater Chem C Mater* **6**, 6543–6548 (2018).
92. Liu, H. *et al.* Modulating the acceptor structure of dicyanopyridine based TADF emitters: Nearly 30% external quantum efficiency and suppression on efficiency roll-off in OLED. *Chemical Engineering Journal* **401**, 126107 (2020).
93. Mahesha, P. *et al.* Synthesis, DFT, and photophysical studies of substituted pyridine carbonitrile derivatives. *J Mol Struct* **1270**, 133958 (2022).
94. Liu, H. *et al.* Efficient Yellow Thermally Activated Delayed Fluorescent Emitters Based on 3,5-Dicyanopyridine Acceptors. *The Journal of Physical Chemistry C* **124**, 25489–25498 (2020).
95. Serevičius, T. *et al.* Achieving efficient deep-blue TADF in carbazole-pyrimidine compounds. *Org Electron* **82**, 105723 (2020).
96. Duan, Y.-C. *et al.* Whether the combination of AIE and TADF functional groups produces AIE-type TADF? –A theoretical study on the synergistic effect of TPE and carbazole donor group/thianthrene-tetraoxide acceptor group. *Dyes and Pigments* **194**, 109547 (2021).
97. Kang, H. *et al.* High-efficiency blue organic light-emitting Diodes using emissive carbazole-triazine-based donor-acceptor molecules with high reverse intersystem crossing rates. *Org Electron* **75**, 105399 (2019).

98. Ma, F. *et al.* Adjusting the photophysical properties of AIE-active TADF emitters from through-bond to through-space charge transfer for high-performance solution-processed OLEDs. *Dyes and Pigments* **188**, 109208 (2021).
99. Wu, C. *et al.* Multifunctional luminophores with dual emitting cores: TADF emitters with AIE properties for efficient solution- and evaporation-processed doped and non-doped OLEDs. *Chemical Engineering Journal* **431**, 133249 (2022).
100. Shi, C. *et al.* tert-Butyltriazine-Diphenylaminocarbazole based TADF materials: π -Bridge modification for enhanced kRISC and efficiency stability. *Dyes and Pigments* **204**, 110430 (2022).
101. Chen, M., Chen, Y., Li, Y., Lin, Y. & Wu, Y. Efficient orange and red thermally activated delayed fluorescence materials based on 1,8-naphthalimide derivatives. *RSC Adv* **14**, 6494–6500 (2024).
102. Vesga-Hernández, C. Diphenyl-substituted pyridine-3,5-dicarbonitrile and fluorenyl-substituted benzothiadiazole derivatives: Synthesis of new fluorescent compounds with extended conjugation for optoelectronic applications. (Pontificia Universidade Católica, Rio de Janeiro, 2023).

APPENDIX

1. DSSCs ^1H and ^{13}C NMR spectraFigure A1: ^1H NMR spectrum of compound 2 (400MHz, $\text{DMSO-}d_6$).Figure A2: ^{13}C NMR spectrum (APT) of compound 2 (100MHz, $\text{DMSO-}d_6$).

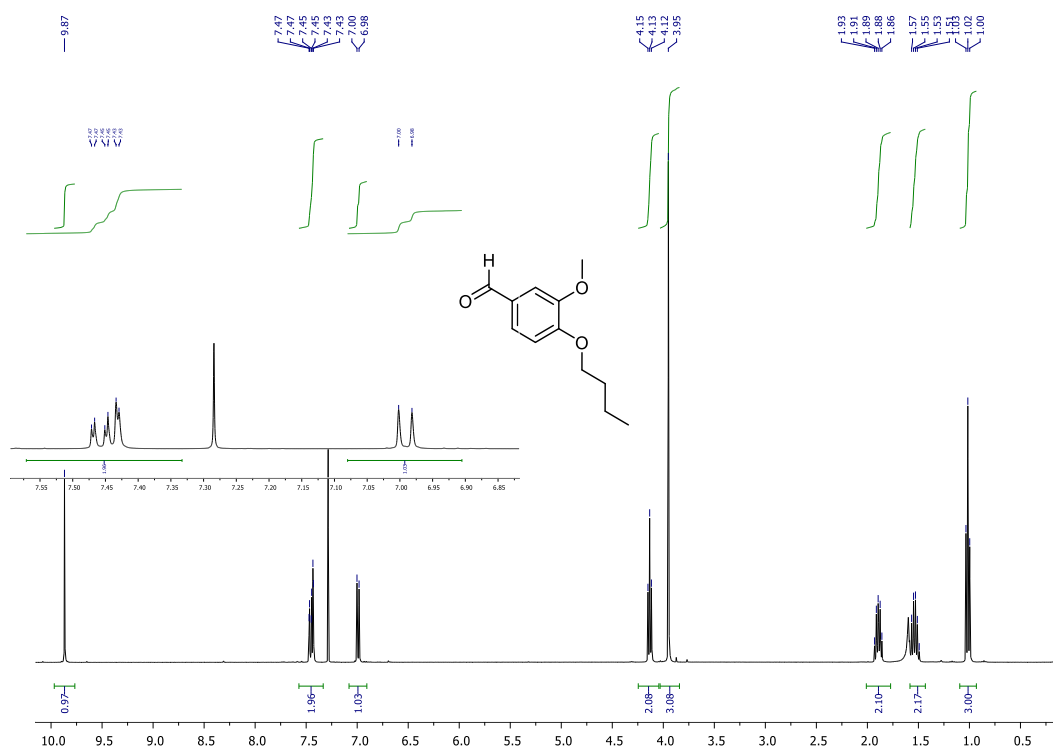


Figure A3: ¹H NMR spectrum of compound **4a** (400 MHz, CDCl₃-d₁).

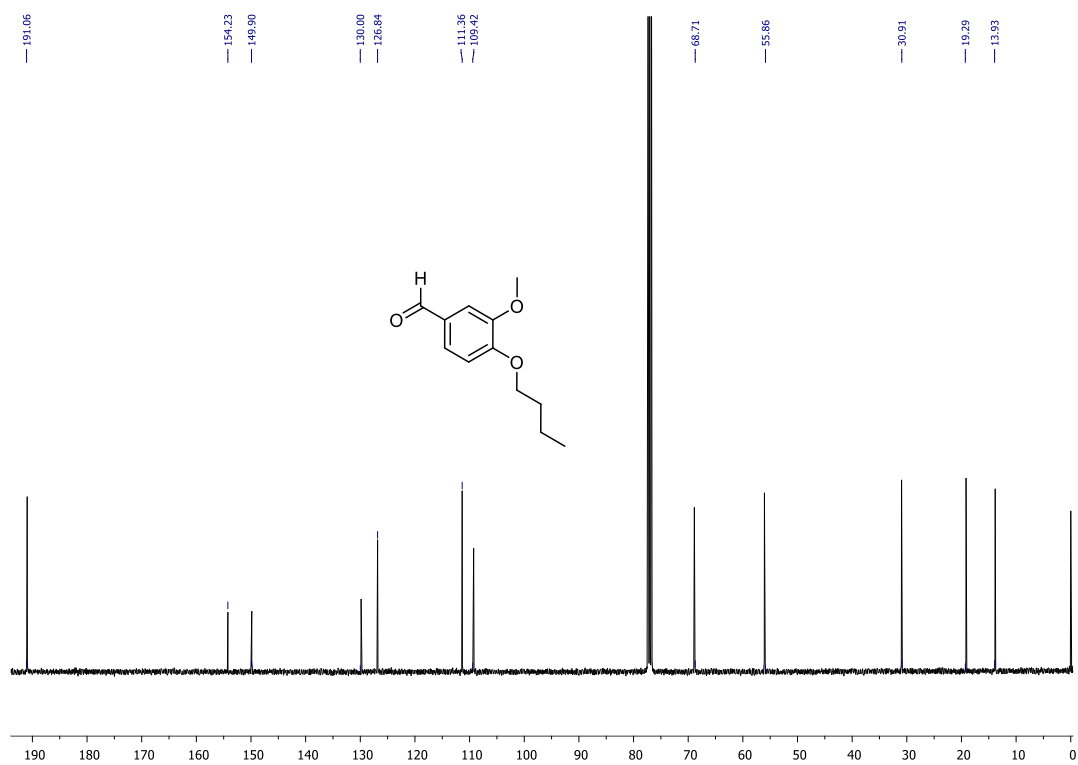


Figure A4: ¹³C NMR (APT) spectrum of compound **4a** (100 MHz, CDCl₃-d₁).

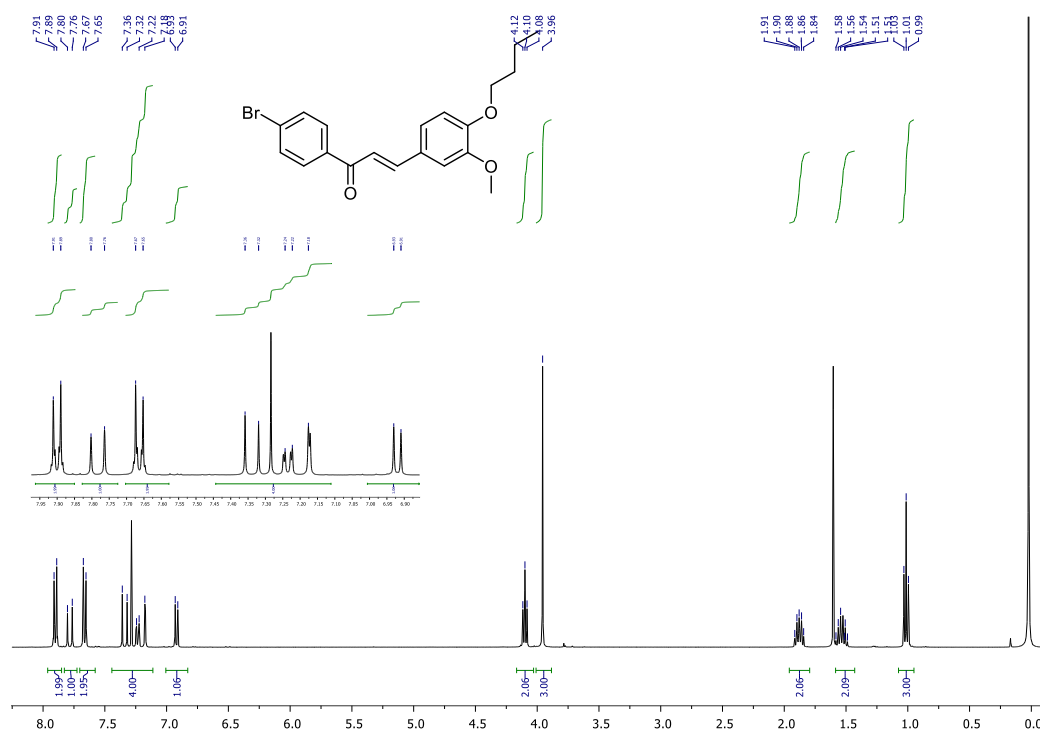


Figure A5: ¹H NMR spectrum of compound **5a** (400 MHz, CDCl₃-d₇).

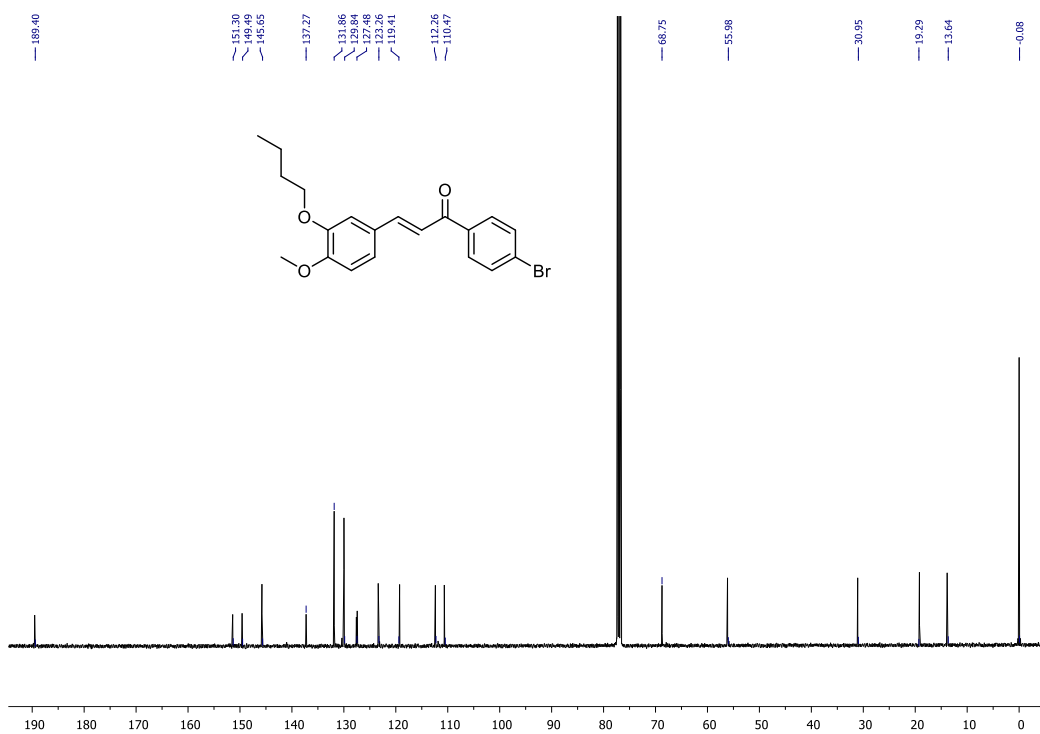


Figure A6: ¹³C NMR (APT) spectra of compound **5a** (100 MHz, CDCl₃-d₇).

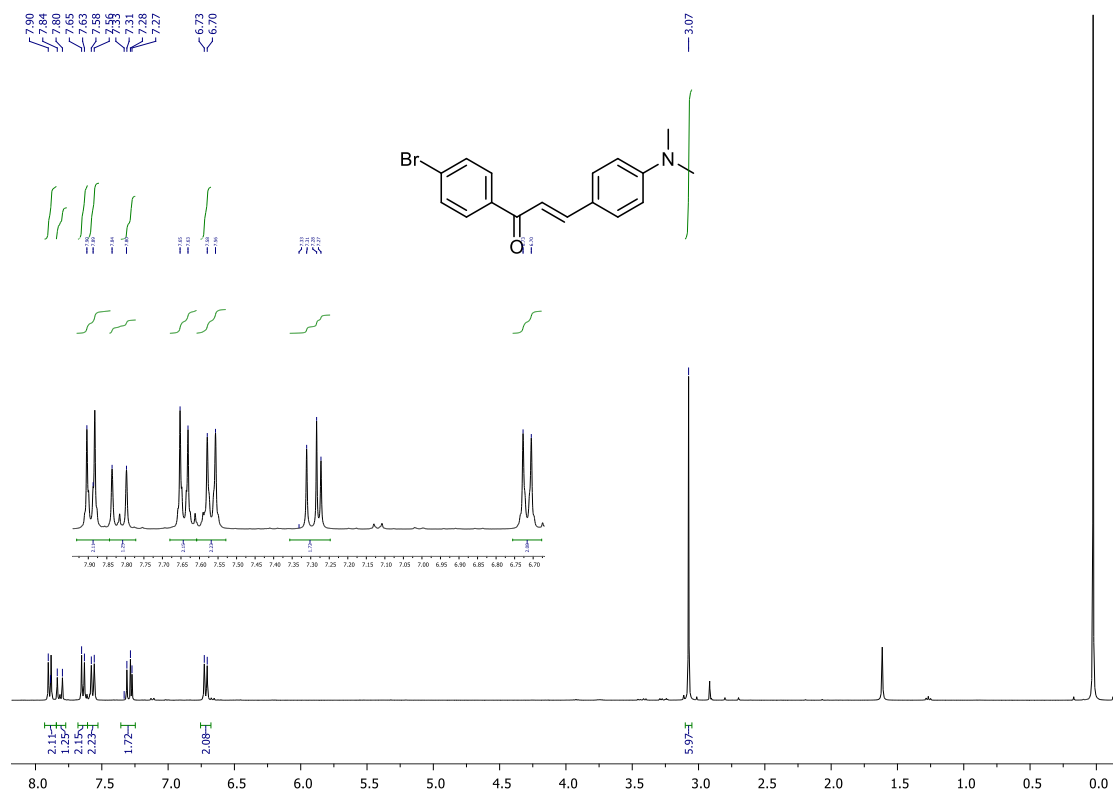


Figure A7: ¹H NMR spectrum of compound **5b** (400 MHz, CDCl₃-d₁).

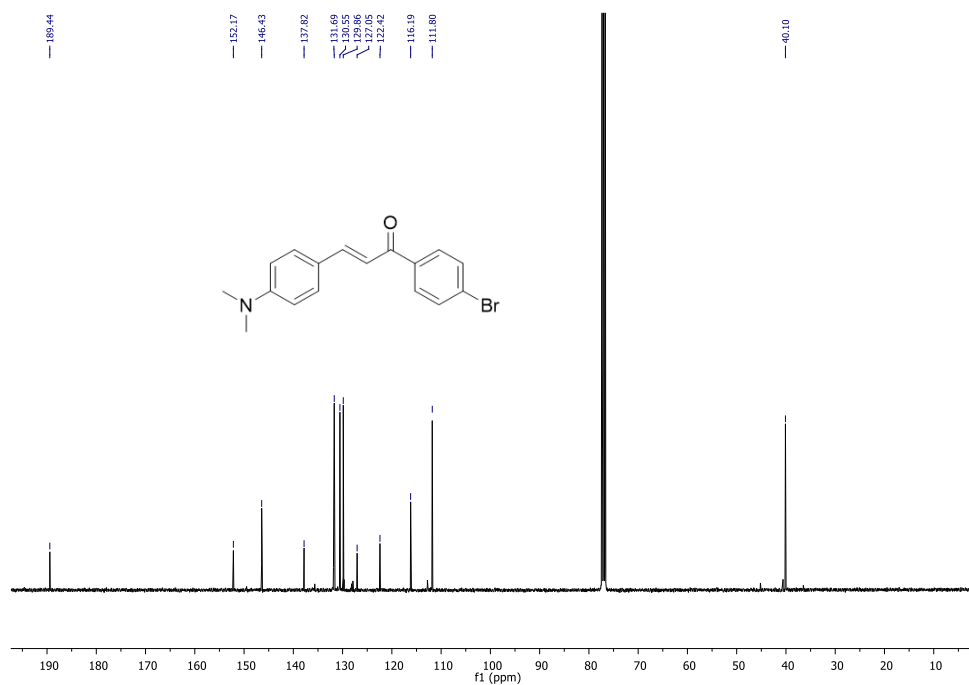
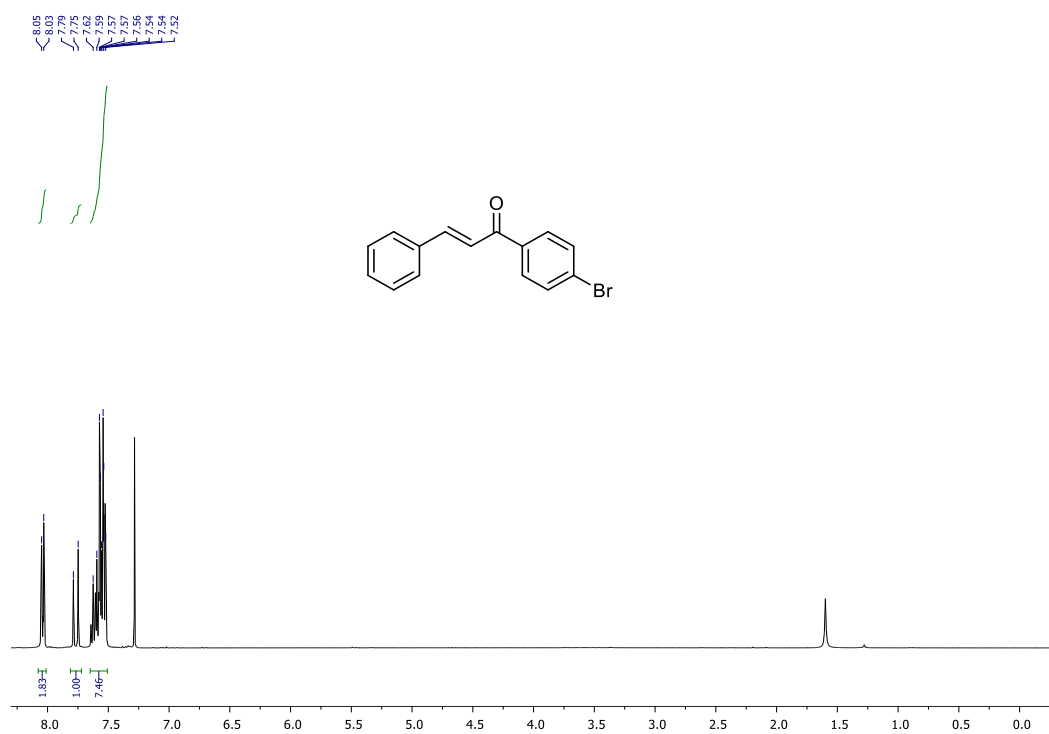
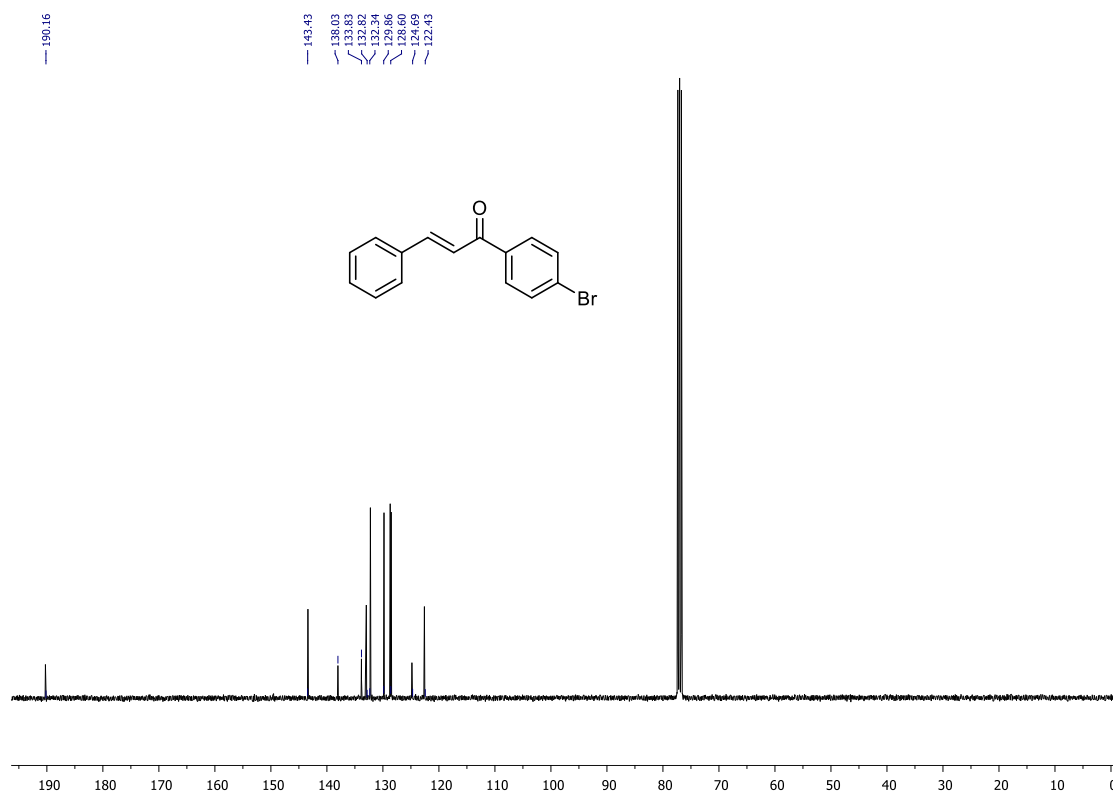


Figure A8: ¹³C NMR (APT) spectra of compound **5a** (100 MHz, CDCl₃-d₁).

Figure A9: ^1H NMR spectrum of compound **5c** (400 MHz, CDCl_3-d_1).Figure A10: ^{13}C NMR (APT) spectrum of compound **5c** (100 MHz, CDCl_3-d_1).

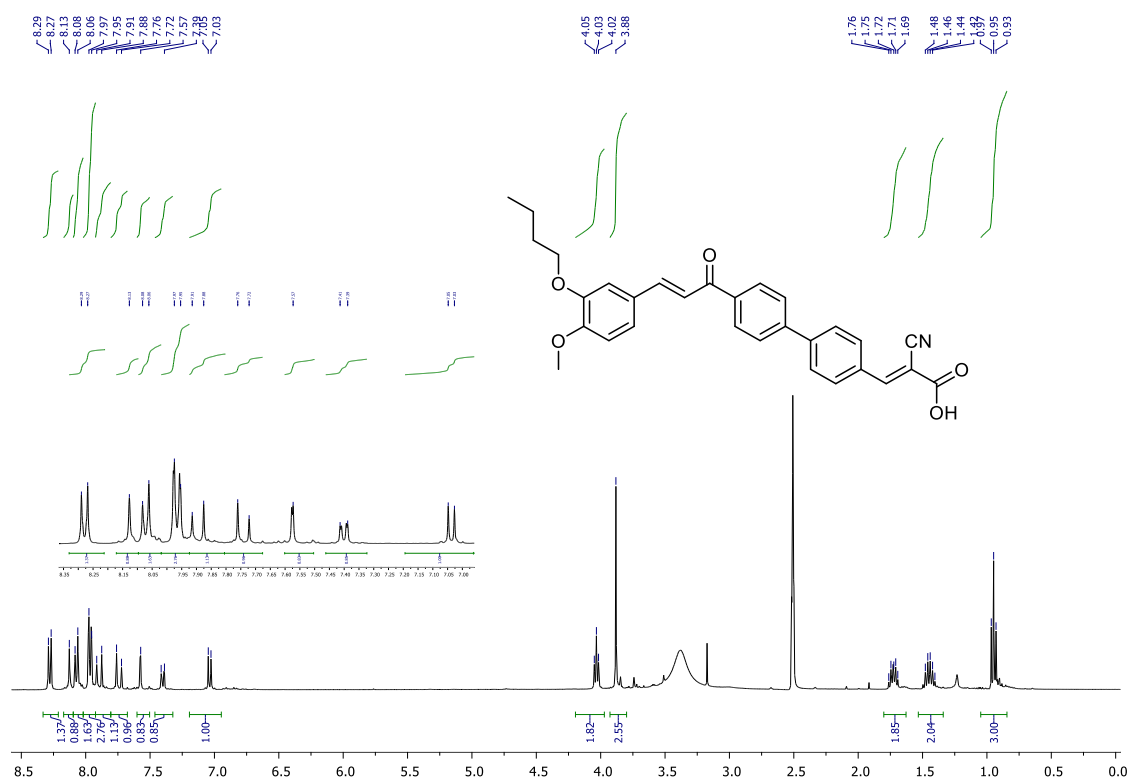


Figure A11: ¹H NMR spectrum of compound **6a** (400 MHz, DMSO-*d*₆).

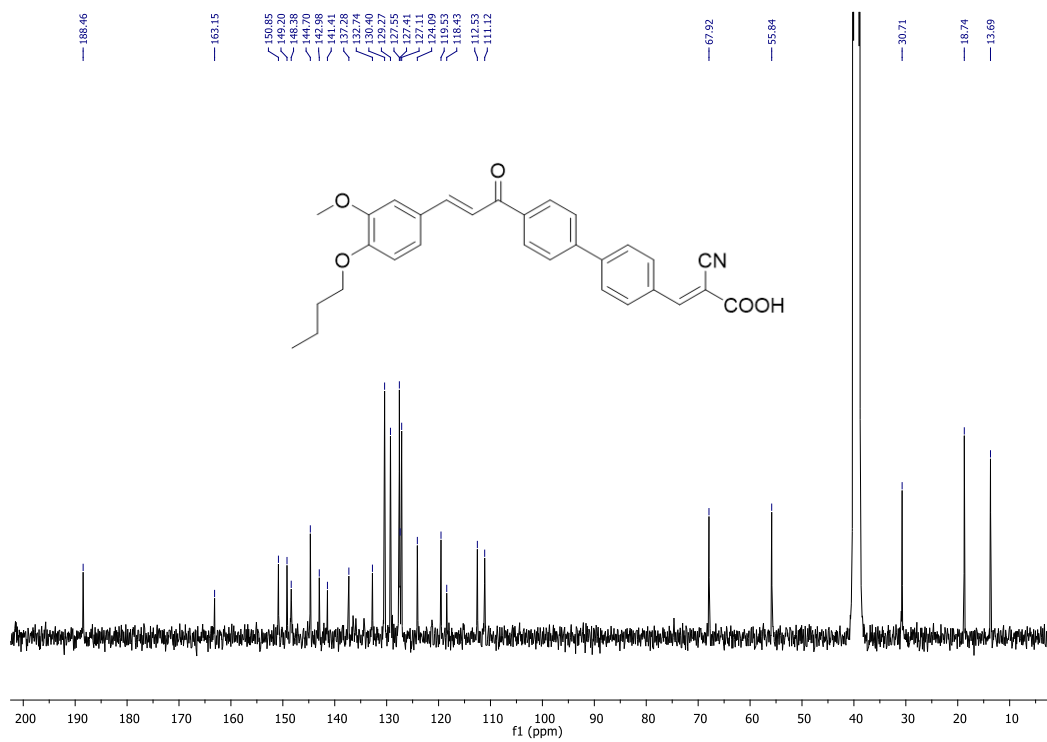


Figure A12: ¹³C NMR (APT) spectrum of compound **6a** (100 MHz, DMSO-*d*₆).

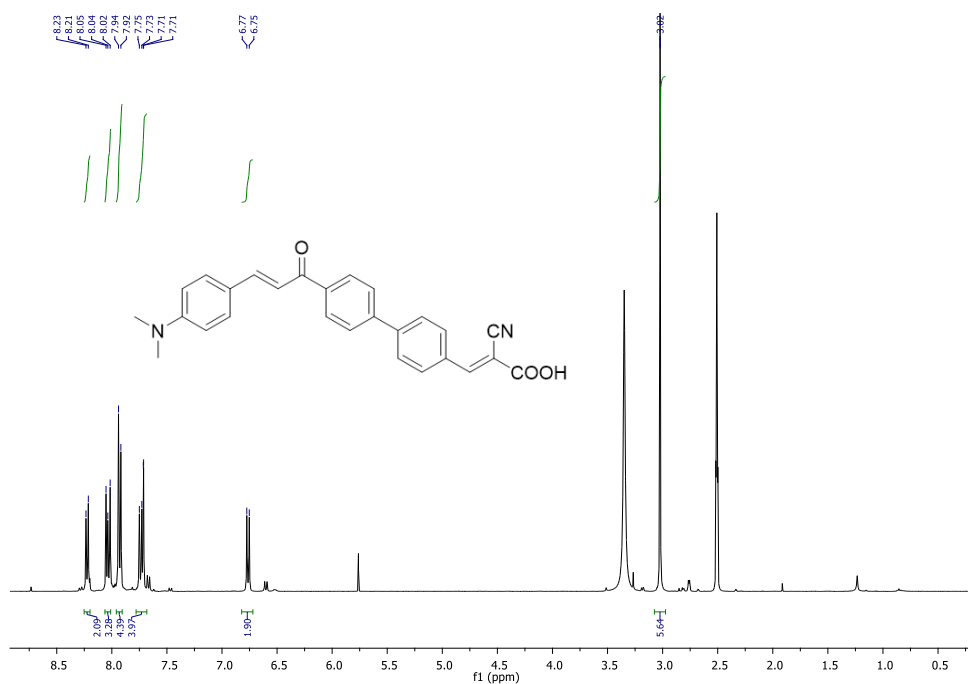


Figure A13: ¹H NMR spectrum of compound **6b** (400 MHz, DMSO-*d*₆).

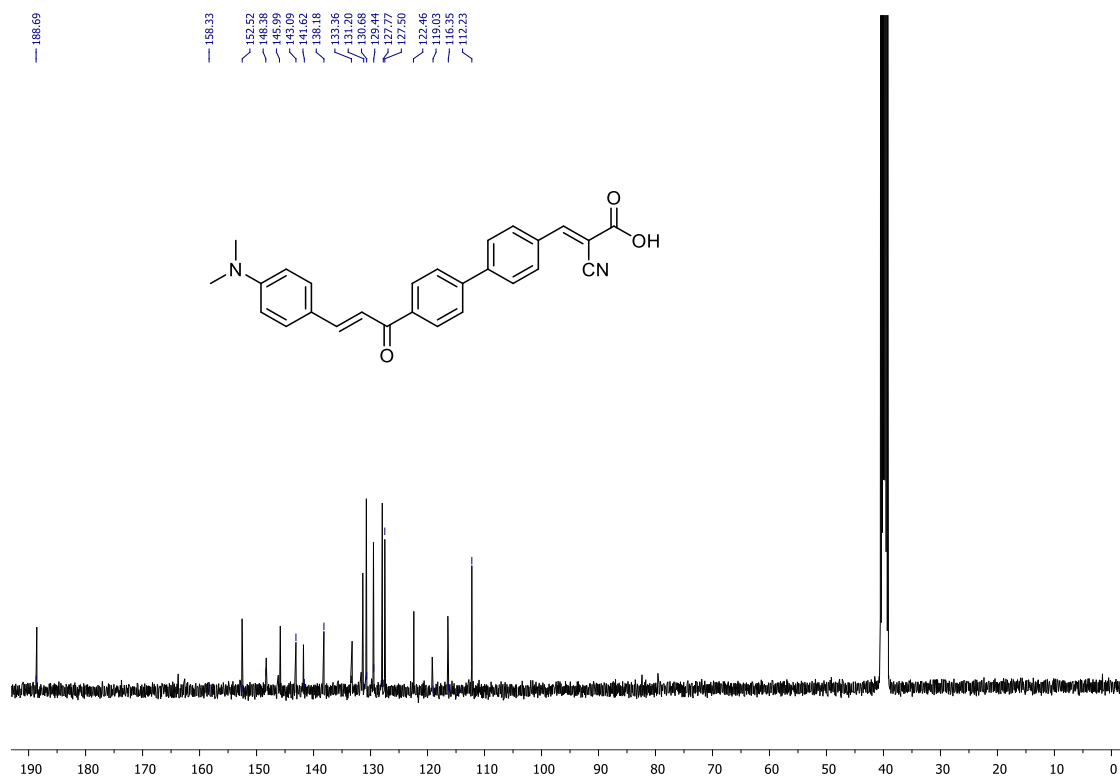
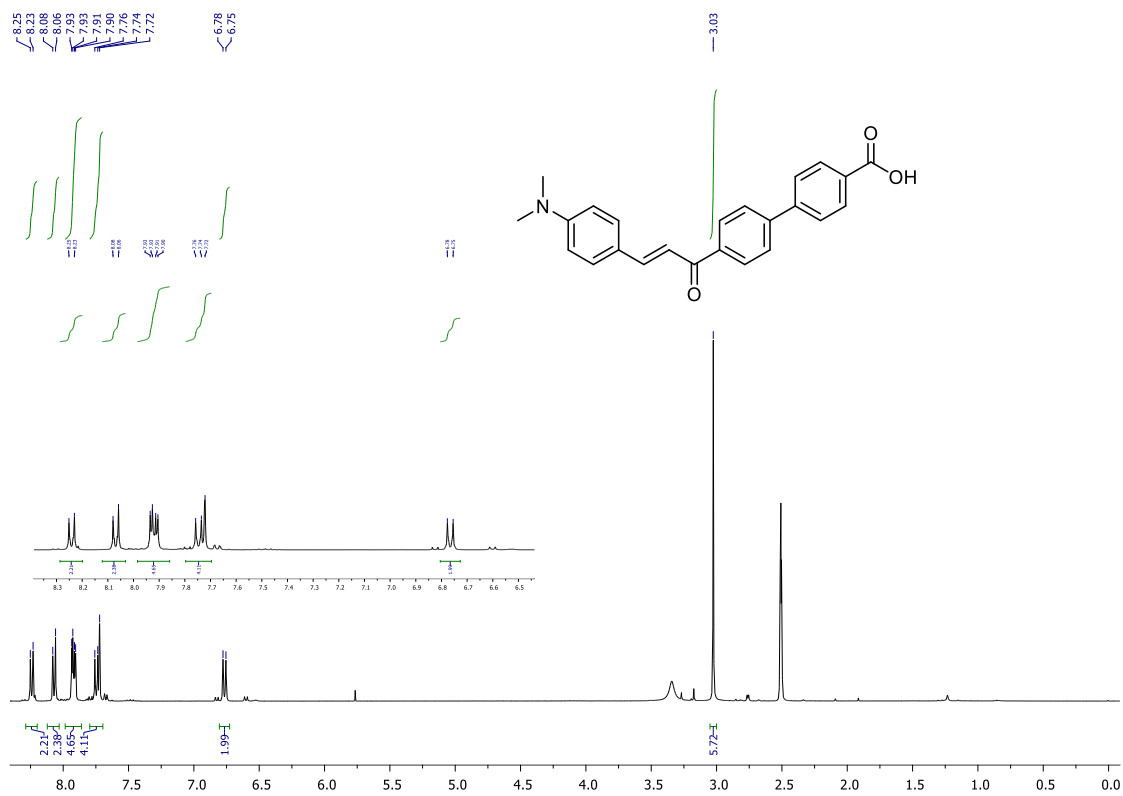
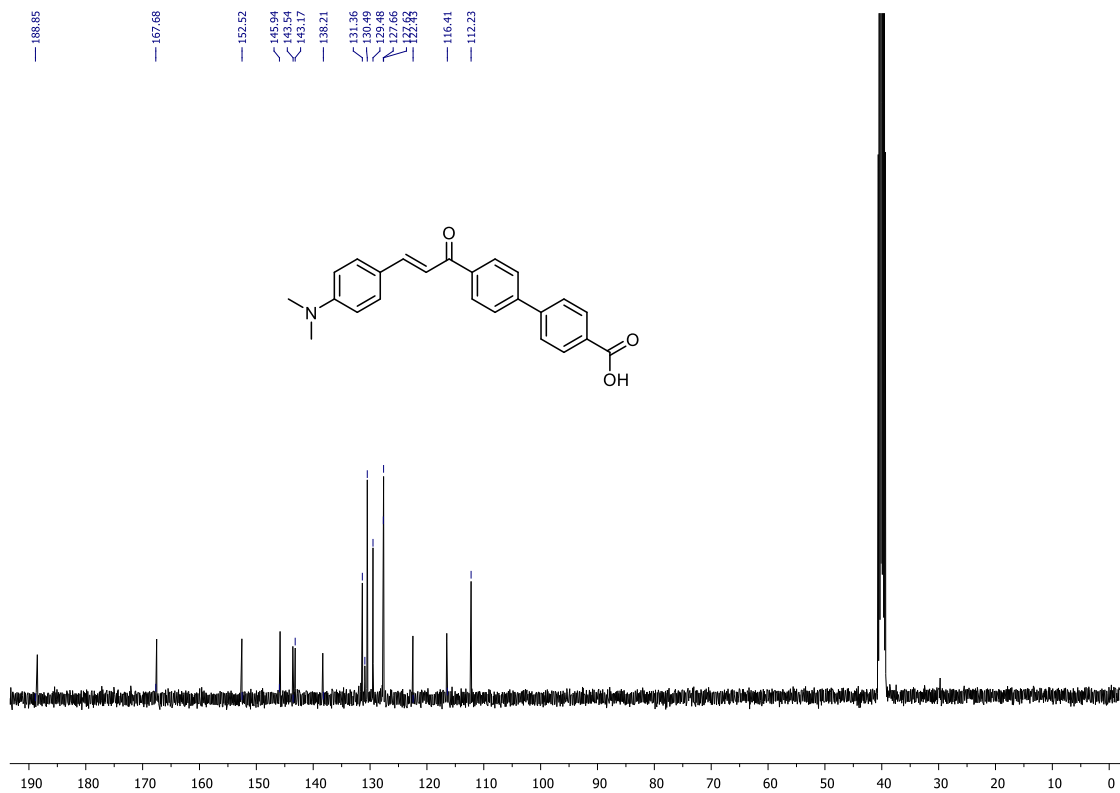
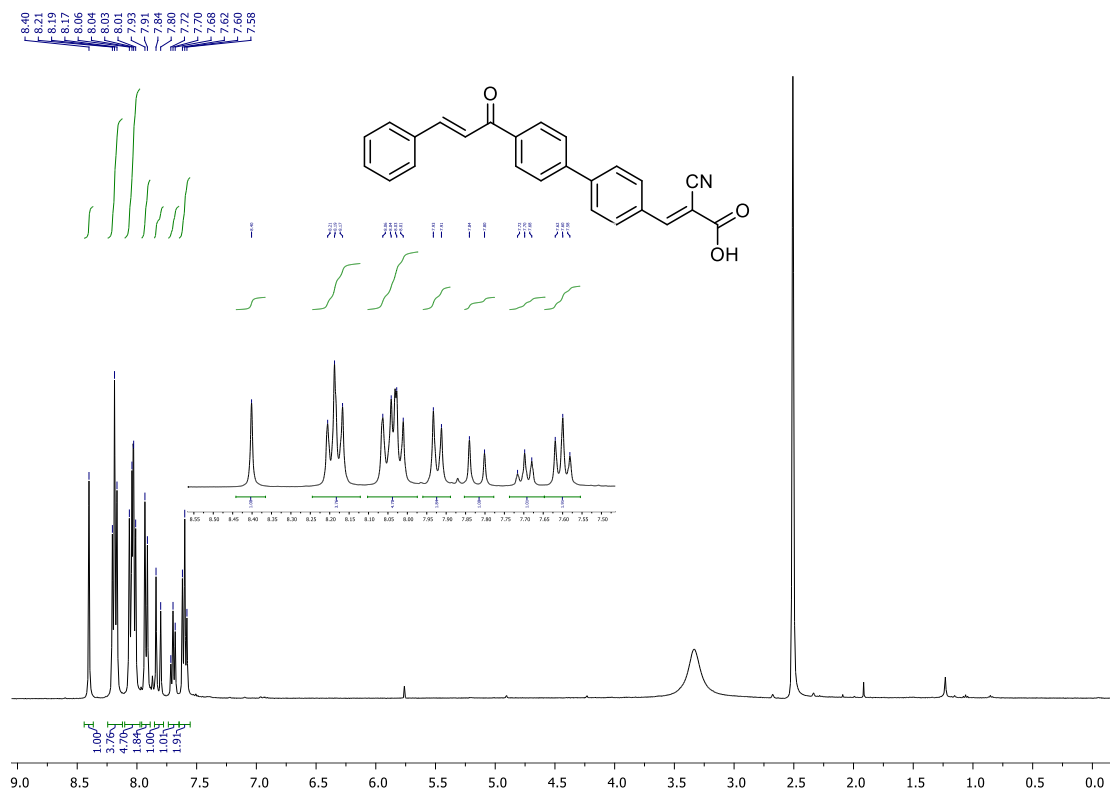
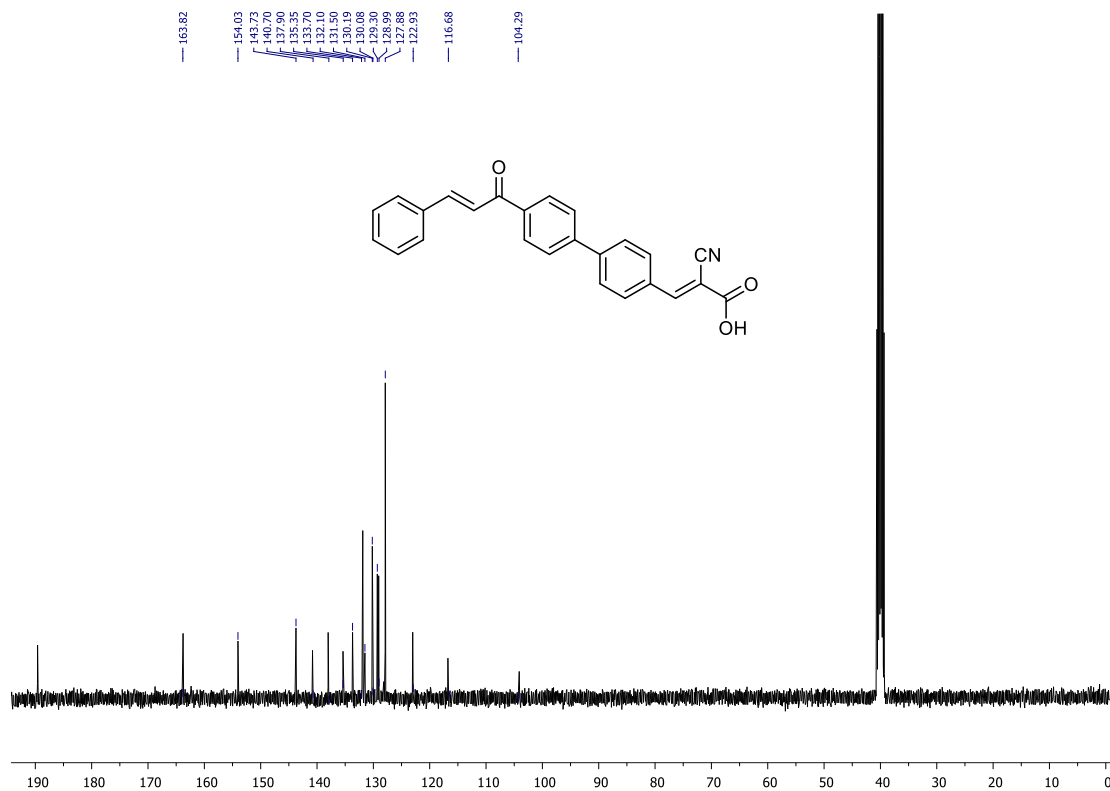


Figure A14: ¹³C NMR (APT) spectrum of compound **6b** (100 MHz, DMSO-*d*₆).

Figure A15: ¹H NMR spectrum of compound **7b** (400 MHz, DMSO-*d*₆).Figure A16: ¹³C NMR (APT) spectrum of compound **7b** (100 MHz, DMSO-*d*₆).

Figure A17: ¹H NMR spectrum of compound **6c** (400 MHz, DMSO-*d*₆).Figure A18: ¹³C NMR (APT) spectrum of compound **6c** (100 MHz, DMSO-*d*₆).

2. HRMS spectra

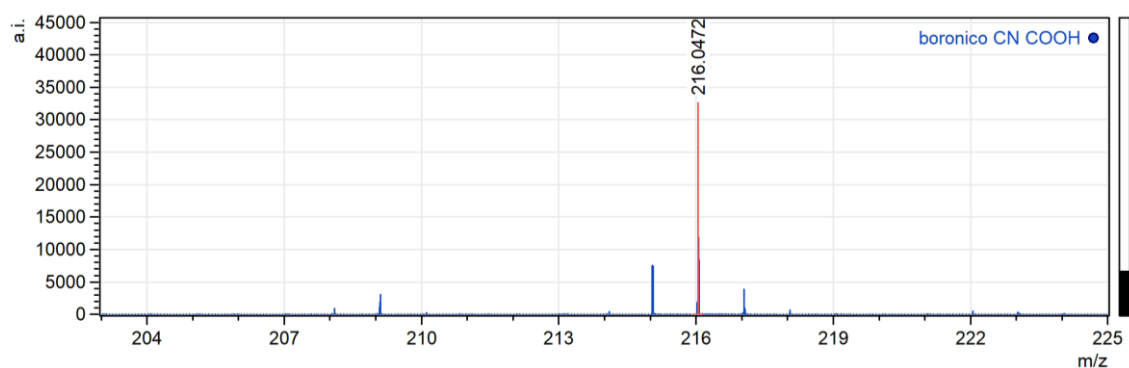


Figure A19: HRMS of compound **2** (ESI; negative mode).

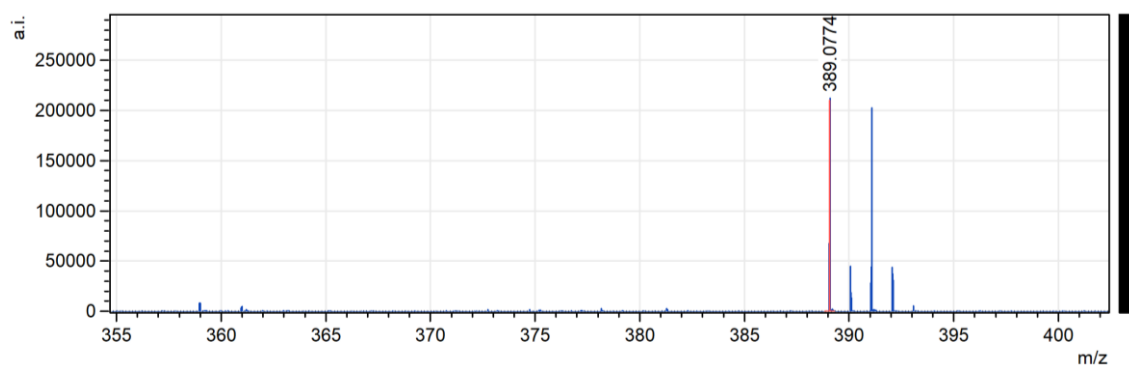


Figure A20: HRMS of compound **2** (ESI; positive mode).

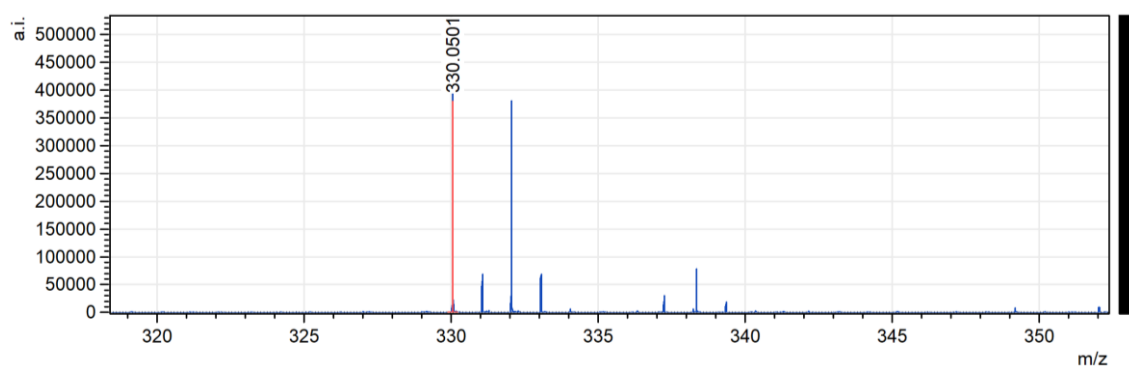
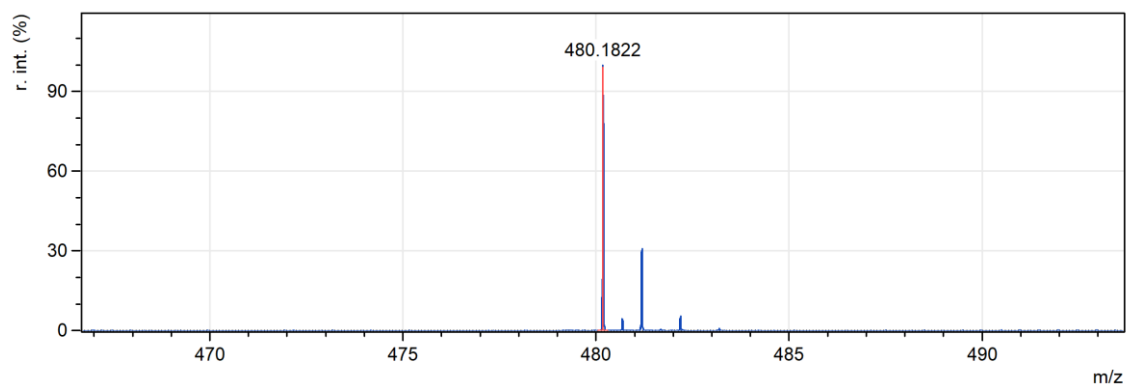
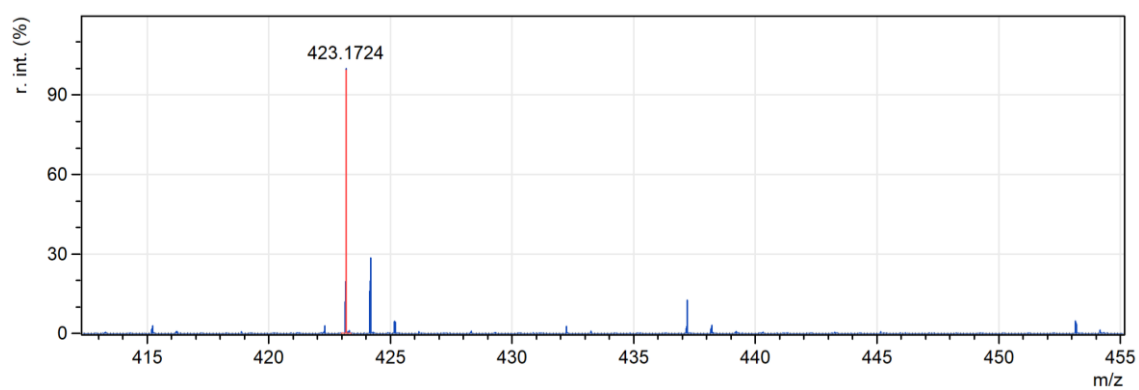
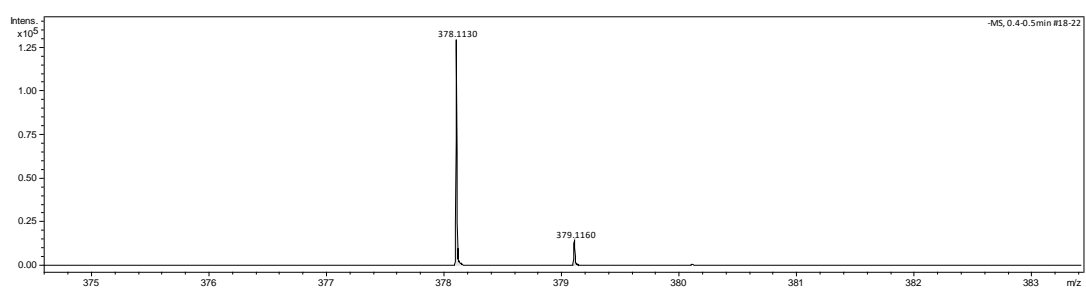
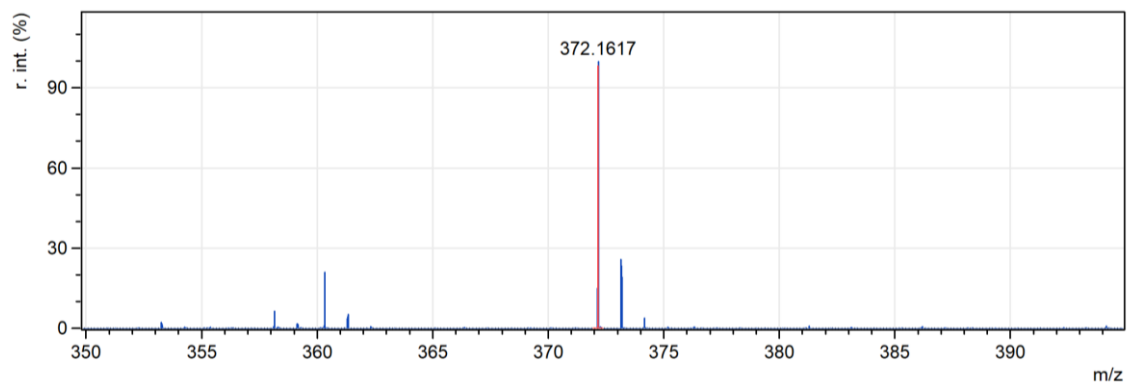
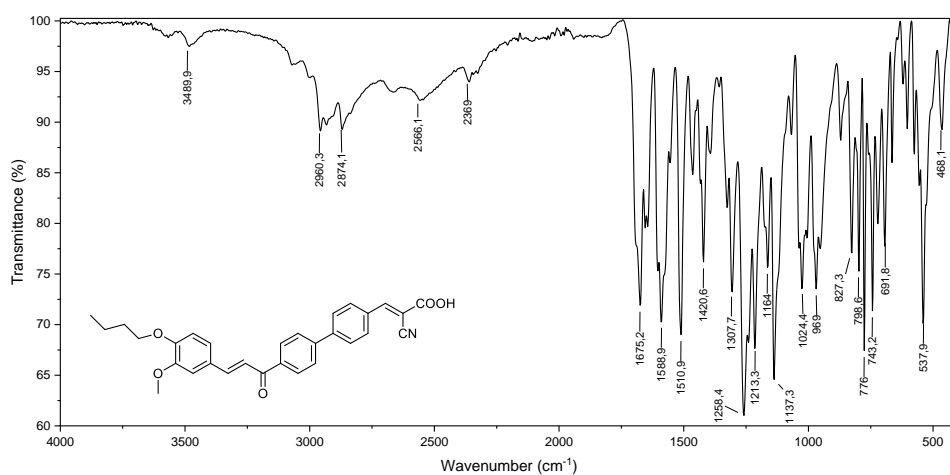
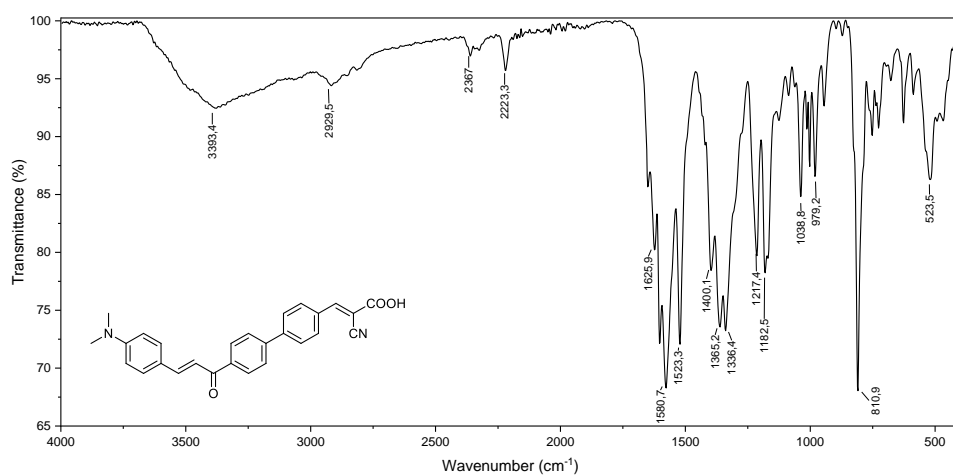


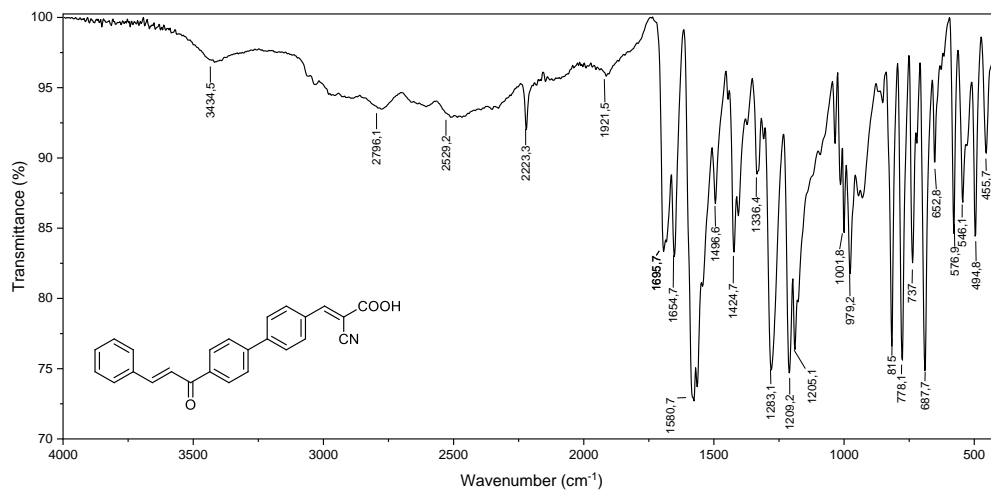
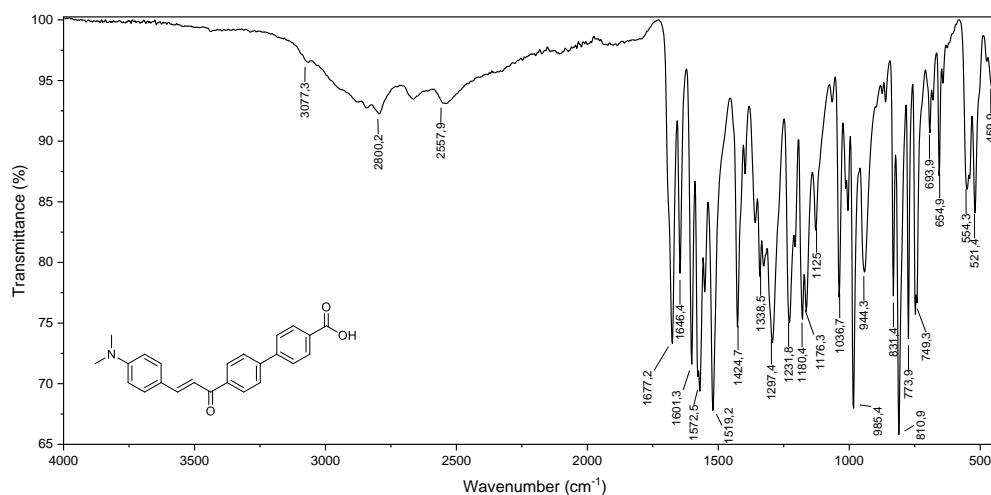
Figure A21: HRMS of compound **5b** (ESI; positive mode).

Figure A22: HRMS of compound **6a** (ESI; negative mode).Figure A23: HRMS of compound **6b** (ESI; positive mode).Figure A24: HRMS of compound **6c** (ESI; negative mode).

Figure A25: HRMS of compound **7b** (ESI; positive mode).

3. FTIR spectra of the photosensitizers

Figure A26: FTIR (ATR) spectrum of compound **6a**.Figure A27: FTIR (ATR) spectrum of compound **6b**.

Figure A28: FTIR (ATR) spectrum of compound **6c**.Figure A29: FTIR (ATR) spectrum of compound **7b**.

3. Dye sensitizers cyclic voltammograms

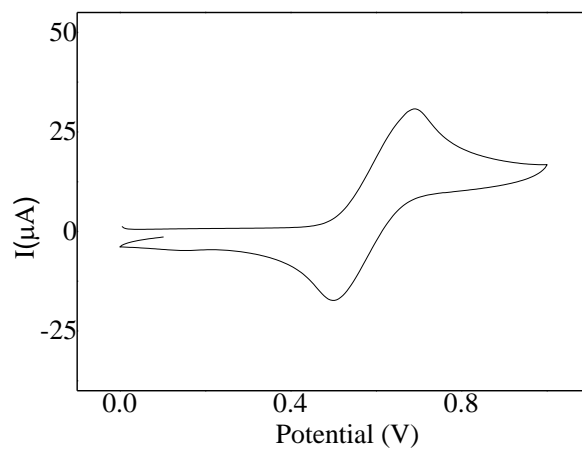


Figure A30: Voltammogram of ferrocene.

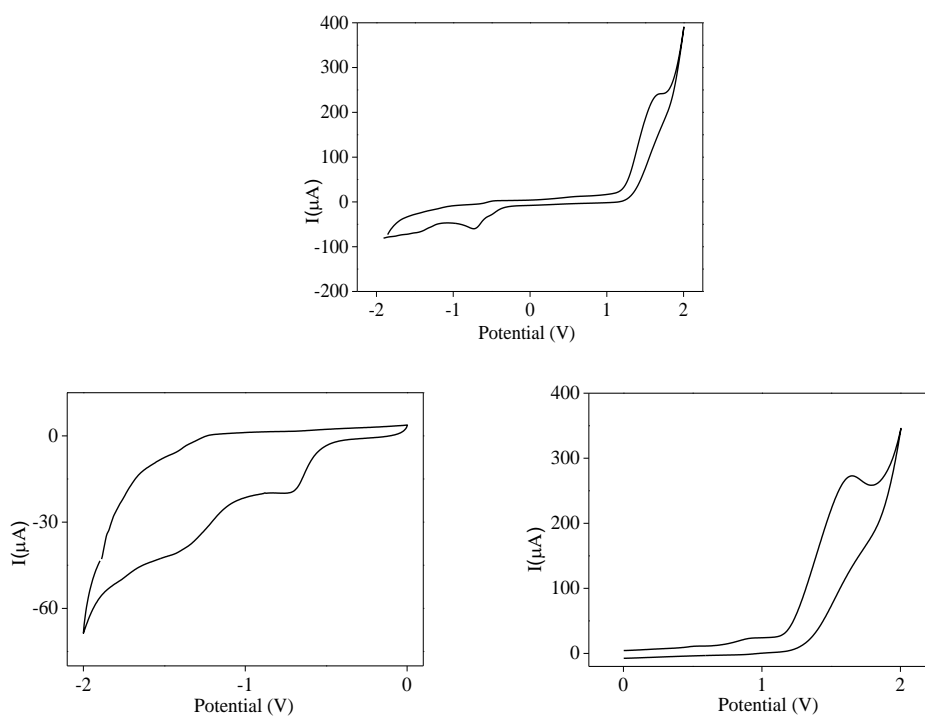
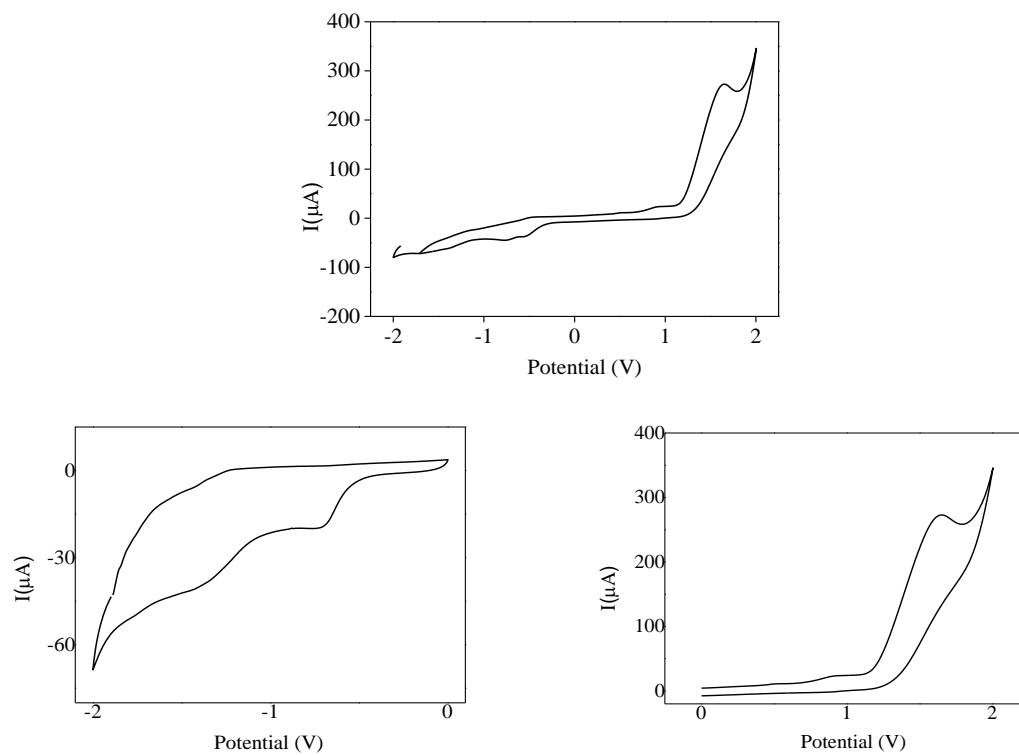
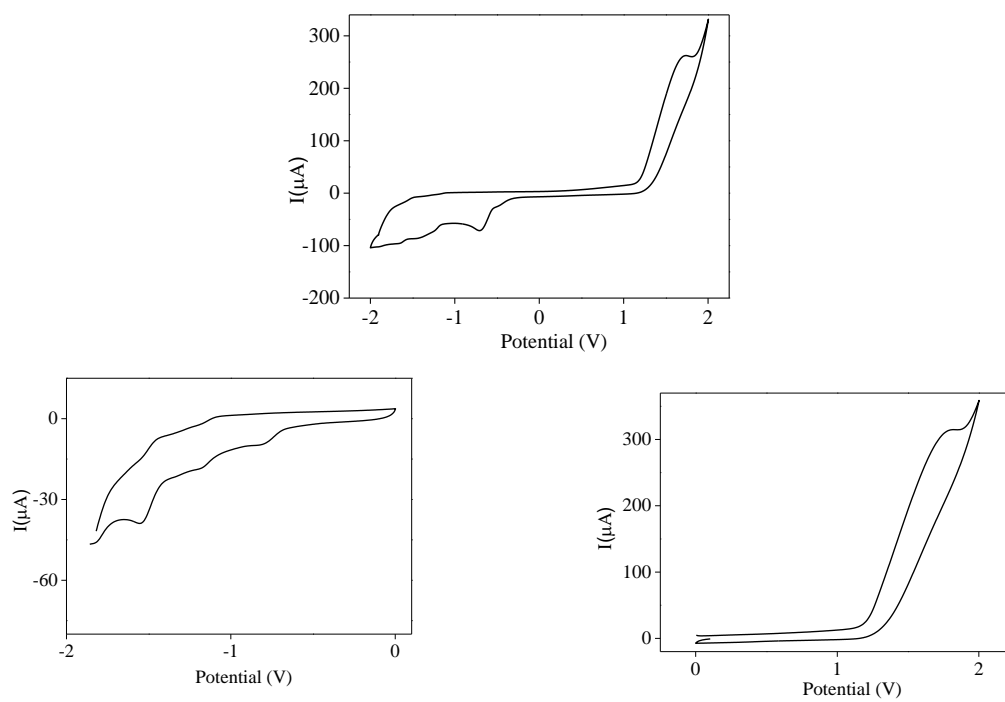
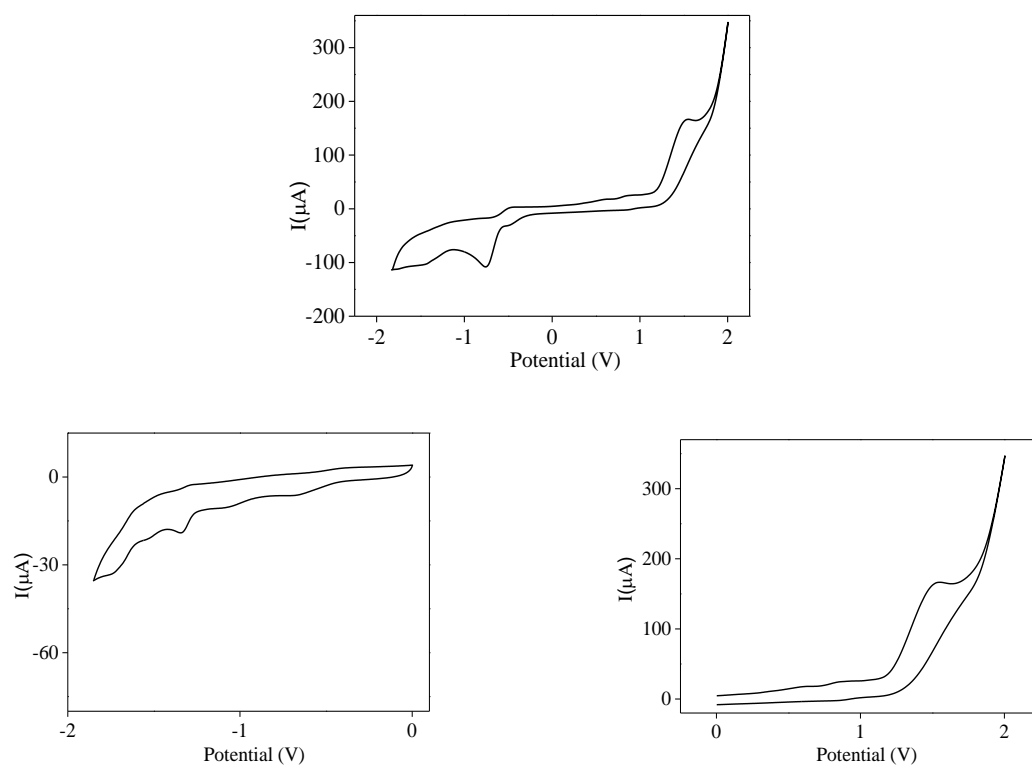
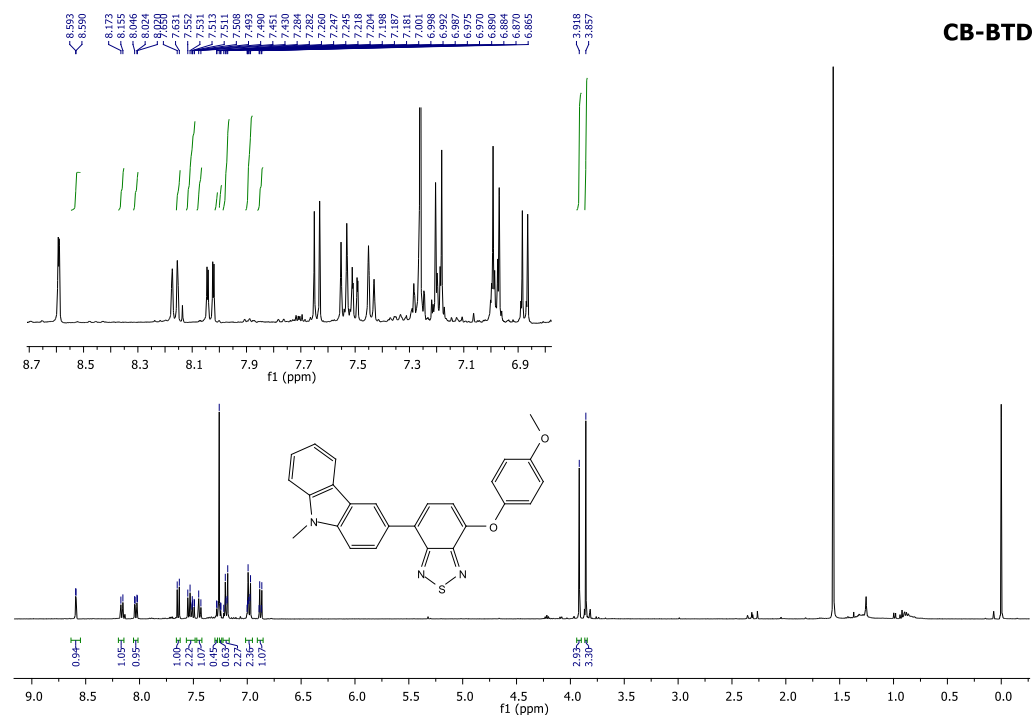
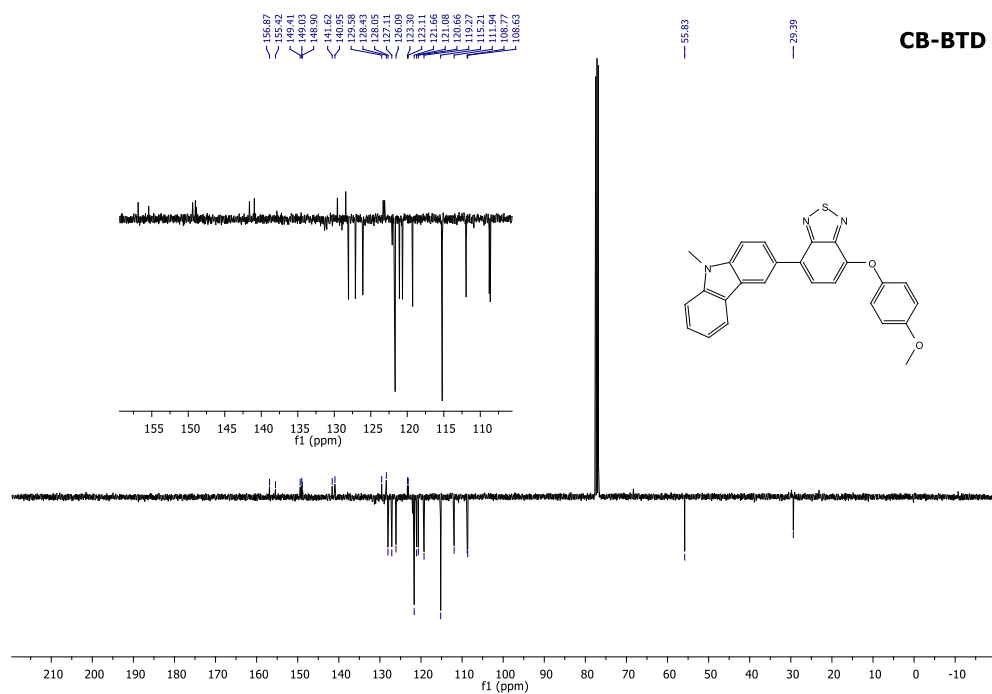
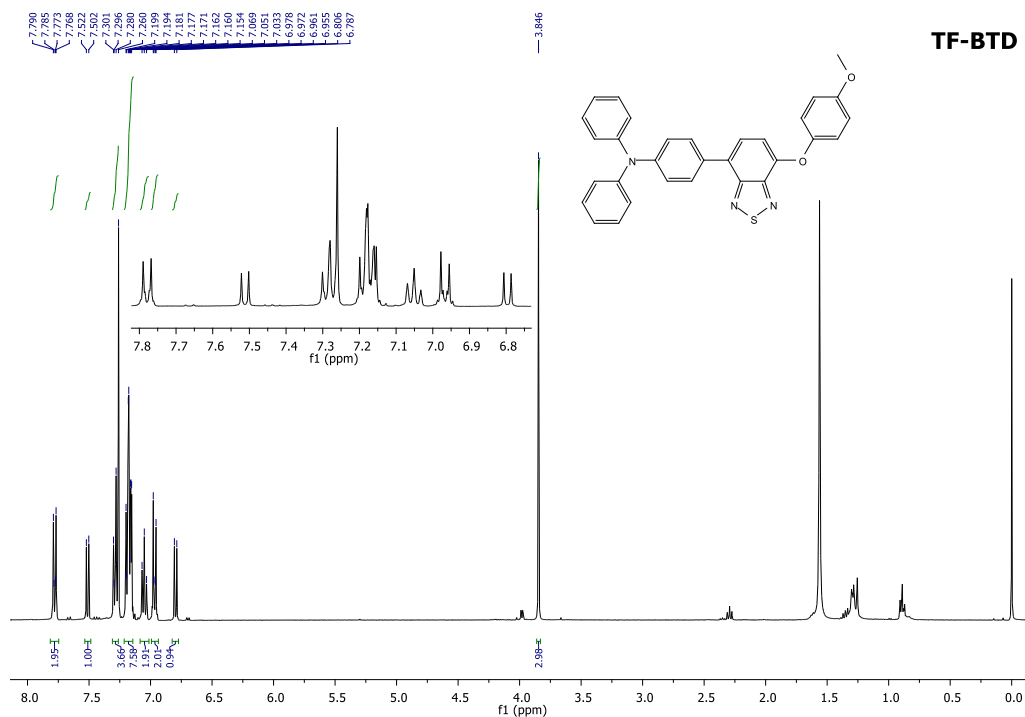
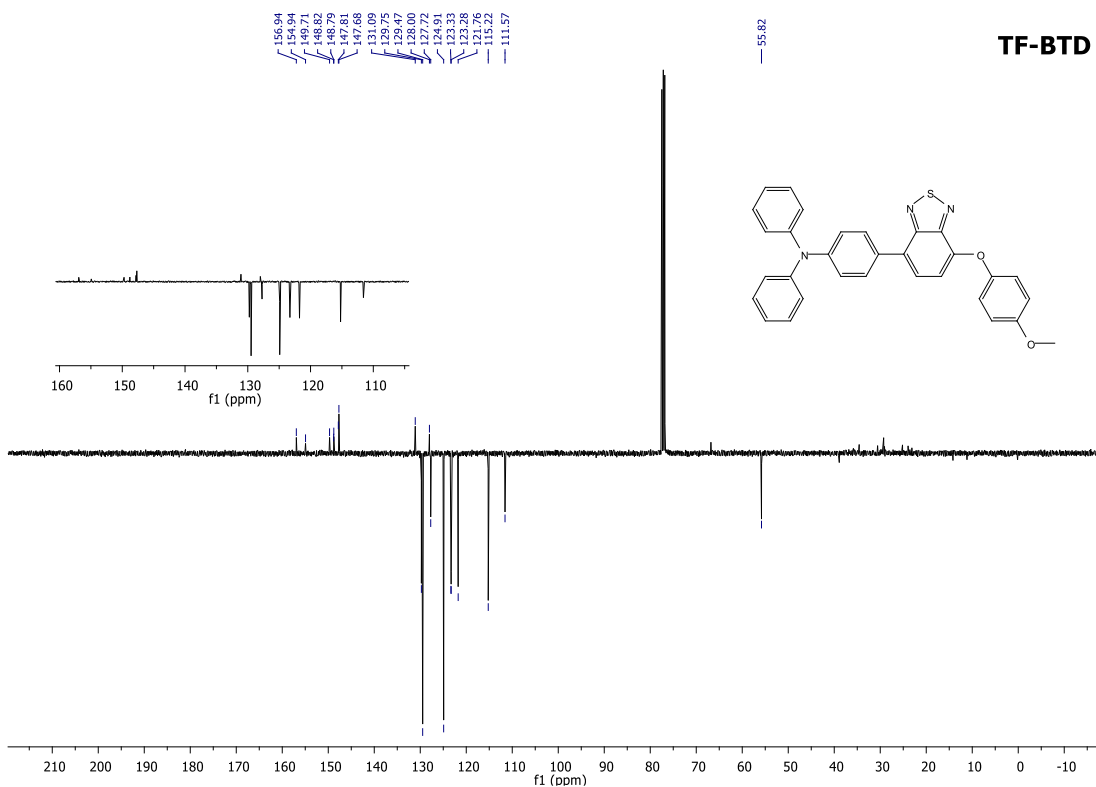


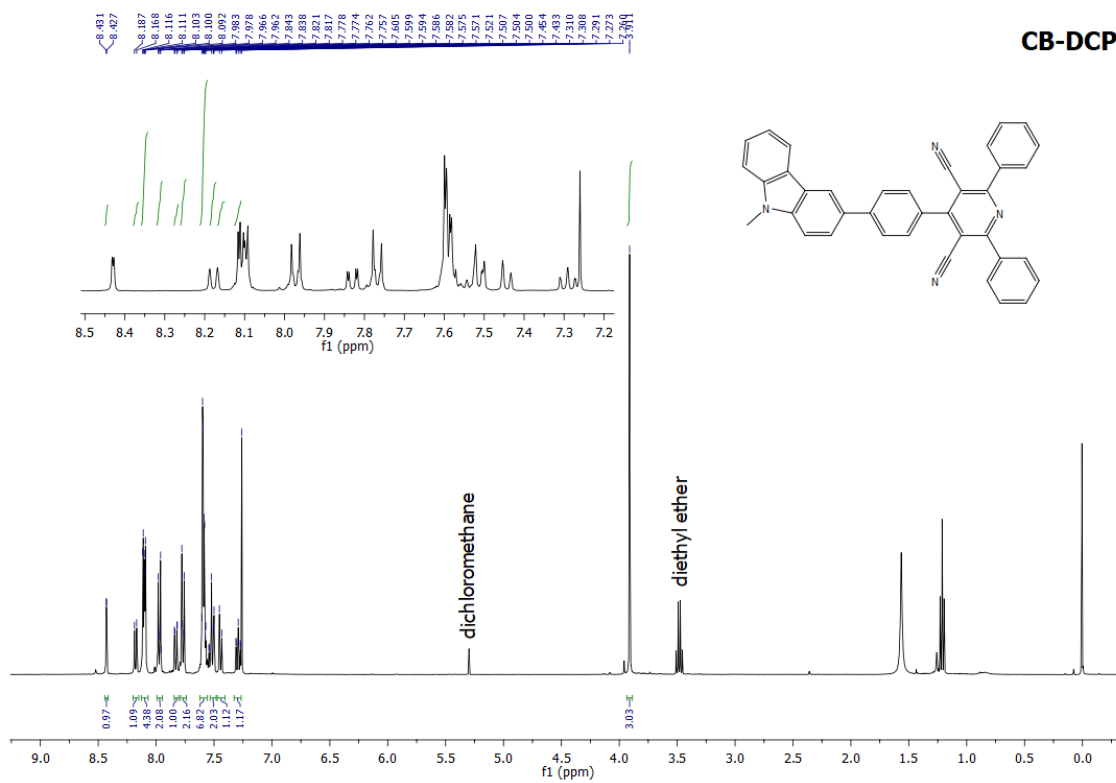
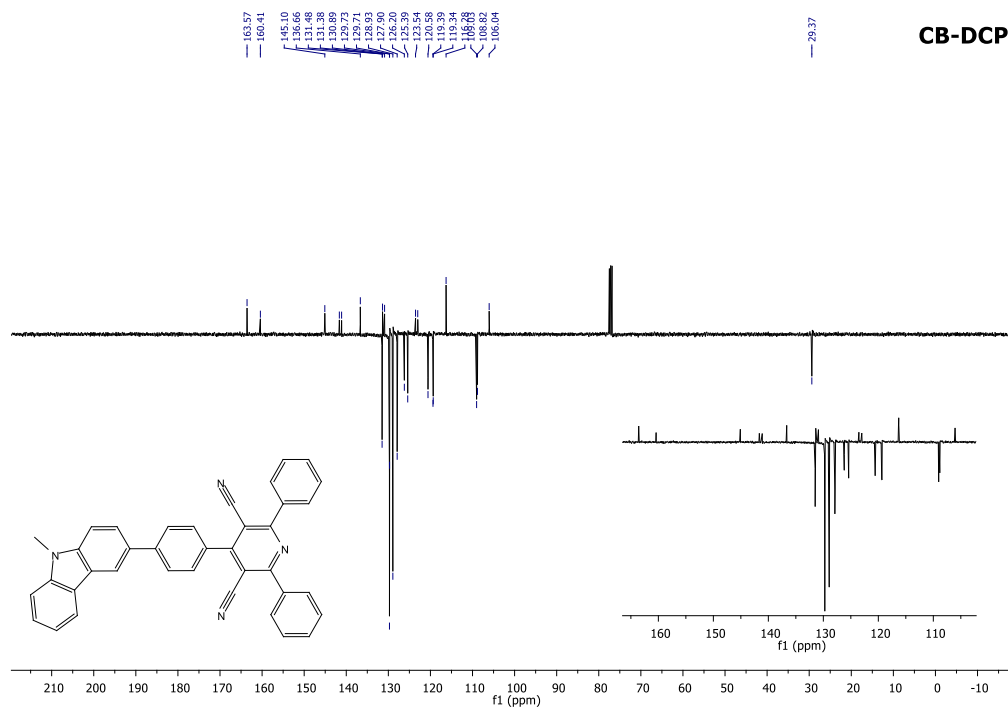
Figure A31: Voltammogram of compound 6a.

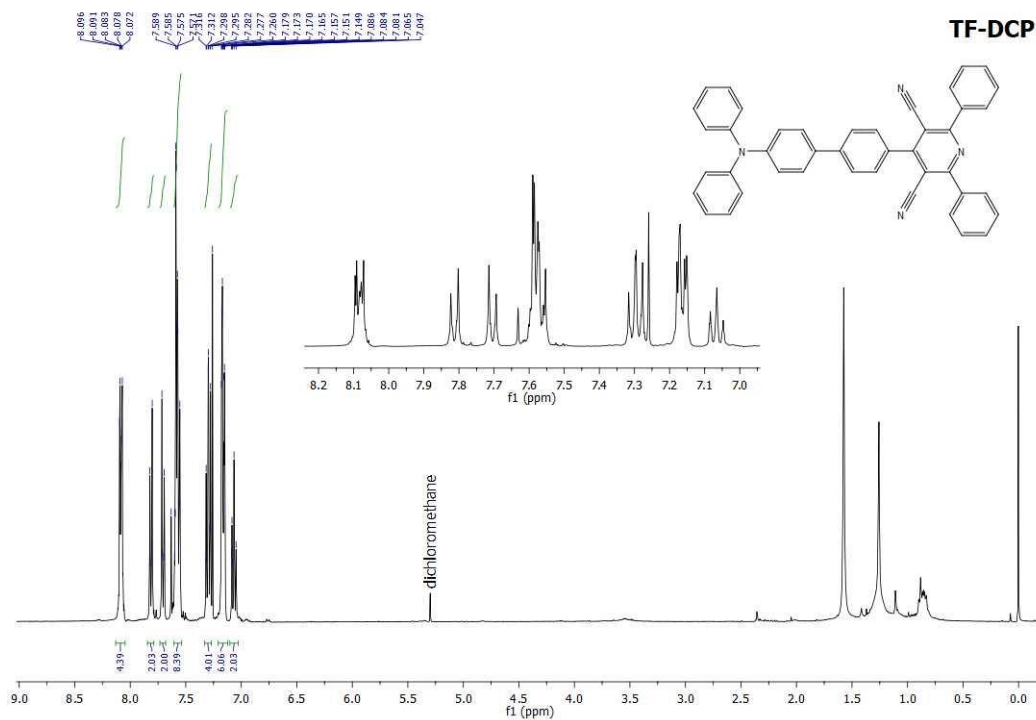
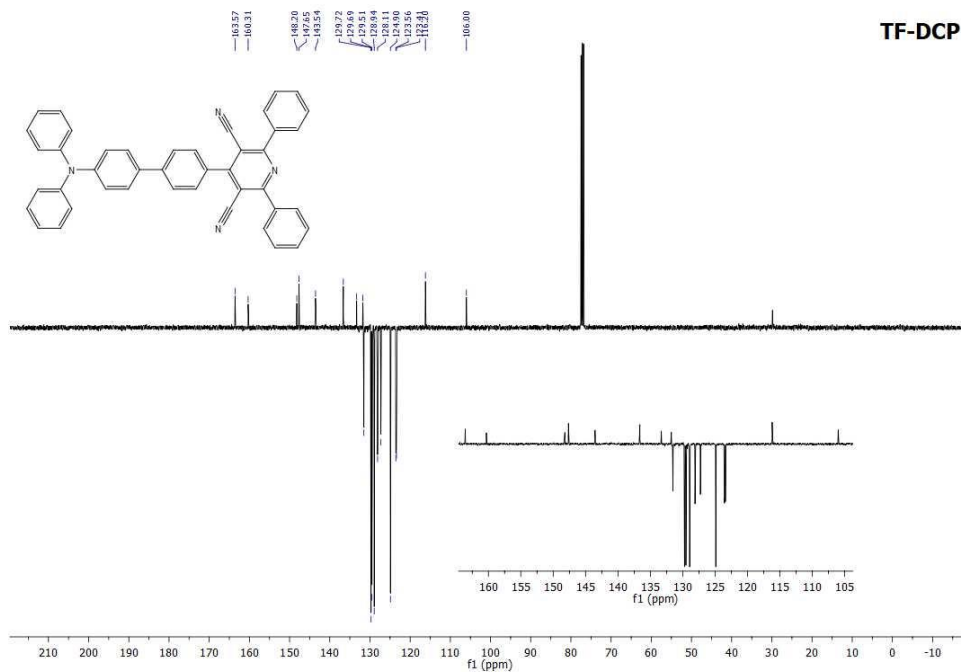
Figure A32: Voltammogram of compound **6b**.Figure A33: Voltammogram of compound **6c**.

Figure A34: Voltammogram of compound **7b**.

4. Luminophores ^1H and ^{13}C NMR spectraFigure A35: ^1H NMR spectrum of CB-BTD (400 MHz, CDCl_3).Figure A36: ^{13}C NMR (APT) spectrum of CB-BTD (101 MHz, CDCl_3).

Figure A37: ¹H NMR spectrum of TF-BTD (400 MHz, CDCl₃).Figure A38: ¹³C NMR (APT) spectrum of TF-BTD (101 MHz, CDCl₃).

Figure A39: ^1H NMR spectrum of CB-DCP (400 MHz, CDCl_3).Figure A40: ^{13}C NMR (APT) spectrum of CB-DCP (101 MHz, CDCl_3).

Figure A41: ^1H NMR spectrum of TF-DCP (400 MHz, CDCl_3).Figure A42: ^{13}C NMR (APT) spectrum of TF-DCP (101 MHz, CDCl_3).

5. Luminophores cyclic voltammetry

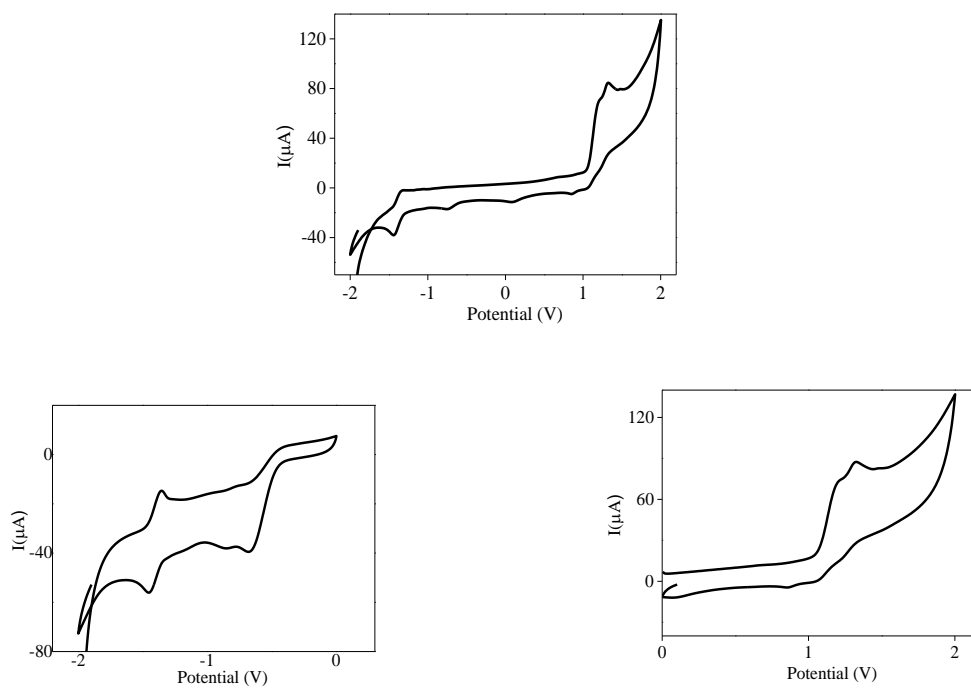


Figure A43: Voltammogram of compound CB-BTD.

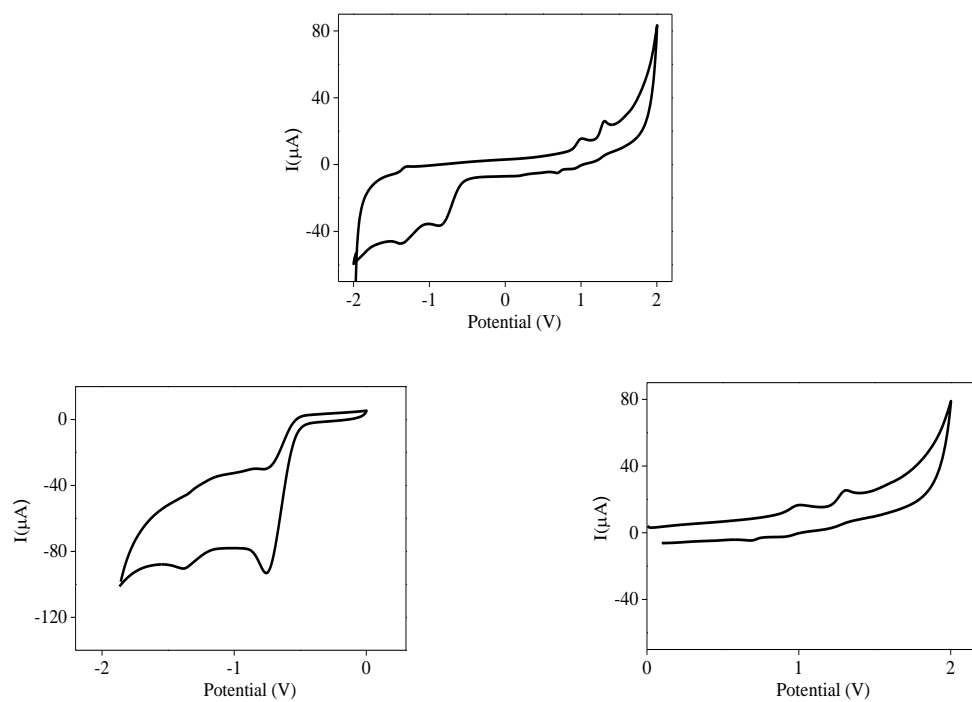


Figure A44: Voltammogram of compound TF-BTD.

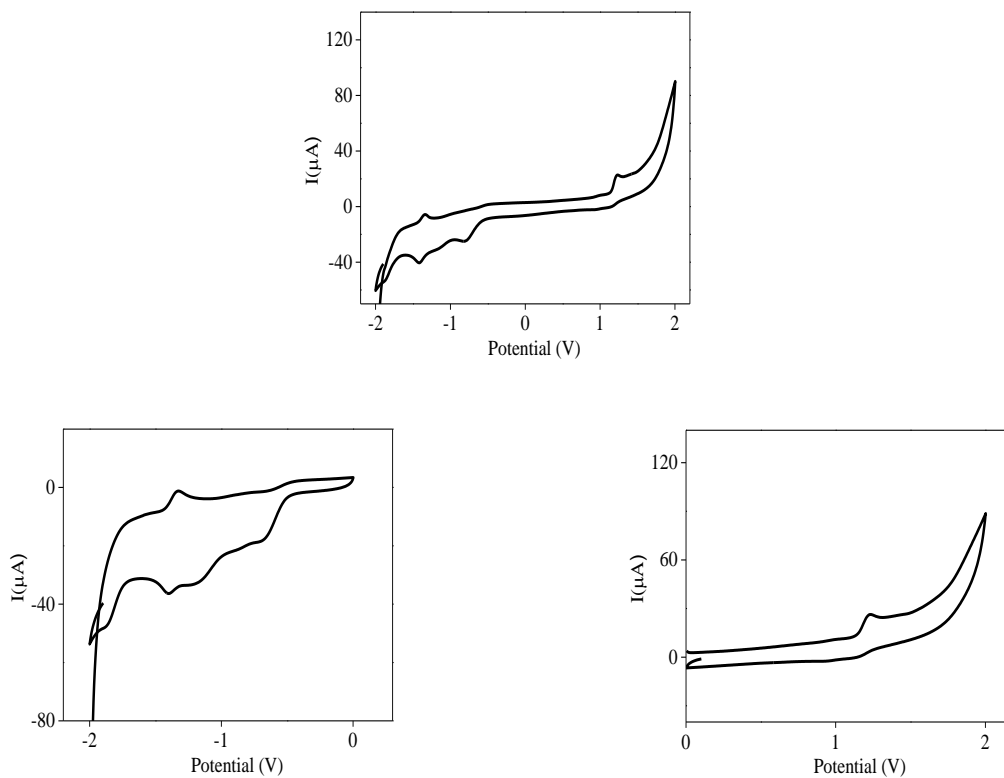


Figure A45: Voltammogram of compound CB-DCP.

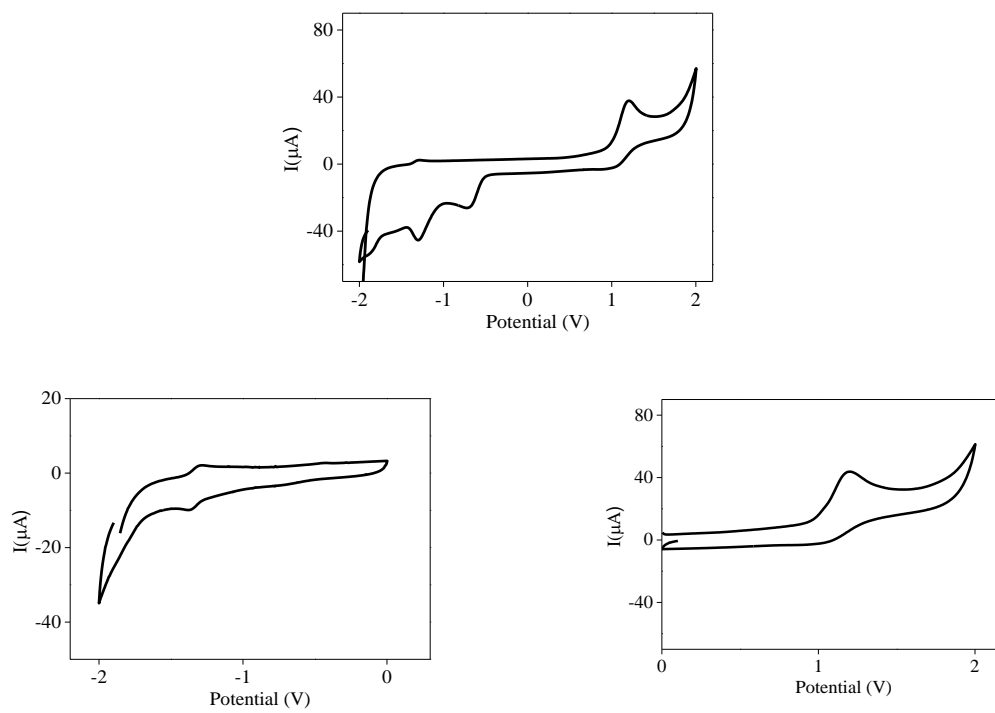


Figure A46: Voltammogram of compound TF-DCP.